

The Pennsylvania State University
The Graduate School
Intercollege Graduate Program in Materials

**SYNTHESIS AND CHARACTERIZATION OF CATALYSTS AND
ELECTROCATALYSTS USING COMBINATORIAL METHODS**

A Thesis in
Materials

By

Ramnarayanan Ramanathan

© 2005 Ramnarayanan Ramanathan

Submitted in Partial Fulfillment
of the Requirements
for the Degree of
Doctor of Philosophy

December 2005

The thesis of Ramnarayanan Ramanathan was reviewed and approved* by the following:

Thomas E. Mallouk
Dupont Professor of Materials Chemistry and Physics
Thesis Advisor
Chair of Committee

Chunshan Song
Professor of Fuel Science

Digby D. Macdonald
Distinguished Professor of Materials Science and Engineering

Darrell Velegol
Associate Professor of Chemical Engineering

Albert E. Segall
Associate Professor of Engineering Science and Mechanics
Co-Chair of the Intercollege Graduate Program in Materials

*Signatures are on file in the Graduate School

ABSTRACT

Thesis Advisor: Thomas E. Mallouk

This thesis documents attempts at solving three problems. Bead-based parallel synthetic and screening methods based on matrix algorithms were developed. The method was applied to search for new heterogeneous catalysts for dehydrogenation of methylcyclohexane. The most powerful use of the method to date was to optimize metal adsorption and evaluate catalysts as a function of incident energy, likely to be important in the future, should availability of energy be an optimization parameter. This work also highlighted the importance of order of addition of metal salts on catalytic activity and a portion of this work resulted in a patent with UOP LLC, Desplaines, Illinois. Combinatorial methods were also investigated as a tool to search for carbon-monoxide tolerant anode electrocatalysts and methanol tolerant cathode electrocatalysts, resulting in discovery of no new electrocatalysts. A physically intuitive scaling criterion was developed to analyze all experiments on electrocatalysts, providing insight for future experiments. We attempted to solve the CO poisoning problem in polymer electrolyte fuel cells using carbon molecular sieves as a separator. This approach was unsuccessful in solving the CO poisoning problem, possibly due to the tendency of the carbon molecular sieves to concentrate CO and CO₂ in pore walls.

CONTENTS

LIST OF FIGURES.....	v
LIST OF TABLES.....	viii
ACKNOWLEDGEMENTS.....	x
CHAPTER 1 Developing directed sorting methods for synthesis of heterogeneous bead based catalysts and testing in a LAMIMS reactor	
Introduction.....	1
Experimental Section.....	3
Results and Discussion.....	6
Conclusions.....	23
References	24
CHAPTER 2 Studies on electrocatalysts and fuel cells	
Introduction.....	70
Background.....	70
Experimental Section.....	84
Results and Discussion.....	87
Transport effects at the electrocatalyst surface during fuel cell runs.....	89
Methanol tolerant cathode electrocatalysts.....	93
Results and Discussion.....	95
Conclusions.....	96
References	97
CHAPTER 3 Coupling Reaction and separation using microporous carbon as gas diffusers	
Introduction.....	116
Experimental Section.....	117
Results and Discussion.....	118
Conclusions.....	123
References	123
APPENDIX A: DIRECTSORT Algorithm	134
APPENDIX B: Total number of physical manipulations for a n component, m step library in a 96 well plate format.....	139

LIST OF FIGURES

Figure 1.1. Schematic illustrating the advantage of replacing beads in vials by beads in wellplates, potentially solving the mixing and tagging problems	53
Figure 1.2a. Home built device for transferring beads across rows and columns	54
Figure 1.2b. A modified home made device for sorting beads across rows	55
Figure 1.2c. Homemade multipipette delivering solutions of 0-20 μ l	56
Figure 1.3a. Color simulation of first adsorption and first row transfer (first split) of a four component-four step split pool library	57
Figure 1.3b. Color simulation of second adsorption and first column transfer (second split) of a four component-four step split pool library	58
Figure 1.3c. Color simulation of third adsorption and second row transfer (third split) of a four component-four step split pool library.....	59
Figure 1.4a. Schematic of Energy Dispersive Spectroscopy (EDS) as a function of position for 0.5wt% Pt on γ -alumina	60
Figure 1.4b. Schematic of Energy Dispersive Spectroscopy (EDS) as a function of position for 0.2wt% Pt on γ -alumina	61
Figure 1.4c. Schematic of Energy Dispersive Spectroscopy (EDS) as a function of position for 1wt% Pt on γ -alumina	62
Figure 1.5. Bead weight (mg) versus bead diameter	63
Figure 1.6a. Electron Probe Micro-Analysis (EPMA) of $\text{Pt}_{0.05}\text{Ni}_{0.05}\text{Cu}_{0.1}\text{Sn}_{0.05}$. Subscripts indicate total metal content in weight%.	64
Figure 1.6b. Electron Probe Micro-Analysis (EPMA) of $\text{Pt}_{0.1}\text{Ni}_{0.05}\text{Cu}_{0.05}\text{Sn}_{0.05}$. Subscripts indicate total metal content in weight%	65
Figure 1.6c. Electron Probe Micro-Analysis (EPMA) of $\text{Ni}_{0.15}\text{Sn}_{0.1}$. Subscripts indicate total metal content in weight%	66
Figure 1.7a. Average normalized Laser Assisted Membrane Introduction Mass Spectroscopy (LAMIMS) area vs. theoretical Pt content (weight%) for three samples with Pt as last adsorption and one sample with Cu as last adsorption	67

Figure 1.7b. Average normalized Laser Assisted Membrane Introduction Mass Spectroscopy (LAMIMS) area vs. theoretical Ni content (weight%) for six samples with Ni as last adsorption	68
Figure 1.7c. Average normalized Laser Assisted Membrane Introduction Mass Spectroscopy (LAMIMS) area vs. theoretical Ni content (weight%) for six samples with Ni as last adsorption	69
Figure 2.1a. Cross sectional view of a polymer electrolyte fuel cell	104
Figure 2.1b. Schematic of an assembled polymer electrolyte fuel cell	104
Figure 2.2. Schematic of kinetic, ohmic and mass transport control in fuel cell curves	105
Figure 2.3. Schematic of voltage losses in anode and cathode due to various fuels.....	106
Figure 2.4a. Horizontal and vertical lines drawn for illustration of negative currents ...	107
Figure 2.4b. Quantitative comparison of electrocatalysts without verifying the pseudo-reference or cathode potential	108
Figure 2.5. Polymer Electrolyte Membrane fuel cell tests for commercial catalysts (Johnson Matthey Pt and PtRu) and two homemade catalysts in a membrane electrode assembly (MEA) as a function of current density.....	109
Figure 2.6. Polymer Electrolyte Membrane fuel cell tests for commercial catalysts (Johnson Matthey Pt and PtRu) and two homemade catalysts in a membrane electrode assembly (MEA) as a function of current.	110
Figure 2.7. Flow rate effects and reproducibility in fuel cell tests for Johnson Matthey Pt on carbon	111
Figure 2.8. Current vs. time for PSU catalysts at 0.5V on the introduction of CO/100ppm H ₂	112
Figure 2.9. Pore Size distribution of carbons (XC72 and XC72R) carbon using chloromethane	113
Figure 2.10. Gas diffusion half cell used in evaluating electrocatalysts for oxygen reduction	114
Figure 2.11. Current-voltage curves of Ru based electrocatalysts for the reduction of oxygen at 60 °C in the presence and absence of methanol in the electrolyte	115
Figure 3.1. Pore size distribution of polyfurfuryl alcohol (PFA) derived carbon using chloromethane as a probe molecule	128

Figure 3.2. Photograph of polyfurfuryl alcohol (PFA) derived carbon web and a schematic of transport through the web	129
Figure 3.3. Membrane module for permeation experiments	130
Figure 3.4. Steady state flux of pure gases through carbon membrane	131
Figure 3.5a. Flow rate of fuel (H_2 or H_2/CO) as a function of time with the membrane held between the gas cylinder and inlet to the flow meter.....	132
Figure 3.5b. Flow rate of fuel (H_2 or H_2/CO) as a function of time with the membrane held between the gas cylinder and inlet to the flow meter.....	132
Figure 3.6. Current- Voltage curves for Johnson Matthey Pt on carbon membrane electrode assembly (MEA) tested in fuel cells as a function of different flow rates of H_2 and H_2/CO as the fuel and O_2 as the oxidizer (in 0.14 and 0.3 standard liters per minute respectively)	133
Figure 3.7. Current- Voltage curves for Johnson Matthey Pt on polyfurfuryl alcohol (PFA) derived carbon membrane electrode assembly (MEA) tested in fuel cells as a function of different flow rates of H_2 and H_2/CO as the fuel and O_2 as the oxidizer (in 0.14 and 0.3 standard liters per minute respectively)	133

LIST OF TABLES

Table 1.1. Results from Row-column directed sorting simulations for four component four step 96-well plate.....	27
Table 1.2. Summary of results for larger numbers of components in larger well plates, using the row-column sorting algorithm	28
Table 1.3. Inductively Coupled Plasma Atomic Emission Spectroscopy (ICPAES) analysis of Pt on γ -alumina	29
Table 1.4a. Theoretical versus actual analysis of standards by Micro-Xray Fluorescence (μ -XRF) and Inductively Coupled Plasma Atomic Emission Spectroscopy (ICPAES) at UOP	29
Table 1.4b. Theoretical versus actual analysis of Pt on γ -alumina by Micro-Xray Fluorescence (μ -XRF) and Inductively Coupled Plasma Atomic Emission Spectroscopy (ICPAES) at UOP	31
Table 1.5. Results from column shuffle for three component four step 96-well plate	32
Table 1.6 Results from manual pipetting for three component 96-well plate	33
Table 1.7 Results of Inductively Coupled Plasma Mass Spectroscopy (ICPMS) analysis of 22 directed sorting synthesized samples.....	34
Table 1.8. Results of average, standard deviation and relative standard deviation in normalized Laser Assisted Membrane Introduction Mass Spectroscopy (LAMIMS) area and Micro-Xray Fluorescence (μ -XRF) of sixteen directed sorting synthesized samples.....	35
Table 1.9. Laser Assisted Membrane Introduction Mass Spectroscopy (LAMIMS) and Micro-Xray Fluorescence (μ -XRF) analysis of samples with Pt as last adsorption from a 3 component (Pt, Cu and Ni), 3 step (4 adsorptions and 3 transfers), 96 wellplate library; synthesized according to the column directed sorting algorithm.....	37
Table 1.10. Laser Assisted Membrane Introduction Mass Spectroscopy (LAMIMS) and Micro-Xray Fluorescence (μ -XRF) analysis of samples with Ni as last adsorption from a 3 component (Pt, Cu and Ni), 3 step (4 adsorptions and 3 transfers), 96 wellplate library; synthesized according to the column directed sorting algorithm.....	42
Table 1.11. Laser Assisted Membrane Introduction Mass Spectroscopy (LAMIMS) and Micro-Xray Fluorescence (μ -XRF) analysis of samples with Cu as last adsorption from a	

3 component (Pt, Cu and Ni), 3 step (4 adsorptions and 3 transfers), 96 wellplate library; synthesized according to the column directed sorting algorithm.....	47
Table 3.1. Permeance of pure component gases from slope of Figure 3.4	126
Table 3.2. Permeance ratios of pure component gases from slope of Figure 3.4	127

ACKNOWLEDGEMENTS

An attempt to mention all the people who have helped me and taught me various scientific and practical approaches during the course of the last six years would fill a thesis chapter. Loss of memory and constraints on space will certainly omit many. My apologies to those left out. The experiments described in this thesis did not follow a linear pattern from concept to conclusion as the text might lead the reader to believe. Writing the thesis in the non-linear fashion would only serve to confuse the reader and I have tried to put experiments, results and conclusions linearly.

I would like to thank everyone past and present in the Mallouk Group for putting up with my behavior. I have had a great time here growing up as an independent thinker. Translating some of those thoughts to practical use is a challenge I look forward to. I would like to thank Tom for the opportunities and Prof. Digby Macdonald for his lectures on electrochemistry and scientific advice. I would like to thank Dr. Deryn Chu at the Army Research Lab at Adelphi, MD for providing support to three hapless graduate students in Fall 2001. It is a pleasure to acknowledge practical advice and constructive critique from Prof. Chunshan Song at Penn State, John Sinfelt and David Vaughan formerly of Exxon-Mobil, Robert Bedard, Michelle Cohn, Richard Willis, Doug Galloway, Evgeny Kolev, Shawn Clisham, Vince Mezera, Gregory Lewis and Anil Oroskar of UOP and discussions with Profs. Larry Duda, Friedrich Helfferich and Paul Weisz. Prof. Weisz deserves a special mention for helping polish random thoughts into ideas based on sound basic science and order of magnitude arguments and helping polish and inculcate strengths in connecting-the-dots. Prof. Helfferich deserves mention for re-emphasizing the importance of thinking through problems apriori and along lines of experiments. I am thankful to Dr. Uday Turaga, currently at Conoco-Philips for constantly challenging me to do better.

The work described in this thesis was largely supported by a grant from the Exploratory and Fundamentals Group of UOP LLC, Des Plaines, IL outside and as part of the U.S. Department of Commerce, National Institute of Standards and Technology, Advanced

Technology Program (Cooperative Agreement Number 70NANB9H3035), through the Collaborative Technology Alliance Program from the Army Research Lab at Adelphi, MD and a semester of Teaching Assistantship from the Department of Chemistry at Penn State. I also thank the National Institute of Standards and Technology, Advanced Technology Program for financial support for my stay at UOP during February-April 2004 and Dr. Richard Willis and Tom for help in securing the same. I would like to thank Falaah Falih, Jason Davis, Richard Willis and Doug Galloway for their timely and invaluable help in the conclusion of Chapter 1 and discussions and fun-filled times during my brief stint with the Exploratory and Fundamentals Group of UOP.

Chapter 1 Developing directed sorting methods for synthesis of heterogeneous bead based catalysts and testing in a LAMIMS reactor

This work was done in collaboration with Douglas Galloway and Falaah Falih (reactor testing of catalyst libraries), Simon Bare and Jason Davis (μ -XRF analysis) and Richard Willis (co-ordination through the project and analytical support) of UOP LLC. The work has resulted in a patent [25] and parts of this chapter have been accepted to the Proceedings of the Petroleum Chemistry Division of the American Chemical Society [24] for Fall 2005 in Washington DC. My advisor (Tom Mallouk) wrote a FORTRAN program to simulate and predict combinations and sequences of metals using a row/column shuffle algorithm. I designed and carried out all the experiments, analyzed results from analytical methods at UOP (SEM, μ -XRF) and Penn State (ICPMS, EPMA and SEM-EDS) and also contributed to troubleshooting and mass and heat transport analysis of the LAMIMS reactor [20] described briefly in this chapter.

Introduction

This chapter describes two approaches to synthesize inorganic materials borrowing techniques developed in the drug industry – the split pool method and a subset, the directed sorting method. We describe here a split-pool directed sorting approach towards the synthesis of inorganic bead libraries [24]. This work builds on an earlier paper from our lab [10] that demonstrated the use of the split-pool concept in solid state materials chemistry. The biggest challenges in our earlier work [10] were to develop a tagging scheme to track metal salt adsorption, and to avoid the mixing of components and dissolution of the alumina support in sequential adsorption steps. These problems resulted in relatively poor control over bead composition as well as an inability to identify individual beads without post-synthesis analysis. The directed sorting approach demonstrated in this paper, based on matrix methods and adsorption in wellplates, enables the synthesis of combinatorial bead libraries without problems of component mixing. The algorithm eliminates the need for post-synthesis bead identification and also eliminates the tagging problem. The inexpensive equipment (well plates, plastic pipettes) used also make this method affordable to laboratories that lack sophisticated synthetic

equipment. To demonstrate the approach, we chose noble metals and 2 mg porous γ -alumina beads of the kind typically used in heterogeneous catalysis [11]. One library was evaluated for catalytic activity by Laser Activated Membrane Introduction Mass Spectrometry (LAMIMS) [20]. We chose methylcyclohexane (MCH) dehydrogenation to toluene as a probe reaction.

The method described here offers an approach mimicking split-pool by choosing n components, which in the case described here are adsorbed onto the beads in n well-plates and m split-pool steps, and has the following advantages: beads (members of a given library) are sorted along a predetermined algorithm that tracks the history of each bead as it adsorbs metal salts, simplifying array layout and controlling redundancy without sacrificing flexibility. These sorting algorithms simplify the mapping of a multidimensional composition space into a 2-D array layout. By changing some of the parameters of the sorting algorithm, such as the sequence of row- and column shuffling steps, it is possible to change the compositional redundancy of the resulting split-pool library. This control is enabled by replacing the vials described in [10] by wells in standard commercial wellplates. This simple modification, illustrated in Figure 1.1, solves the component mixing problem by isolating each bead in a unique well, physically separated from the adjacent beads. Each bead absorbs the same amount of solution in each step. The tagging problem is solved by indexing every bead by four coordinates (well plate identity, row and column number, and split pool step). The most important outcome is the direct correlation of the response of the library (to a probe reaction or signal) with the composition and sequence of metal adsorption steps on each bead without physical tagging.

The concept of spatially addressing a large number of experiments can be traced to the work of Mittasch [1], who tested large numbers of catalysts, and in essence kept track of every sample and its processing history. Computers were not invented in 1903 and one can assume that lab notebooks and entries therein served as tags. To our knowledge, the earliest documented systematic way of designing experiments following a specific algorithm can be traced to the work by Fisher and Yates [15], who were interested in

problems in biology and agriculture, leading to useful concepts such as analysis of variance (ANOVA) and design of experiments (DOE). With the advent of combinatorial methods pioneered by Hanak [2] and popularized by numerous researchers [3-9, 12], sophistication increased along with the use of computers and robotics. Labor saving DOE constructs were generally not used in this early work, because they were not easily integrated into the array deposition methods used [13]. The current chapter uses computer simulations and pen-and-paper approaches to synthesize deterministic combinatorial libraries with controlled redundancy.

Split-pool combinatorial approaches have been widely used in organic and bio-organic chemistry, and have been extensively reviewed [11, 13, 17]. Directed sorting approaches to making split-pool materials libraries have been studied by Schunk et al., and our group [10, 14]. Schunk et al. [14] describe the synthesis and characterization of a 3000 member Mo-Bi-Co-Ni-Fe on γ -alumina library. Their synthetic procedure for adsorption involved adsorbing metal salts on γ -alumina in a porcelain dish, replacing the vials described in our work [10]. Post analysis of beads was still required in their work to identify bead compositions.

Experimental Section

Materials H_2PtCl_6 , $\text{SnCl}_2 \cdot 2\text{H}_2\text{O}$, $\text{CuCl}_2 \cdot 2\text{H}_2\text{O}$ and $\text{NiCl}_2 \cdot 6\text{H}_2\text{O}$ were purchased from Alfa Aesar and used as received. Pt, Co, Cu and Ni (1mg and 10mg) in 1ml of 2 and 10 % HCl were purchased from Hi-Purity standards and used as received. Porous 2mg γ -alumina beads from UOP LLC, made by an oil drop technique [23], had a surface area of 195 m^2/g and an average diameter of 1.5 μm . The average mass of the support beads was 2.3 mg. Prior to first adsorption, γ -alumina beads were washed in DI water at room temperature. The beads were then calcined at 400 $^\circ\text{C}$ for 3 hours and cooled down to room temperature to remove excess water. Vacu-pette 96, well plates and pipettes were purchased from VWR. Cascade Blue, Fluorescein-5-isothiocyanate, Lucifer Yellow and Sulforhodamine 101 were used as received from Molecular Probes.

One Sphere at-a-time (OSAAT) experiments under incipient wetness In OSAAT experiments, one alumina sphere was placed manually into each well of a 96 V-bottom well plate (Nalge Nunc International). To reduce effects of diameter and weight of the beads during these experiments, we manually sorted about 700 beads by weight (2.3 ± 0.2 mg) and diameter (sieved using a 1536 well plate). The beads were then divided into six equal lots (~ 100 beads). Metal salts were dissolved in 0.5M HCl to a final concentration of 0.09 g/ml. In a typical procedure to adsorb 0.05wt% Pt onto each bead, approximately 1.8 g of H_2PtCl_6 (Alfa-Aesar) and 530 μl of concentrated hydrochloric acid was dissolved in 20 ml of water. The solutions were heated to boiling for 15 min., cooled to room temperature, and then diluted to 25 ml. During the adsorption experiments, one alumina sphere was placed manually into each well and 12 μl of solution containing metal salt was delivered to each well manually using a pipette. Adsorption under these conditions was close to incipient wetness. Adsorption was done at room temperature for 30 minutes followed by a drying step at 60°C for 1 h. The beads were then cooled to room temperature.

Modifying the Vaccupette for bead transfer and as a multi-pipetter In combinatorial chemistry experiments to date and in OSAAT experiments described in our earlier paper [10, 11 and references therein], commercial robotic plotters have been routinely programmed to deliver the metal salt solutions to synthesize large libraries. Here, a Vaccu-pette from VWR, an inexpensive plastic multi-tip pipettor was modified into a multi-pipette syringe and bead transfer device. To use the Vaccu-pette as a bead transfer device, Samco Transfer pipet tips were cut to 4.4cm in length and attached to the Vaccu-pette bottom using a 96 well plate. Holes were drilled into the wells of a 96 well plate and the pipet tips were held onto the Vaccupette using the hollow plate and Scotch tape, as shown in Figures 1.2a and 1.2b. To use the Vaccupette as a multi-pipettor, paraffin wax was melted in a crystallization dish. Pipet tips used to deliver (0-20 μl) were held onto the pegs of the Vaccupette and the whole assembly immersed in hot paraffin wax. The wax was cooled to room temperature and the assembly was removed from the wax using a heated chisel. The bottom of the multi-pipettor was encased in Parafilm as shown in Figure 1.2c. This set of tools eliminates the need for expensive synthetic equipment,

such as commercial plotters and solid handling devices routinely used in combinatorial chemistry.

Elemental analysis Metal loadings and distribution on representative beads were determined using Energy Dispersive X-ray Spectroscopy (EDS), Micro X-ray Fluorescence (μ -XRF) and Inductively Coupled Plasma Atomic Emission Spectrometry (ICP-AES) at UOP, Electron Probe Microanalysis (EPMA) and Inductively Coupled Plasma Mass Spectrometry (ICP-MS) at Penn State. ICPAES analysis was performed on Leeman Labs PS3000 using calibration standards (Specpure from Alfa Aesar and Hi-Purity standards). ICPMS analysis was done using a Finnigan MATELEMENT high resolution instrument using the same calibration standards as ICPAES. For ICPMS analysis, the beads were digested for one hour at 80 °C in a mixture of 2ml DI water, 2ml concentrated H_3PO_4 (VWR) and 1 ml concentrated HCl (VWR) in an erlenmeyer covered with a watch glass, cooled to room temperature and diluted to 50ml with DI water. Calibration standards containing Cu, Co and Ni were also diluted to 50ml in the same matrix as the samples. 750 μ l of 10ppb of Indium was used as an internal standard in all samples during ICPMS and data were normalized to Indium counts in the mass spectrometer. For some of the samples that had errors greater than 20% by ICPMS, Cu and Ni calibration standards (Hi-Purity) were spiked together with Indium and samples reanalyzed. EPMA analysis used a Cameca SX-50 by sectioning each bead in two halves and mounting in epoxy. EPMA profiles were recorded from the edge to the center in 50 μ m steps with a 20 μ m spot size; epoxy penetration prevented us from getting closer than 20 μ m from the true bead edge. EDS spectra for the beads adsorbed with Pt were collected on a Scanning Electron Microscope (JEOL 840) from the true edge of the bead at UOP and was operated at 15kV and a beam current of 600nA with counting time of 200s and spot size of 10 μ m². The elemental concentrations were extracted by a linear least squares fit to spectra of standards recorded in the same instrument under the same conditions and peak deconvolution, integration and conversion to wt% done using Noran software. The EDS elemental maps for the beads adsorbed with Pt, Ru, Ni, Au, Pd, Re, Ir, and Rh were collected on a Scanning Electron Microscope (JEOL JSM 5400) at Penn State with the IMIX-PC version 10.593. The spectra were recorded at a take off angle of

30 degrees, accelerating voltage of 20KV at a magnification of 75X. Each EDS elemental map was collected for 1 hour. Under these conditions, the detection limits of the EDS system were reached at 0.3 wt%. We therefore concluded that the EDS system was able to detect 0.5 wt% metal loading on the beads. Samples were also analyzed by Micro-XRF (Eagle III μ Probe from EDAX) using a Rh-K α source at an excitation energy of 25 keV. The spot size was 1mm and the collection time used was 300s per bead. Based on the beam excitation energy, the escape depth was estimated to correspond to the outer 200 μ m of the γ -alumina bead.

Directed sorting experiments The first step in this process was adsorption. This was done by transferring beads using the modified Vaccupette shown in Figure 1.2a. Once the beads were adsorbed and dried, the first quarter of each plate along the rows in a given plate was transferred using the row-sorter shown in Figure 1.2b to another well plate. The process was repeated cyclically i.e., the next quarter of each well plate receives the beads from the next plate and so on. This process happens four times per plate for a 4 component row shuffle. The same procedure was used for the column shuffle, with the transfer being perpendicular to that described above. The row/column shuffle alternated with row shuffle after every odd adsorption step (counting the first as odd) and column shuffle after every even adsorption step and proceeds to four steps, with total number of adsorptions being five. These steps are repeated for m sorting steps, making the total number of adsorptions $m+1$. In the sorting algorithm represented by Fig. 1.3 and Tables 1.2 and 1.3, a shift by one row and one column was added after every pair of row/column directed sorting steps in order to maximize the diversity of the bead libraries. For example, in the synthesis of a four-component bead library occupying four 96-well plates (12 rows x 8 columns), rows of beads were moved in groups of three and columns in groups of two. In the first row shuffle, rows 1-3 from plate 1 were transferred to plate 1, rows 4-6 to plate 2, etc. In the second row shuffle, rows 12, 1, and 2 from plate 1 were transferred to plate 1, rows 3-5 to plate 2, etc., as illustrated in Fig. 1.3c In the third row sort, rows 11, 12, and 1 from plate 1 were transferred to plate 1, rows 2-4 to plate 2, etc. The adsorption and sorting operations were alternated until the desired number of split-pool steps was achieved. The experimental procedure for directed sorting experiments thus replaces vials described in [10] by well-plates.

Test for methylcyclohexane dehydrogenation to toluene using LAMIMS Hydrogen gas was passed through the reactor at 50 ml/min and a 25 Watt laser (Synrad) was held over each bead for 6 minutes at 25% laser power, to reduce metal salts to metal at each bead. The feed was switched to a mixture of H₂ (50 ml/min) and MCH (0.02ml/min). The laser was switched to 55% peak power and held at each bead for 40 seconds to provide energy heat the gas surrounding the bead, the metal supported on alumina and provide necessary energy for the endothermic reaction (MCH to toluene) and for Toluene to desorb.

Results and Discussion

Adsorption of metal salts onto individual beads in well plates

We first studied the adsorption of metal salts onto individual beads to optimize the conditions for synthesizing direct sorted split-pool bead libraries in wellplates. Our initial experiments involved adsorbing Pt from H₂PtCl₆ to determine metal distribution and uniformity on γ -alumina. We developed One-Sphere-at-a-time (OSAAT) approach for these experiments. Briefly, one alumina sphere was placed manually into each well of a 96 V-bottom well plate and one or more adsorption/drying cycles were performed in that well. In a typical procedure to adsorb Pt onto each bead, beads were equilibrated in each well plate with 3 μ l of solution such that metal solution corresponding to desired metal weight was adsorbed onto each bead. Table 1.3 shows the results of ICPAES analysis of 3 beads from each lot, indicating a good correlation between theoretical and measured compositions. The measurements were carried out at six different Pt loadings and indicated that the beads were uniform in Pt impregnation (+/- 4% variation from the average with a relative error of 5%). We concluded that ICPAES on Pt was not sensitive to variation in bead weight (406%) and variation in bead diameter (7.7%) and possibly reflected variation in pipetting (3%). Figures 1.4a-c show EDS spectra as a function of position on cross-sectioned beads containing Pt. We also extended the OSAAT mode of adsorption to Ru, Ni, Au, Pd, Re, Ir, and Rh. using 3 μ L of metal salts in 0.5M HCl and found by EDS-SEM that the metal salts were evenly distributed [26]. These experiments suggested to us that the OSAAT mode of adsorption could be applied to make directed

sorting split-pool libraries using the modified Vaccupettes as multi-pipettors and for suction during bead transfer.

Adsorption of metal salts under incipient wetness conditions onto beads using row/column algorithms in well plate arrays

Conceptually, the difference between OSAAT and directed split-pool was one of adsorption. In our original split-pool experiments [10], beads were loaded into dram vials and then adsorbed under impregnation (excess solvent) conditions. The beads were in close proximity and we postulated that eliminating this would solve homogeneity and mixing problems. In OSAAT experiments, each bead sat in its own well and adsorbed solution under incipient wetness conditions. Chan's experiments under OSAAT conditions for adsorption of Pt, Ru, Ni, Au, Pd, Re, Ir, and Rh produced evenly distributed metal loaded beads [26]. The use of a well plate solves the problem of beads in close proximity. Therefore, each OSAAT adsorption is similar to an adsorption step in the split-pool scheme. The beads in individual wells could be loaded with metal salt solutions, dried, pooled and split again. We thus optimized adsorption under OSAAT conditions and then applied the same conditions to split-pool.

Directed sorting algorithm

Bead libraries were synthesized using a sorting algorithm conceptually similar to the randomization of colors in a Rubik's cube. One of the objectives in solving the Rubik's cube puzzle is to start from disjoint faces of the cube i.e., a mixture of colors, and end up with uniform color on each face of the cube. This is done by moving sections of the cube along row or column, similar to viewing each well plate as a matrix ($\mathbf{k} \times \mathbf{l}$) and shuffling rows and columns. Thus the 3*3 Rubik's cube can be mapped onto a 3 layer well-plate structure. The objective of our simulations and experiments however, was the reverse, i.e., start with uniform colors (first adsorption) and end up with a disjoint hypercube (the result of many adsorption steps and sequences in >3 compositional dimensions).

Conceptually, one can view each well plate as a bead positional matrix ($\mathbf{k} \times \mathbf{l}$) with a third variable \mathbf{j} serving as the well plate identifier. The number of components in a split-pool library (\mathbf{n}) is fixed by the number of well-plates (indexed by \mathbf{j}), analogous to the number

of vials or reaction flasks in conventional split-pool synthesis, giving us the flexibility of choosing large or small split-pool libraries. We simulated the transfer sections of each well plate (i.e., beads along sets of rows/ columns) to other well plates, with uniform metal salt adsorption in each well plate between split-pool steps.

In order to rapidly simulate the split-pool algorithms and assess the diversity of bead libraries they produced, a FORTRAN program (DIRECTSORT) was written, treating beads in wells (that replace vials) as members of a matrix (Appendix 1). The program simulated different sorting algorithms and ran in a few seconds on a PC allowing one to change the algorithm and see the results quickly. The first step in the process is adsorption of each component onto all the beads in each well plate. The program treats every adsorption step as unique in a given well plate and tracks this by adding the well plate index (\mathbf{j}) to every bead (\mathbf{k},\mathbf{l}) of a given well plate.

After the first adsorption there are rectangles of height (\mathbf{h}) and width (\mathbf{w}), where (\mathbf{h}) is the total number of rows and (\mathbf{w}) is the total number of columns in every well plate (See Figure 1.3a, top). The next step is to move members of a given row (\mathbf{k}) in a well plate (\mathbf{j}) to the same (\mathbf{j}) or another ($\mathbf{j}+1, \mathbf{j}+2$, etc) plate. This implies that after the first adsorption and first row transfer there are rectangles of height (\mathbf{h}/\mathbf{n}) and width (\mathbf{w}), in each well plate (Figure 1.3a, bottom). This row shuffle is followed by a second adsorption step, as shown in Figure 1.3b (top). At the end of the two adsorptions and one row transfer, each member of the matrix has two components (the first and second adsorption) and is deterministically identified. The next step is to move members of a given column (\mathbf{l}) in a well plate to the same or to another well plate. This first column shuffle results in rectangles of height (\mathbf{h}/\mathbf{n}) and width (\mathbf{w}/\mathbf{n}), as shown in Figure 1.3b (bottom). The row/column shuffle alternates, with row shuffle after every odd adsorption step (counting the first as odd) and column shuffle after every even adsorption step and proceeds to \mathbf{m} steps, with total number of adsorptions being $\mathbf{m}+1$. The DIRECTSORT program counts the number of unique sequences of components and compositions (tallied as the total number of times a given component is present in the index of each element), and also gives a map of the final compositions.

Figures 1.3a-c illustrates the concept of a row/column shuffle using a four component, four step 96 well plate (12 rows and 8 columns) library. The results of the alternate row/column sorting algorithm are shown in 1.1 and 1.2 for four components in four 96-well plates. The row/column shuffle algorithm captured 52 of the 56 possible compositions. We found that the algorithm missed four binaries (combinations of two of four elements) out of a possible 24 accounting for the difference (Table 1.1). Table 1.2 illustrates the number of unique compositions and sequences for libraries made with different well plate sizes and number of split-pool steps.

We can see from Tables 1.1 and 1.2 that for small libraries (384 beads), there are as many unique sequences as there are wells (or beads) in the array, but there is some redundancy of compositions. The simulation procedure accounts for moving members along a row/column of a given wellplate to a row/column of another wellplate. This process can thus reduce or eliminate the need for physical tagging. The number of physical manipulations (bead transfer and solution adsorption) for a n component m step directed sorting library was $m(n^2+1)+3n$ or on the order of mn^2 , where n is the number of components and m , the number of split-pool steps (Appendix 2).

Synthesis of noble metal libraries using metal salt solutions and DIRECTSORT

We found that slurry impregnation in aqueous solution of metal salts (containing 2 wt% HCl on 1 bead basis), without thermal treatment, led to desorption of metals and dissolution of alumina when the beads adsorbed metal salts in glass vials. Switching to ethanol as the solvent solved the desorption problem but led to non-homogeneous impregnation of metal on the beads. Switching ligands from chloride to acetylacetonate did not solve the homogeneity problem. We then experimented with using adsorption under incipient wetness conditions (3 μ l) and slurry conditions (6 and 12 μ l) in well plates.

Metal salts were dissolved in 0.5M HCl to a final concentration of 0.09 g/ml. The Vaccupette multi-pipette was modified with small pipet tips (Figure 1.2c) to reproducibly deliver small solution volumes (0-50 μ l) by calibrating the syringe that delivered the solution and visual examination of pipet tips. In each adsorption step, beads were equilibrated in each well plate with 12 μ l of solution such that metal loading was 0.05wt%

in each step. A qualitative check after addition of solution was done by noting the difference in total weight of the plates before and after adsorption. This value was close to 1.15g ($96 \text{ wells} * 12 \mu\text{l/well} * 1 \text{g/ml} * 10^{-3} \mu\text{l/ml}$). Adsorption under these conditions is close to incipient wetness. Adsorption was done at room temperature for 30 minutes followed by a drying step at 60°C for 1 h. The beads were cooled to room temperature, removed along a given row or column (pool) and distributed equally 4 receiving wellplates (split). Fresh solution was prepared prior to every adsorption step and stored in the dark until they were used. The steps were repeated until the desired loading was achieved.

Using ICPMS standards for error analysis and column shuffle

Although the row/column shuffle algorithm and the synthesis of libraries were easy to implement experimentally, the battery of analytical techniques examined (Electron probe Microanalysis and Inductively Coupled Plasma Mass Spectrometry at PSU and μ -XRF at UOP) for a four metal library (H_2PtCl_6 , $\text{SnCl}_2 \cdot 2\text{H}_2\text{O}$, $\text{CuCl}_2 \cdot 2\text{H}_2\text{O}$ and $\text{NiCl}_2 \cdot 6\text{H}_2\text{O}$), did not provide absolute quantification with the designed compositions. We postulated that there could be six reasons for this discrepancy

- 1) Interference from the Rhodium x-ray source at the μ -XRF prevented quantification of Tin and might have contributed to some of the discrepancies in these plots. Based on a synthesis error of 3% (estimated by description below) and an analysis error of 10%, the μ -XRF data indicated that the trends are appropriate for elements other than tin; only for 30% of the samples.
- 2) Adsorption of metals and its analysis was composition dependent. This hypothesis was only supported for a few random compositions and was tough to quantify as the reason for the observed discrepancy.
- 3) Pipetting error for home made Vaccupettes
- 4) Contamination from well plates
- 5) Contamination from pipet tips
- 6) Diameter and weight of each bead

Variation in pipetting and error analysis

To check for errors in synthesis across 96 wells, 12 μ l of 1×10^{-9} M fluorescein-5-isothiocyanate (FITC) dye was added to each well. The standard deviation in fluorescence intensity across the wells measured with an HTS 7000 Plus Bio Assay Reader using a Vaccupette or manual pipetting was 10% and of the blank wellplates was 5%. To reduce the magnitude of this error, absorbance experiments in the same plate reader were carried out using micromolar concentrations of the three dyes (Cascade Blue, Sulforhodamine 101 and Lucifer Yellow) used in our previous experiments [10]. The 96-well V-bottom plates used in the metal and food coloring experiments gave an analytical error of 15% for known concentration of dyes in each well plate due to the conical shape of the wells in the direction of the light path. To overcome the above problems, analytical measurements checking for pipetting errors were carried out in 96 well flat plates, by manually pipetting 40 μ l in each well (forming a 1 mm path length, the minimum possible to get uniform coverage of each well by the dye). The absorbance error reduced to 0.1% for single dyes and 3% for mixtures.

Variation in bead diameter

To account for variation in nominal diameter (0.065 inch) of the γ -alumina beads, approximately 18000 beads were analyzed by optical microscopy at UOP. The standard deviation of beads with nominal diameter 0.065 inch was 0.005, with a relative standard error of 7.7%.

Variation in bead weight

To account for variation in bead weight, 388 beads were analyzed by a Sartorius Balance, accurate to four digits at Penn State. The standard deviation of beads with average weight 2.5 mg was 10.5 with relative error of 406%. Figure 1.5 shows the measured bead weight (mg) versus number of beads.

Synthesis and analysis of libraries by row-column and column only shuffle algorithms and μ -XRF analysis

For proof-of-concept metal libraries, a 4 component (Pt, Sn, Cu and Ni), 4 step (5 adsorptions and 4 transfers), 96 wellplate library was synthesized according to the row/column directed sorting algorithm. γ -alumina beads in these experiments were sorted by a commercial roller grader and total metal content after four split pool cycles (5 adsorption steps) was 0.25wt% metal. The choice of metals was based on previous work on the methylcyclohexane (MCH) dehydrogenation reaction by Haensel *et al.*, and Sinfelt *et al.* [19].

To validate the μ -XRF technique, we synthesized samples with Pt, Cu and Ni on γ -alumina and checked the same by ICPAES and μ -XRF and found large analytical errors. Tables 1.4a and b shows the relative errors in ICPAES and μ -XRF for nine samples chosen as standards. The relative errors in μ -XRF, defined as the ratio of standard deviation to average of difference in theoretical amounts and measured μ -XRF values, were 36.6% in Pt, 47.2% in Ni and 20% in Cu for 0.05wt% theoretical metal content on γ -alumina. The relative errors increased to 86.6% in Pt and decreased to 21.7% in Ni for 0.1wt% theoretical metal content on γ -alumina and were 89.2% in Ni and 69.9% in Cu for 0.2wt% theoretical metal content on γ -alumina. We found that five to seven samples were required to reduce error due to μ -XRF (Tables 1.4a and 1.4b). We conclude that bead weight was the controlling factor for the deviation in μ -XRF based on relative errors due to bead diameter (7.7%), bead weight (406%) and pipetting (3%).

The second approach (column only sort) using pen-and-paper was developed to answer a different question. We asked the reverse question of the earlier approach i.e., what are the minimum number of physical manipulations for reasonably diverse libraries and what sub-matrix method would achieve the objective. We were motivated to ask this question based on analytical data for metal loaded beads synthesized using row/column sorting. We chose shuffling columns alone for simplicity, four adsorptions and three metals for this purpose and indexed beads in wellplates as members of a matrix as in the row/column sorting algorithm. The column shuffle algorithm resulted in 3mn compositions and sequences using 4mn steps. The total number of steps can be reduced by a factor of 2, if we use suitably designed masks. The algorithm also has a redundancy of 8 i.e., each row based on the minimum required to lower errors by μ -XRF based on

analytical results by row/column sorting. The shuffle algorithm resulted in 36 compositions and used 48 physical manipulations for a library of 288 beads. The algorithm addressed four adsorptions of each element, 9 binary combinations (with two unique order of additions each) and 3 ternary combinations with one of three components twice (with five unique order of additions each) as shown in Table 1.5. We synthesized all combinations of binary and ternary combinations of elements by manual pipetting. The total number of physical manipulations was 332, four times the number of pipetting steps as beads (82) and four plate transfers, shown in Table 1.6.

To remove discrepancies due to interference from tin and to check for analytical errors upto 1wt%, we synthesized libraries with Pt, Cu and Ni using ICPMS standards of the three metals in a solution of 2% HCl (Hi-Purity Standards) using the column shuffle algorithm. We postulated using pre-analyzed standards would help in resolving analytical errors and help in determining discrepancies due to μ -XRF. Two libraries were synthesized, one using the Vaccupette (Table 1.5 and Tables 1.9 through 1.11) and another by manual pipetting (Table 1.6) using fresh wellplates sealed in plastic prior use. We postulated that this would help estimate the errors in synthesis through analysis of directed sorting combinatorial libraries prepared by manual pipetting and the Vaccupette.

Table 1.5 summarizes order of addition using column shuffle. The shuffle algorithm resulted in 36 compositions and used 48 physical manipulations for a library of 288 beads. The algorithm addressed four adsorptions of each element, 9 binary combinations (with a redundancy of 2) and 3 unique ternary combinations (with a redundancy of 5 each). In a typical procedure, γ -alumina beads were washed in DI water at room temperature. The beads were then calcined at 400 °C for 3 hours and cooled down to room temperature. The beads were suction transferred from a Petri dish and dropped onto a 96 well plate such that each well contained one bead. Metal salt solutions (containing 1 μ g/ μ l Pt, Cu and Ni in HCl from High-Purity standards) were adsorbed onto the beads. The Vaccupette multi-pipette was modified with small pipet tips to reproducibly deliver small solution volumes (0-50 μ l). In each adsorption step, beads were equilibrated in each well plate with 6 μ l of solution such that metal loading was 0.25 wt% in each step. Adsorption was done at room temperature for 30 minutes followed by a drying step at

60°C for 1 h. The beads were cooled to room temperature, removed along a given row or column (pool) and distributed equally over 4 receiving well plates (split). Fresh solution was prepared prior to every adsorption step and stored in the dark until they were used. The steps were repeated until the desired loading was achieved (1 wt%).

The results of predicted versus measured compositions by element and by order of addition using μ -XRF are part of Tables 1.9 through 1.11. The relative errors in μ -XRF, defined as the ratio of standard deviation to average of difference in theoretical amounts and measured μ -XRF values were 39.2% in Pt, 34.9% in Ni and 42.6% Cu for 1wt% theoretical metal content on γ -alumina as shown in tables 1.4, 1.9, 1.10 and 1.11. We conclude that bead weight was the controlling factor for the deviation in μ -XRF based on relative errors due to bead diameter (7.7%), bead weight (406%) and pipetting (3%). We found that analysis by μ -XRF was inconsistent and independent of order of addition of elements and differed from theoretical concentrations in a non-predictive way. We concluded based on the current data (Tables 1.4, 1.8-1.11) that μ -XRF is not a useful analytical tool in evaluating directed sorting metal adsorption by incipient wetness on porous γ -alumina. We speculate that the reason for inconsistent and large errors in the μ -XRF is the sampling depth (200 μ m), representing 13% of bead diameter and large variation in bead weight (406%). Future experiments reducing the variation in bead weight should address this important issue. Analytical errors estimate by μ -XRF for manual pipetting were consistently large (50% and more) and these were not evaluated for catalytic activity.

EPMA analysis of libraries by row/column shuffle

A few random samples were analyzed for tin content using Electron Probe Microanalysis (EPMA). Figures 1.6a -c show elemental profiles as a function of distance along each bead using EPMA, indicating that the metals are distributed throughout each bead with variation as a function of distance. We also observed that the signal from the EPMA saturated at 0.2wt% metal.

ICPMS analysis of metal loaded beads made by the column shuffle algorithm

The objective of these experiments was to test whether using the column shuffle algorithm adsorbed the desired quantities of metal on each bead, independent of variations in bead diameter (406%) and bead weight. To compensate for matrix and order of addition effects on the analysis, we synthesized mixed solutions of Cu, Co and Ni from ICPMS standards of the three metals in 10% HCl (Hi-Purity Standards) by the column shuffle algorithm and described in Table 1.5. We then made a bead library by the same algorithm using 10 μg of metal from ICPMS standards per adsorption step and four steps resulting in a total metal content of 1.7wt% after four adsorptions. One library was synthesized using the Vaccupette in fresh wellplates that were sealed in plastic prior use. The internal measurement errors due to the instrument, confirmed using Cu and Ni spikes in pre-analyzed standards were $\pm 8\%$ in samples containing Cu and Ni alone and 15% in combinations of samples containing Cu and Ni and no Co. Pipetting had errors of $\pm 5\%$ for all samples and drifts in plasma resulted in errors of $\pm 6\%$. The internal measurement errors due to the instrument, confirmed for Co in pre-analyzed standards were $\pm 22\%$ in the presence of at least two additions each of Ni or Cu and one addition of Co; 15% for two or three additions of Co and combinations of Cu and Ni and 10% for samples containing Co alone. We speculated that Co formed cobalt phosphate and experimented with addition of spikes of Ni and Cu i.e., adding more labile metals, but were unsuccessful in reducing the magnitude of this analytical error. We also observed that presence of Co led to large analytical errors in the instrument. Assuming that errors due to pipetting, drifts in plasma and metal analyses do not cancel each other and can be modeled based on the pythagoras theorem for propagation of errors, we estimated root mean square errors for samples containing Co and no other metal in the samples ($\pm 12.7\%$), Ni and no other metal in the samples ($\pm 11.2\%$), Cu and no other metal in the samples ($\pm 12.7\%$), combinations of Cu and/or Ni with no cobalt ($\pm 16.9\%$) in the samples, combinations of Cu and/or Ni with one addition of Co ($\pm 23.3\%$) in the samples and combinations of Cu and/or Ni with two or three additions of Co with errors of ($\pm 30\%$) in the samples.

We examined 22 out of 36 compositions in Table 1.5; one sample each of four adsorptions of each element (1111, 2222 and 3333), one sample each of the 9 binary combinations (2221, 2211, 2111, 3111, 1133, 1333, 2333, 3322, 3222) and 14 samples

from ternary combinations (1321, 3211 and 2113; 2213, 2132, 3221 and 2321; 3321, 3132, and 3213). The fourteen samples of ternary combinations also served to test order of addition trends in ICPMS analysis. We also examined nine duplicates (2221, 2111, 2213, 2132, 2321, 3121, 3111, 1333 and 1223) with and without Nickel spikes. The results of predicted versus ICPMS analysis are part of Table 1.7. Although the agreement is not absolute, these results from table 1.7 confirm the sorting algorithm at the single bead level using ICPMS. ICPMS was the only analytical technique capable of characterizing direct sort samples at a single bead level at weight percent below SEM detection limits (0.5 wt% for mixture of metals).

Tests for catalytic activity using LAMIMS

We evaluated three well plates (a total of 288 beads) synthesized by the column shuffle algorithm for catalytic activity using dehydrogenation of methylcyclohexane (MCH) as a probe reaction. The beads were evaluated in a LAMIMS reactor described in detail in [20]. In a typical LAMIMS experiment, 96 metal loaded beads were placed in a LAMIMS reactor. The metal loaded beads were reduced under hydrogen by passing a 25Watt laser at 25% of peak power over each bead for six minutes. The gas flow was switched to a mixture of methylcyclohexane (MCH) and hydrogen and the reduced beads were serially heated and product (toluene) detected using a quadrupole mass spectrometer at a mass to charge ratio of 91 for toluene [20, 29]. At a mass to charge ratio of 91, the mass spectrometer only detects fragments of toluene [29]. To quantify the mass spectrometer signal, a 1 wt% Pt on γ -alumina catalyst with a metal dispersion of 75% [20a] served as an internal standard in each run and subjected to the same conditions (reduction and analysis for activity) as the directed sorting synthesized samples. We did an energy balance to verify that the laser sufficiently heats up the samples during reduction and reaction (described below).

Reduction of metal loaded alumina

We did an energy balance to verify that the laser sufficiently reduces the samples. The main assumption in this part of the analysis is that the energy from the laser is used to heat the gas surrounding the bead, the alumina bead and the metal supported on alumina.

Heat in = laser power at full capacity * % of total laser power * activation time

$$= 25\text{W} * (25/100)*360\text{s}$$

$$= 6.25\text{J/s} * 360\text{s} = 2250\text{J}$$

Thermal energy needed to heat H₂

$$= \text{Molar flow rate (in mol/s)} * \text{Specific heat at constant pressure (J mol}^{-1} \text{ K}^{-1}) * \text{Temperature difference (K) assuming a 220 K rise}$$

$$= 6.25 * 10^{-4} * 29 * 220$$

$$= 3.98 \text{ J/s}$$

Thermal energy needed to heat alumina

$$= \text{thermal conductivity of alumina (W m}^{-1} \text{ K}^{-1}) * \text{Temperature difference (K)} * \text{characteristic length (Volume/Area in m)}$$

$$= 2 * 220 * 0.1066 * 10^{-2}$$

$$= 0.47 \text{ J/s}$$

Assuming steady state,

$$\text{Heat In} = 2250\text{J}$$

$$\text{Heat required} = (3.98 + 0.47) * 360 = 1602 \text{ J}$$

We see that we have 648J excess heat, assuming steady state and steady laser power.

Ratio of Molecules/Sites

To call a solid a catalyst, the ratio of number of reactant molecules to sites should be large. This follows from the definition of closed cycles [28].



where,

S is a site on a catalyst surface

R is reactant

P is product

We can get a ratio of molecules/sites using the formula below

Molecules = Flow rate (mol/s) * time(s) * Avogadro's number

Sites = Metal surface area (m²/g) * weight metal /bead (g) * (1.5 * 10¹⁹) sites / m²

Using,

$$\text{Pt surface area of } 276 \text{ m}^2_{\text{Pt/g Pt}} [19] = (6.023 * 10^{23}) / (195.09 * 10^4 * 1.1 * 10^{15})$$

$$1 \text{ wt\% Pt on alumina } (2.3 \text{ mg bead} * 0.01 \text{ g Pt/g bead} * 10^{-3} \text{ g bead/ mg bead}) = 23 * 10^{-6} \text{ g Pt/bead}$$

$$\text{Flow rate of MCH } 0.26 * 10^{-5} \text{ mol/s (0.02 ml/min)}$$

Total time of 40s

$$\begin{aligned} \text{Ratio of molecules/sites} &= (0.26 * 10^{-5} * 40 * 6.023 * 10^{23}) / (276 * 23 * 10^{-6} * 1.5 * 10^{19}) \\ &= 657 \text{ on a 1 bead basis.} \end{aligned}$$

This tells us that sites are rate limiting and we are in a position to measure catalysts. A good rule of thumb is to have at least a 100-fold excess of molecules to sites to account for effects like bypass of catalyst sites.

Energy Balance

We did an energy balance to verify that the laser sufficiently heats up the samples. The main assumption in this part of the analysis is that the energy from the laser is used to heat the gas surrounding the bead, the metal supported on alumina and provide necessary energy for the endothermic reaction (MCH to toluene) and for Toluene to desorb.

$$\begin{aligned} \text{Heat in} &= \text{laser power at full capacity} * \% \text{ of total laser power} * \text{activation time} \\ &= 25\text{W} * (55/100) * 40\text{s} \\ &= 13.75\text{J/s} * 40\text{s} = 550\text{J} \end{aligned}$$

Thermal energy needed to heat H₂ and MCH

$$\begin{aligned} &= \text{Sum of [(molar flow rate in mol/s) * Specific heat at constant pressure (J mol}^{-1} \text{ K}^{-1}) * \\ &\text{Temperature difference (K)] for each species} \\ &= 6.25 * 10^{-4} * 29 * 220 \text{ (H}_2\text{)} + 0.26 * 10^{-5} * 229 * 220 \text{ (MCH)} \\ &= 4.118 \text{ J/s} \end{aligned}$$

Heat consumed by reaction

$$\begin{aligned}
 &= \text{Molar flow rate of MCH (mol/s)} * \text{Heat of reaction (J/mol)} \\
 &= 0.26 * 10^{-5} \text{ mol/s} * 205 * 10^3 \text{ J/mol} \\
 &= 0.533 \text{ J/s}
 \end{aligned}$$

Thermal energy needed to heat alumina

$$\begin{aligned}
 &= \text{thermal conductivity of alumina (W m}^{-1} \text{ K}^{-1}) * \text{Temperature difference (K)} * \\
 &\text{characteristic length (Volume/Area) in m} \\
 &= 2 * 220 * 0.1066 * 10^{-2} \\
 &= 0.47 \text{ J/s}
 \end{aligned}$$

Thermal energy needed to desorb Toluene

$$\begin{aligned}
 &= \text{Conversion} * \text{Molar flow rate of MCH} * \text{Energy for Desorption [19]} \\
 &= 0.1 * 0.26 * 10^{-5} \text{ mol/s} * 126 * 10^3 \text{ J/mol} \\
 &= 0.0312 \text{ J/s}
 \end{aligned}$$

Assuming steady state,

$$\text{Heat In} = 13.75 \text{ J/s}$$

$$\begin{aligned}
 \text{Heat required} &= 4.118 + 0.553 + 0.47 + 0.0312 \text{ J/s} \\
 &= 5.172 \text{ J/s}
 \end{aligned}$$

We see that we have 8.58 J/s excess heat, assuming steady state and steady laser power.

We then ask what happens if we lower laser power. Obviously, inlet heat decreases and part of that heat is transferred to reaction, heat dissipation and desorption. Conversion also decreases at lower temperatures. This means the signal in the LAMIMS Mass Spec should drop. We have seen this effect qualitatively in the LAMIMS (lower signal at low temperatures) at lower laser power (not shown in current chapter). All the above analysis should be treated with caution since time needed for steady state conditions is greater than 1000s (using $t = \text{radius of bead}^2 / (2D_{\text{eff}})$) and D_{eff} of $10^{-7} \text{ cm}^2/\text{s}$ following Weisz [27] i.e., we are operating far from steady-state, probably in a transient mode.

Three lots of 96 beads (total of 288 beads) were tested in a LAMIMS reactor for the methylcyclohexane dehydrogenation reaction. We examined eight replicates of 36

compositions including pure metals (Pt, Cu and Ni with 1wt% on γ -alumina), 9 binary combinations (with a redundancy of 2) and 3 unique ternary combinations (with a redundancy of 5 each). The LAMIMS area and peak height of the directed sorting samples were normalized to the 1 wt% Pt on γ -alumina catalyst, described above.

Details of the μ -XRF and LAMIMS analysis of all 288 beads are part of Tables 1.9 through 1.11. We found that not all samples gave a detectable LAMIMS signal. The standard deviation in normalized LAMIMS analysis (area and peak height) was consistent between 0 and 0.1. To simplify the analysis, we only chose to examine compositions that had a detectable LAMIMS signal, (reducing the number of examined compositions to 23). We also chose average LAMIMS peak height and area of 0.2 as lower bound based on standard deviation in normalized LAMIMS peak height and area, reducing the number of compositions to 16 i.e., seven of 23 that had detectable LAMIMS signals had a LAMIMS peak height and area lower than 0.2 (usually on the order of 0.05) with a relative standard deviation of 50%. Table 1.8 shows average, standard deviation and relative standard deviation of LAMIMS peak height and area and μ -XRF analysis of 16 selected samples.

We found that all eight Pt on alumina samples synthesized by the column shuffle algorithm compared well to 1wt% Pt on γ -alumina described above. The relative errors in the normalized LAMIMS peak and area were 9.6% and 10.6% respectively indicating that the errors in the LAMIMS technique were lower than the μ -XRF (39.2%) for Pt on γ -alumina. We also found that the LAMIMS technique using MCH dehydrogenation to toluene as a probe was not sensitive to relative error in bead weight (406%), but possibly reflected relative errors in bead diameter (7.7%) and errors due to ICPAES analysis of 1 wt% Pt from table 1.2 (4%). We also concluded earlier that errors due to ICPAES analysis of 1 wt% Pt from table 1.2 (4%) was mainly due to pipetting (3%). We estimated a molecule/site ratio of 657 on a one bead basis, using theoretical Pt surface area of 276 m^2/g [19] and concluded that sites were limiting under the conditions of the experiment. Our objective was to evaluate the bead-based libraries for catalytic activity, followed by detailed microanalysis. We then examined the normalized LAMIMS area as a function of

order of addition. Figures 1.7a-c shows the average normalized LAMIMS area as a function of Pt content and Pt as the last adsorption step (1.7a) and Ni content and last adsorption step (1.7b and 1.7c). The error bars in Figures 1.7a-c represent the standard deviation in average LAMIMS area. We found only one composition with Cu as the last adsorption step (PtPtPtCu) had average LAMIMS peak height and area greater than 0.2 and we included this composition as part of Figure 1.7a.

Based on average normalized LAMIMS area and relative standard deviation in normalized LAMIMS area and data from Table 1.8 and Figures 1.7a-c, we ranked the 16 selected samples for MCH dehydrogenation (assuming normalized LAMIMS area measured activity for MCH turnover) as PtPtPtPt > CuPtPtPt > (NiCuNiNi=CuPtCuNi=PtCuNiNi) > (PtPtCuNi=PtNiNiNi) > NiCuCuNi > (CuCuCuNi=NiNiNiNi=NiPtCuNi) > (CuCuNiNi = PtCuCuNi) > (PtPtPtCu = NiNiPtPt) > CuNiNiNi.

Overall, the most surprising trend was the variation in activity for the same nominal composition on the order of addition in almost all samples that showed some level of activity for MCH turnover, defined as average LAMIMS peak height and area of 0.2 as lower bound. We observed from Figure 1.7a that the activity of Pt_{0.75}Cu_{0.25} (subscripts in total metal weight %) varied depending on order of addition of Pt or Cu to the alumina beads. When Cu was adsorbed from ICPMS standard solutions first, followed by three adsorptions of Pt, the average LAMIMS area was 47% of pure Pt. When adsorption of copper followed three additions of Pt, the average LAMIMS area halved. We observed from Figure 1.7b that the activity of Ni_{0.75}Cu_{0.25} (subscripts in total metal weight %) varied depending on order of addition of Ni or Cu to the alumina beads. When Cu was adsorbed from ICPMS standard solutions preceded by one adsorption of Ni followed by two adsorptions of Ni the average LAMIMS area was 44% of pure Pt, but when adsorption of copper preceded three additions of Ni, the average LAMIMS area halved. Order of addition trends were seen with a few combinations of Pt, Cu and Ni consistently, in a non-predictive fashion as shown in Figure 1.7c.

The order of addition information could provide a very valuable tool in evaluating and/or optimizing catalysts of the same nominal composition. We believe that this could be the most powerful use of the current method. This study also evaluated catalytic activity as a function of precise amounts of energy (laser power) and should be useful in evaluating activity of catalyst, should availability of energy be an optimization parameter. As expected, we were unsuccessful in finding a combination of elements on alumina that matched the activity of Pt for the MCH dehydrogenation reaction in this model system. In actual combinatorial catalyst development, the next step would be to choose interesting compositions (based on average LAMIMS peak height and area comparable to a reference catalyst), and evaluate the same in micro-reactors.

Using direct sorted LAMIMS libraries in catalyst discovery

The experiments in this chapter have quantified errors in synthesis and analysis of combinatorial libraries and the subsequent evaluation in a LAMIMS reactor. This study also showed that very little sample (2mg) is required in analyzing catalytic activity of samples that demonstrated minimal (about 20% of that of Pt on alumina) to high conversion (Pt on alumina at 100%) and therefore provides an alternative to screening using microreactors [18], for reactors that employ catalysts in the form of beads. Gembicki et al. [21] argue that catalysts and reactors have evolved over the years to operate in a transient mode. The LAMIMS reactor inherently couples separation and reaction and can be adapted to run as a multifunctional transient reactor. We speculate that tools such as LAMIMS used in evaluation of combinatorial libraries will open up new applications and reactor designs.

Conclusions

The work described above demonstrates a bench-top route to prepare large bead libraries that do not require tagging or post-synthesis analysis. The main advantages of the method are its simplicity, ease of preparation and low cost. In principle, use of a multi-pipettor and corresponding analysis eliminates the need for commercial plotters routinely used in combinatorial chemistry, resulting in large cost savings. We concluded that variation in bead weights account for large analytical errors by μ -XRF in preparation through

analysis of direct sorted bead based combinatorial libraries. Future experiments designed to check this with more uniform bead weights may help resolve this issue. ICPMS was the only analytical technique we used that was capable of analyzing mixtures of elements at the single bead level. The directed sorting technique described in this chapter also highlights the importance of order of addition in experiments seeking to optimize catalytic activity or other catalytic figures of merit. Difficulties with the analytical techniques and bead weight variation can partly be offset with the use of a chemical probe of bead activity, such as methylcyclohexane, using the LAMIMS reactor configuration [20, 22].

References

1. Mittasch, A., *Advances in Catalysis*, Academic Press Inc., New York, NY, **1950**, 2, 81-101.
2. Hanak, J.J., *J.Mater.Sci.* **1970**, 5, 964.
3. (a) Xiang X.-D., Sun, X., Briceno, G., Lou Y., Wang, K.-A., Chang, H., Wallace-Friedman, W. G., Chen S. and Schultz, P. G., *Science*, **1995**, 268, 1738. (b) Briceno, G., Chang, H., Sun, X., P., Schultz, P. G. and Xiang X.-D., *Science*, **1995**, 270, 273.
4. (a) Moates, F.C., Somani, M., Annamalai, J., Richardson, J. T., Luss, D., Willson, R. C., *IECR*, **35**, 4801 (1996); (b) Senkan, S., *Angew. Chem. Int. Ed.* **2001**, 40, 312; (c) Jandeleit, B.; Schaefer, D. J.; Powers, T. S.; Turner, H. W. and Weinberg, W. H., *Angew. Chem. Int. Ed.* **1999**, 38, 2494.
5. (a) Reddington, E.; Sapienza, A.; Gurau, B.; Viswanathan, R.; Sarangapani, S.; Smotkin, E. S.; Mallouk, T. E. *Science* **1998**, 280, 1735. (b) Chen, G.; Delafuente, D. A.; Sarangapani, S.; Mallouk, T. E. *Catal. Today* **2001**, 2443, 1.
6. (a) Danielson, E.; Golden, J. H.; McFarland, E. W.; Reaves, C. M.; Weinberg, W. H.; Wu, X. D. *Nature* **1997**, 389, 944; (b) Danielson, E.; Devenney, M.; Giaquinta, D. M.; Golden, J. H.; Haushalter, R. C.; McFarland, E. W.; Poojary, D. M.; Reaves, C. M.; Weinberg, W. H.; Wu, X. D. *Science* **1998**, 279, 837.
7. Van Dover, R. B., Schneemeyer, L. F. and Fleming, R. M., *Nature*, **1998**, 392, 162.
8. (a) M. Lebl, *J. Comb. Chem.*, **1999**, 1, 3; (b) Lam, K. S.; Lebl, M.; Krchák, V. *Chem. Rev.* **1997**, 97, 411.
9. (a) Lam, K. S.; Salmon, S. E.; Hersh, E. M.; Hruby, V. J.; Kazmierski, W. M.; Knapp, R. J., *Nature* **1991**, 354, 82; (b) Houghten, R. A.; Pinilla, C.; Blondelle, S.

- E.; Appel, J. R.; Dooley, C. T. and Cuervo, J. H., *Nature* **1991**, 354, 84.;c) Kozmin, S. A., Wang, Y., *Angew. Chem. Intl. Ed.*, **2003**, 42, 903
10. Sun, Y., Chan, B. C., Ramnarayanan, R., Leventry, W. M., Bare, S. R., Willis, R. R., and Mallouk, T. E., *J. Comb. Chem.*, **2002**, 4 (6), 569
 11. a) *Applied Catalysis A: General*, **2003**, 254(1), 1-170, focuses on applying combinatorial techniques to heterogeneous catalysis; b) *Macromolecular Rapid Communications*, **2004**, 25(1), 1-386, focuses on applying tools and instruments used in combinatorial techniques and describes applications of the combinatorial technique to problems in polymers and other materials (semiconductors, catalysts).; c) *Measurement Science and Technology*, **2005**, 16(1), 1-316 is devoted to various aspects of combinatorial methods.
 12. Miller, C. T., Mann, G., Havrilla, G. J., Wells, C. A., Warner, B. P., and Baker, R. T., *J. Comb. Chem.*, **2003**, 5 (3), 245.
 13. "Experimental Design for Combinatorial and High Throughput Materials Development", edited by Cawse J. N., John Wiley and Sons, NJ, **2003**
 14. Klein, J., Zech, T., Newsam J. M. and Schunk, S. A., *Appl. Catal. A: General*, **2003**, 254 (1), 121.
 15. a) "Statistical Methods, Experimental Design and Scientific Inference", Fisher R. A., Oxford University Press, Oxford, **1990**. b) "Experimental Design", selected papers of Frank Yates, Hafner Publishing Company, Connecticut, **1970**.
 16. "Computability and complexity theory," Steven Homer and Alan L. Selman, Springer, NY, **2001**.
 17. "Combinatorial Chemistry: A Practical Approach," edited by Fenniri, H., Oxford University Press, Oxford, UK, **2000**.
 18. Baertsch, C. D., Schmidt, M. A. and Jensen K. F, *Chem. Comm.*, **2004**, 22, 2610.
 19. a) Haensel, V. and Donaldson, G. R., *IECR*, **1951**, 43, 2102; b) Sinfelt, J. H., Hurwitz, H, Schulman, R. A., *J. Phys. Chem*, **1960**, 64, 1559.; c) Sinfelt, J. H., *J. Mol. Catal. A: Chemical*, **2000**, 163, 123 (2000).; d) Reyes, S. C., Sinfelt, J. H., DeMartin, G. J., *J. Phys. Chem. B*, **2005**, 109, 2421.
 20. a) Nayar, A.; Kim, Y. T.; Rodriguez, J.; Willis, R. R.; Galloway, D. B.; Falaah, H. F.; Smotkin, E. S., *Applied Surface Science*, **2004**, 223(1-3), 118.; b) Nayar, A.; Liu, R.; Allen, R. J.; McCall, M. J.; Willis, R. R.; Smotkin, E. S., *Anal. Chem.*, **2002**, 74(9), 1933.; c) Nayar, A., Liu R., Willis, R. R., Smotkin, E.S., *US Patent Application, Publication*, 2004/0077096, April 22, **2004**.; d) Nayar, A., Liu R., Willis, R. R., Smotkin, E.S., *US Patent* 6923939, **2005**.
 21. Gembicki, S.A., Vanden Bussche, K.M., and Oroskar, R. A., *Chem. Engg. Sci.*, **2003**, 58, 549.

22. a) Swenson, L. R.; Brandvold, T. A.; McCall, M. J.; Vanden Bussche, K. M.; Willis, R. R., *PCT Int. Appl.*, **2002**, WO 2002088675; b) Swenson, L. R.; Brandvold, T. A.; McCall, M. J.; Willis, R. R., *PCT Int. Appl.*, **2002**, WO 2002088674
23. a) Mitsche, R. T., U.S., **1976**, US 3943070 19760309; b) Steenberg, L. R.; Vesely, K. D., Ger. Offen., **1972**, DE 2048434 19720406.
24. Ramnarayanan R., Chan B.C., Salvitti M.A., Mallouk T. E., Falih F. M., Galloway D. B., Bare S. R., and R. R. Willis, "Directed sorting method for synthesis of supported metal catalysts for methylcyclohexane dehydrogenation", accepted in Preprints of Symposia - American Chemical Society, Division of Petroleum Chemistry, **2005**.
25. Mallouk, T. E.; Ramnarayanan, R.; Willis, R. R.; Gillespie, R. D., *Patent Int. Appl.*, **2004**, WO 2004102197.
26. Chan B.C., PhD Thesis, The Pennsylvania State University, 2003.
27. a) Weisz P. B., Prater C. D., Rittenhouse K. D., *J. Chem. Phys.*, **1953**, *21*, 2236; b) Weisz P. B.; Prater C. D.; Rittenhouse K. D., *J. Chem. Phys.*, **1955**, *23*, 1965; c) Weisz P. B., *Z. Phys Chem*, **1957**, *11*, 1;d) Weisz P. B., *Science*, **1973**, *179(4072)*, 433.
28. a) Madon R. J. and Boudart M, *I&EC Fundamentals*, **1982**, *21*, 438; b) Boudart M and Djega-Mariadassou, "Kinetics of heterogeneous catalytic reactions," Princeton University Press (**1984**).; c) Boudart M, *J. Mol. Catal. A: Chemical*, **1999**, *141*, 1.
29. NIST Mass Spec Data Center, S.E. Stein, director, "Mass Spectra" in "NIST Chemistry WebBook, NIST Standard Reference Database Number 69", Eds. P.J. Linstrom and W.G. Mallard, **June 2005**, National Institute of Standards and Technology, Gaithersburg MD, 20899 (online at <http://webbook.nist.gov>).

Table 1.1 Results from Row-column directed sorting simulations for four component four step 96-well plate

Row-column directed sorting using four components in four 96-well plates. The results shown are for one of four well plates for four directed sorting cycles. Each well or bead is identified with a 5-digit adsorption sequence. For example, the first entry on row three (44411) signifies a bead history of three adsorptions of component 4, followed by two adsorptions of component 1 and indicates order of addition. The four-digit composition below this sequence (3002) indicates that the bead contains three parts component 4, and

two parts component 1. Note that the last adsorption step (the last digit in the 4-digit sequence) is the same for all beads in a given well plate. Note also that all compositions sum to 5, which is the number of adsorption steps in 4 split-pool cycles.

The algorithm generated all four components twice (0005, 0050, 0500 and 5000), 20 binaries with varied redundancy [0041, 0410, 1004 and 4100 (once), 0014, 1400, 0140 and 4001 (thrice), 3002 (six times), 0032, 0320, 2003 and 3200 (five times), 0023, 0230, 0203, 0302, 3020, 2030 and 2300 (six times)], 24 ternaries with varied redundancy [0311, 3110, 1103 and 1031 (two times), 1013, 0131, 1310 and 3101 (three times), 0113, 1301, 3011 and 1130 (four times), 1022 and 2210 (ten times), 0122, 2012, 1220 and 2201 (thirteen times), 0221 (eleven times), 2102 (twelve times), 0212, 1202, 2021 and 2120 (fourteen times)] and four quarternaries twenty seven times each (2111, 1211, 1112 and 1121). The missing binaries were 0104, 0401, 4010 and 1040.

STEPS	NCOMP	ROWS	COLS	PLATE			
4	4	12	8	96			
TOTAL NUMBER OF WELLS							
384							
NUMBER OF UNIQUE COMPOSITIONS							
52							
NUMBER OF POSSIBLE COMPOSITIONS							
56							
NUMBER OF UNIQUE SEQUENCES							
256							
11111	44441	33441	22331	11331	44221	33221	22111
0005	4001	2201	0221	0203	2021	0221	0023
11111	44441	33441	22331	11331	44221	33221	22111
0005	4001	2201	0221	0203	2021	0221	0023
44411	33341	22341	11231	44231	33121	22121	11411
3002	1301	1121	0113	2111	0212	0032	1004
34411	23341	12341	41231	34231	23121	12121	41411
2102	1211	1112	1112	1211	0122	0023	2003
34411	23341	12341	41231	34231	23121	12121	41411
2102	1211	1112	1112	1211	0122	0023	2003
23311	12241	41241	34131	23131	12421	41421	34311
0212	1022	2012	1202	0212	1022	2012	1202
13311	42241	31241	24131	13131	42421	31421	24311
0203	2021	1112	1112	0203	2021	1112	1112

13311	42241	31241	24131	13131	42421	31421	24311
0203	2021	1112	1112	0203	2021	1112	1112
42211	31141	24141	13431	42431	31321	24321	13211
1022	1103	2012	1202	2111	0212	1121	0113
32211	21141	14141	43431	32431	21321	14321	43211
0122	1013	2003	2201	1211	0122	1112	1112
32211	21141	14141	43431	32431	21321	14321	43211
0122	1013	2003	2201	1211	0122	1112	1112
21111	14441	43441	32331	21331	14221	43221	32111
0014	3002	3101	0311	0212	1022	1121	0113

Table 1.2 Summary of results for larger numbers of components in larger well plates, using the row-column sorting algorithm

Components	Steps	Plate size	Compositions	Sequences	No. of wells
4	4	96	52	256	384
4	8	96	104	384	384
8	4	96	304	768	768
8	8	96	576	768	768
4	4	384	52	256	1536
4	8	384	148	1024	1536
8	4	384	520	2048	3072
8	8	384	1752	3072	3072
8	8	1536	1256	6144	12288

Table 1.3 Inductively Coupled Plasma Atomic Emission Spectroscopy (ICPAES) analysis of Pt on γ -alumina

Theoretical wt%	Sample #1	Sample #2	Sample #3	Average wt% [Experimental]	Standard Deviation
0.05	0.048	0.052	0.054	0.051	0.003
0.1	0.11	0.103	0.104	0.106	0.004
0.15	0.162	0.149	0.146	0.152	0.009
0.2	0.181	0.196	0.178	0.185	0.01
0.5	0.444	0.442	0.482	0.456	0.023
1	0.953	1.02	0.986	0.986	0.034

Table 1.4a Theoretical versus actual analysis of standards by Micro-Xray Fluorescence (μ -XRF) and Inductively Coupled Plasma Atomic Emission Spectroscopy (ICPAES) at UOP

Pt theo.	Pt XRF	Pt ICP	%Dif XRF	%Dif ICP	Ni theo.	Ni XRF	Ni ICP	% Dif XRF	% Dif ICP
0.05	0.03	0.03	40	32	0.05	0.03	0.04	40	30
0.05	0.03	0.04	40	26	0.05	0.04	0.04	20	24
0.05	0.04	0.03	20	32					
Average	0.03	0.04	33.33	30.00		0.04	0.04	30.00	27.00
Std. dev	0.01	0.00	11.55	3.46		0.01	0.00	14.14	4.24
%Std dev/ Average	17.32	4.95	34.64	11.55		20.20	5.81	47.14	15.71
0.1	0.09	0.11	10	5	0.1	0.12	0.12	20	20

0.1	0.10	0.10	0	3	0.1	0.13	0.12	30	18
0.1	0.11	0.10	10	3	0.1	0.13	0.04	30	63
Average	0.10	0.10	6.67	3.67		0.13	0.09	26.67	33.67
Std. dev	0.01	0.00	5.77	1.15		0.01	0.05	5.77	25.42
%Std dev/ Average	10	1.11	86.60	31.49		4.56	51.66	21.65	75.51
0.15	0.16	0.16	6.67	6.67	0.2	0.16	0.20	20	1
0.15	0.17	0.18	13.33	20	0.2	0.17	0.19	15	4
0.15	0.17	0.16	13.33	7.33	0.2	0.20	0.19	0	5
Average	0.17	0.17	11.11	11.33		0.18	0.19	11.67	3.33
Std. dev	0.01	0.01	3.85	7.51		0.02	0.00	10.41	2.08
%Std dev/ Average	3.46	6.75	34.64	66.29		11.78	2.15	89.21	62.45

Table 1.4a continued Theoretical versus actual analysis of standards by Micro-Xray Fluorescence (μ -XRF) and Inductively Coupled Plasma Atomic Emission Spectroscopy (ICPAES) at UOP

Cu theo	Cu XRF	Cu ICP	% Dif XRF	% Dif ICP
0.05	0.04	0.04	20	16
0.05	0.05	0.04	0	20
0.05	0.05	0.04	0	18
Average	0.05	0.04	6.67	18.00
Std. dev	0.01	0.00	11.55	2.00
%Std dev/ Average	12.37	2.44	173.21	11.11

0.2	0.16	0.20	20	1
0.2	0.17	0.19	15	4
0.2	0.20	0.19	0	5
0.2	0.18	0.20	10	0.5
0.2	0.19	0.22	5	10.5
0.2	0.24	0.21	20	5.5
Average	0.19	0.20	11.67	4.42
Std. dev	0.03	0.01	8.16	3.63
%Std dev/ Average	14.89	5.91	69.99	82.08

Table 1.4b Theoretical versus actual analysis of Pt on γ -alumina by Micro-Xray Fluorescence (μ -XRF) and Inductively Coupled Plasma Atomic Emission Spectroscopy (ICPAES) at UOP

Nominal Pt wt%	Pill #	XRF wt% Pt	XRF average wt%	XRF Std. Dev.	% XRF std dev/average	ICP wt% Pt
0.05	1	0.025				
0.05	2	0.05				
0.05	3	0.02				
0.05	4	0.06				
0.05	5	0.04				
0.05	6	0.04				
0.05	7	0.06	0.042	0.015	37	0.047
0.15	1	0.19				
0.15	2	0.16				
0.15	3	0.125				
0.15	4	0.17				
0.15	5	0.14				
0.15	6	0.175				
0.15	7	0.19	0.164	0.025	15	0.151

0.3	1	0.35				
0.3	2	0.325				
0.3	3	0.35				
0.3	4	0.33				
0.3	5	0.275	0.326	0.031	9.4	0.294

Table 1.5 Results from column shuffle for three component four step 96-well plate

Column directed sorting using four components in four 96-well plates. The results shown are for all three well plates for three directed sorting cycles. Each well or bead is identified with a 4-digit adsorption sequence indicating order of addition. For example, the first entry on column two (2221) indicates order of addition and signifies a bead history of three adsorptions of component 2, followed by two adsorptions of component 1. Note that the last adsorption step (the last digit in the 4-digit sequence) is the same for all beads in a given well plate. Note also that all compositions sum to 4, which is the number of adsorption steps in 3 split-pool cycles. The algorithm addressed four adsorptions of each element (1111, 2222 and 3333), 9 binary combinations with two unique order of additions each (2221 and 1222; 2211 and 1221; 2111 and 1211; 3111 and 1113; 1133 and 3113; 1333 and 3133; 2333 and 3332; 3322 and 2332; 3222 and 2322) and 3 ternary combinations with one of three components twice and with five unique order of additions each (1132, 1321, 1213, 3211 and 2113; 2213, 1322, 2132, 2321 and 3221; 3321, 1332, 3132, 2133 and 3213). The algorithm also has a redundancy of 8 i.e., each row. The shuffle algorithm resulted in 36 compositions and used 48 physical manipulations for a library of 288 beads. Each row in the following table represents a **unique well plate** and each row replicated eight times in the algorithm (8*12 columns = 96 = 1 well plate; 96*3 = 288 = 3 well plates). Analytical results (μ -XRF) and LAMIMS analysis for 16 samples from the library are in Table 7; based on (μ -XRF) and LAMIMS analysis in Tables 9 through 11 for all the samples.

1111	2221	2211	3321	2111	3221	3211	1321	3111	1221	1211	2321
------	------	------	------	------	------	------	------	------	------	------	------

2222	3332	3322	1132	3222	1332	1322	2132	1222	2332	2322	3132
3333	1113	1133	2213	1333	2113	2133	3213	2333	3113	3133	1213

Table 1.6 Results from manual pipetting for three component 96-well plate

Each well or bead is identified with a 4-digit adsorption sequence indicating order of addition. For example, the first entry on column two (1112) indicates order of addition and signifies a bead history of three adsorptions of component 1, followed by one adsorptions of component 2. Note also that all compositions sum to 4, which is the number of adsorption steps in 3 split-pool cycles. Nil refers to no adsorption and was used to check for background.

1111	1112	1112	1131	1122	1123	1121	1132	1133	1211	1212	1213
1231	1311	1312	1312	1221	1222	1223	1232	1322	1323	1333	1331
1332	1233	1321	2222	2223	2221	2232	2233	2231	2212	2213	2211
2322	2323	2321	2313	2122	2123	2121	2332	2333	2331	2133	2131
2111	2112	2113	2311	2313	2132	3333	3331	3332	3313	3332	3313
3311	3312	3323	3321	3322	3133	3131	3132	3123	3233	3231	3232
3113	3111	3112	3211	3212	3222	3223	3221	3122	3121	3213	nil
nil											

Table 1.7 Results of Inductively Coupled Plasma Mass Spectroscopy (ICPMS) analysis of 22 directed sorting synthesized samples. Each theoretical eight digit element code represented a total of four adsorption steps resulting in a total of 1.7wt% metal on γ -alumina. We estimated analytical root mean square errors for samples containing Co and no other metal in the samples (+/-12.7%), Ni and no other metal in the samples (+/-11.2%), Cu and no other metal in the samples (+/-12.7%), combinations of Cu and/or Ni with no cobalt (+/-16.9%) in the samples, combinations of Cu and/or Ni with one addition of Co (+/-23.3%) in the samples and combinations of Cu and/or Ni with two or three additions of Co with errors of (+/-30%) in the samples.

Theoretical Composition	Analytical composition by ICPMS (wt./0.43%)	ICP-MS analysis within analytical error range?
CoCoCoCo	Co _{3.7}	Yes
NiNiNiNi	Ni _{3.8}	Yes
CuCuCuCu	Cu ₄	Yes
NiNiNiCo	Co ₁ Ni _{2.9}	Yes
NiNiCoCo	Co _{1.8} Ni _{1.8}	Yes
NiCoCoCo	Co _{2.1} Ni _{0.9}	Yes
CuCoCoCo	Co _{2.7} Cu _{0.9}	Yes
CoCoCuCu	Co ₂ Cu _{1.6}	Yes
CoCuCuCu	Co _{0.9} Cu _{2.6}	Yes
NiCuCuCu	Ni _{0.9} Cu _{2.3}	No for Cu
CuCuNiNi	Ni _{1.9} Cu _{1.7}	Yes
CuNiNiNi	Ni _{2.9} Cu _{0.9}	Yes
CoCuNiCo	Co _{1.4} Ni _{0.8} Cu _{0.3}	No for Co and Cu
CuNiCoCo	Co ₂ Ni ₁ Cu ₁	Yes
NiCoCoCu	Co ₂ Ni ₁ Cu _{0.95}	Yes
NiNiCoCu	Co _{0.8} Ni _{0.9} Cu _{0.9}	No for Ni
NiCoCuNi	Co _{0.6} Ni _{1.6} Cu _{0.9}	No for Co
NiCuNiCo	Co _{0.6} Ni _{1.3} Cu _{0.95}	No for Co and Ni
CuNiNiCo	Co _{0.8} Ni _{1.6} Cu ₁	No for Ni
CuCuNiCo	Co _{0.8} Ni ₁ Cu _{1.9}	Yes
CuCoCuNi	Co _{0.7} Ni _{0.9} Cu _{1.6}	No for Co
CuNiCoCu	Co _{0.6} Ni _{0.9} Cu _{1.8}	No for Co

Table 1.8 Results of average, standard deviation and relative standard deviation in normalized Laser Assisted Membrane Introduction Mass Spectroscopy (LAMIMS) area and Micro-X-ray Fluorescence (μ -XRF) of 16 directed sorting synthesized samples. Numbers in brackets next to composition denote number of samples (out of eight) included in the analysis. The remainder (out of eight) in each case had no detectable normalized LAMIMS area.

Composition	Average LAMIMS area normalized to 1wt% Pt	Standard Deviation in LAMIMS area	Relative Standard Deviation in LAMIMS area	Average μ -XRF Difference from theoretical composition	Standard Deviation in μ -XRF	Relative Standard Deviation in μ -XRF
NiNiPtPt (7)	0.23	0.1	43.3	35.5(Pt) 30 (Ni)	10.1(Pt) 10.3(Ni)	28.5(Pt) 34.2(Ni)
CuPtPtPt (8)	0.47	0.11	23.7	29(Pt) 32 (Cu)	17.7(Pt) 15(Cu)	60.9(Pt) 46.8(Cu)
PtPtPtCu (7)	0.23	0.05	21.4	19.2(Pt) 23(Cu)	11.7(Pt) 8.5 (Cu)	61.1(Pt) 36.9 (Cu)
PtPtPtPt (8)	1.17	0.11	9.6	29.1	11.4	39.2
CuCuCuNi (5)	0.31	0.06	18.9	32.0(Ni) 32.8(Cu)	12.1(Ni) 11.6 (Cu)	37.8(Ni) 35.3 (Cu)
NiCuCuNi (4)	0.33	0.1	31.4	29.3(Ni) 26.8(Cu)	10.9(Ni) 13.7 (Cu)	37.3(Ni) 51.3 (Cu)
CuCuNiNi (5)	0.27	0.08	29.1	27.0(Ni) 25.25(Cu)	9.0(Ni) 8.7(Cu)	33.4(Ni) 34.4 (Cu)
NiCuNiNi (4)	0.41	0.11	26.8	26.8(Ni) 30.0(Cu)	7.70(Ni) 7.1(Cu)	28.8(Ni) 23.6(Cu)
CuNiNiNi (4)	0.22	0.07	31.5	28.7(Ni) 35.5(Cu)	12.4(Ni) 12.0(Cu)	43.3(Ni) 33.8(Cu)
NiNiNiNi (4)	0.31	0.08	24.9	26.6	9.3	34.9
CuPtCuNi (4)	0.42	0.18	42.1	36.5(Pt) 31(Ni) 31(Cu)	20.5(Pt) 13.7(Ni) 13.9(Cu)	56.0(Pt) 44.0(Ni) 44.8(Cu)

PtPtCuNi (4)	0.35	0.12	34.2	21.3(Pt) 31.5(Ni) 30.5(Cu)	15.0(Pt) 13.3(Ni) 13.2(Cu)	70.6(Pt) 42.1(Ni) 43.2(Cu)
PtCuCuNi (4)	0.26	0.1	37.8	35.5(Pt) 32.5(Ni) 32.0(Cu)	17.2(Pt) 14.7(Ni) 14.2(Cu)	48.4(Pt) 45.3(Ni) 44.3(Cu)
PtCuNiNi (7)	0.44	0.24	53.9	37.5(Pt) 28.0(Ni) 42.0(Cu)	19.5(Pt) 13.9(Ni) 16.3(Cu)	51.9(Pt) 49.8(Ni) 38.8(Cu)
NiPtCuNi (4)	0.32	0.11	33.1	38.0(Pt) 36.8(Ni) 35.0(Cu)	20.3(Pt) 13.6(Ni) 16.0(Cu)	53.4(Pt) 36.9(Ni) 45.6(Cu)
PtNiNiNi (4)	0.34	0.12	35.5	32.5(Pt) 34.8(Ni)	30.1(Pt) 11.6(Ni)	92.7(Pt) 33.2(Ni)

Table 1.9 Laser Assisted Membrane Introduction Mass Spectroscopy (LAMIMS) and Micro-Xray Fluorescence (μ -XRF) analysis of samples with Pt as last adsorption from a 3 component (Pt, Cu and Ni), 3 step (4 adsorptions and 3 transfers), 96 wellplate library; synthesized according to the column only directed sorting algorithm. Eight replicates are represented by a two or three digit sample well identifier; alphabet (A through H) followed by a number (1 through 12). The eight alphabet code indicates order of addition of elements (Pt, Cu and Ni) from solutions in 2% HCl. LAMIMS analysis was carried out under a mixture of H₂ (50 ml/min) and MCH (0.02ml/min). The laser was switched to 55% peak power and held at each bead for 40 seconds, resulting in a power input of 550J. The LAMIMS area and height were normalized to 1wt% Pt on γ -alumina [20a]. N/A denotes no signal.

Sample	Pt Target	Pt XRF	% Dif Pt	Ni Target	Ni XRF	% Dif Ni	Cu Target	Cu XRF	% Dif Cu	Normalized LAMIMS Area	Normalized LAMIMS Height
Well											
A1	1.00	1.22	22.0							1.18	1.10
B1	1.00	1.42	42.0							1.15	1.16
C1	1.00	1.41	41.0							1.11	1.05
D1	1.00	1.38	38.0							1.03	1.00
E1	1.00	1.17	17.0							1.03	0.97
F1	1.00	1.13	13.0							1.28	1.26
G1	1.00	1.20	20.0							1.24	1.18
H1	1.00	1.40	40.0							1.34	1.30
Average	1.00	1.29	29.13							1.17	1.13
Std. Dev.		0.122	11.43							0.11	0.12
%Avg/Std. Dev		9.462	39.2393							9.63	10.59
A2	0.25	0.32	28.0	0.75	0.89	18.7				0.10	0.12
B2	0.25	0.32	28.0	0.75	0.90	20.0				0.08	0.08
C2	0.25	0.33	32.0	0.75	1.01	34.7				0.15	0.16
D2	0.25	0.43	72.0	0.75	1.07	42.7				0.06	0.08
E2	0.25	0.28	12.0	0.75	0.85	13.3				0.10	0.12
F2	0.25	0.33	32.0	0.75	1.00	33.3				0.21	0.22

A5	0.75	1.11	48.0	0.25	0.38	52.0					N/A	N/A
B5	0.75	1.08	44.0	0.25	0.37	48.0					N/A	N/A
C5	0.75	1.11	48.0	0.25	0.35	40.0	NiPtPtPt				N/A	N/A
D5	0.75	0.85	13.3	0.25	0.27	8.0					N/A	N/A
E5	0.75	0.99	32.0	0.25	0.33	32.0					N/A	N/A
F5	0.75	1.20	60.0	0.25	0.36	44.0	NiPtPtPt				N/A	N/A
G5	0.75	1.10	46.7	0.25	0.40	60.0					N/A	N/A
H5	0.75	0.97	29.3	0.25	0.32	28.0					N/A	N/A
Average	0.75	1.05	40.17	0.25	0.35	39.00						
Std. Dev.		0.11	14.53		0.04	16.25						
%Avg/Std. Dev		10.36	36.17		11.69	41.66						
A6	0.25	0.26	4.0	0.50	0.54	8.0	0.25	0.29	16.0	0.248	0.266	
B6	0.25	0.40	60.0	0.50	0.70	40.0	0.25	0.36	44.0	N/A	N/A	
C6	0.25	0.27	8.0	0.50	0.54	8.0	0.25	0.30	20.0	N/A	N/A	
D6	0.25	0.30	20.0	0.50	0.59	18.0	0.25	0.31	24.0	N/A	N/A	
E6	0.25	0.32	28.0	0.50	0.57	14.0	0.25	0.30	20.0	N/A	N/A	
F6	0.25	0.31	24.0	0.50	0.62	24.0	0.25	0.31	24.0	N/A	N/A	
G6	0.25	0.31	24.0	0.50	0.60	20.0	0.25	0.31	24.0	N/A	N/A	
H6	0.25	0.30	20.0	0.50	0.63	26.0	0.25	0.32	28.0	N/A	N/A	
Average	0.25	0.31	23.50	0.50	0.60	19.75	0.25	0.31	25.00	0.25	0.27	
Std. Dev.		0.04	16.89		0.05	10.55		0.02	8.49			
%Avg/Std. Dev		13.68	71.89		8.81	53.43	CuNiNiPt	6.79	33.94			
A7	0.50	0.51	2.0	0.25	0.28	12.0	0.25	0.29	16.0	N/A	N/A	
B7	0.50	0.54	8.0	0.25	0.28	12.0	0.25	0.30	20.0	0.173	0.202	
C7	0.50	0.62	24.0	0.25	0.31	24.0	0.25	0.34	36.0	0.289	0.280	
D7	0.50	0.78	56.0	0.25	0.22	12.0	0.25	0.36	44.0	N/A	N/A	
E7	0.50	0.78	56.0	0.25	0.39	56.0	0.25	0.39	56.0	N/A	N/A	
F7	0.50	0.71	42.0	0.25	0.32	28.0	0.25	0.34	36.0	N/A	N/A	
G7	0.50	0.65	30.0	0.25	0.32	28.0	0.25	0.33	32.0	N/A	N/A	

H7	0.50	0.63	26.0	0.25	0.32	28.0	0.25	0.34	36.0	N/A	N/A
Average	0.50	0.65	30.50	0.25	0.31	25.00	0.25	0.34	34.50	0.23	0.24
Std. Dev.		0.1	20.05		0.05	14.62		0.03	12.64	0.08	0.05
%Avg/Std. Dev		15.36	65.74		15.87	58.48	CuNiPtPt	9.40	36.63	35.36	22.77
A8	0.50	0.56	12.0	0.25	0.29	16.0	0.25	0.32	28.0	N/A	N/A
B8	0.50	0.71	42.0	0.25	0.32	28.0	0.25	0.33	32.0	N/A	N/A
C8	0.50	0.75	50.0	0.25	0.34	36.0	0.25	0.36	44.0	N/A	N/A
D8	0.50	0.66	32.0	0.25	0.31	24.0	0.25	0.34	36.0	N/A	N/A
E8	0.50	0.61	22.0	0.25	0.27	8.0	0.25	0.30	20.0	N/A	N/A
F8	0.50	0.58	16.0	0.25	0.27	8.0	0.25	0.32	28.0	N/A	N/A
G8	0.50	0.63	26.0	0.25	0.31	24.0	0.25	0.30	20.0	N/A	N/A
H8	0.50	0.57	14.0	0.25	0.27	8.0	0.25	0.29	16.0	N/A	N/A
Average	0.50	0.63	26.75	0.25	0.30	19.00	0.25	0.32	28.00		
Std. Dev.		0.07	13.73		0.03	10.64		0.02	9.32		
%Avg/Std. Dev		10.83	51.33		8.94	55.98	PtCuNiPt	7.28	33.28		
A9	0.75	0.90	20.0				0.25	0.31	24.0	0.680	0.649
B9	0.75	1.12	49.3		CuPtPtPt		0.25	0.37	48.0	0.533	0.527
C9	0.75	0.85	13.3				0.25	0.29	16.0	0.343	0.326
D9	0.75	0.93	24.0				0.25	0.31	24.0	0.437	0.416
E9	0.75	1.12	49.3				0.25	0.36	44.0	0.557	0.513
F9	0.75	0.85	13.3				0.25	0.31	24.0	0.423	0.415
G9	0.75	1.13	50.7				0.25	0.39	56.0	0.352	0.368
H9	0.75	0.84	12.0				0.25	0.30	20.0	0.472	0.480
Average	0.75	0.97	29.00				0.25	0.33	32.00	0.47	0.46
Std. Dev.		0.13	17.66					0.04	14.97	0.11	0.10
%Avg/Std. Dev		13.69	60.88					11.34	46.77	23.72	22.24
A10	0.50	0.65	30.0	0.50	0.68	36.0				N/A	N/A

B10	0.50	0.72	44.0	0.50	0.68	36.0	PtNiNiPt			N/A	N/A	
C10	0.50	0.59	18.0	0.50	0.58	16.0				N/A	N/A	
D10	0.50	0.77	54.0	0.50	0.71	42.0				N/A	N/A	
E10	0.50	0.75	50.0	0.50	0.72	44.0				N/A	N/A	
F10	0.50	0.70	40.0	0.50	0.67	34.0		PtNiNiPt			N/A	N/A
G10	0.50	0.80	60.0	0.50	0.71	42.0					N/A	N/A
H10	0.50	0.64	28.0	0.50	0.62	24.0					N/A	N/A
Average	0.50	0.70	40.50	0.50	0.67	34.25						
Std. Dev.		0.07	14.33		0.05	9.71						
%Avg/Std. Dev		10.20	35.39		7.23	28.34						
A11	0.75	0.89	18.7	0.25	0.29	16.0	PtNiPtPt			N/A	N/A	
B11	0.75	0.99	32.0	0.25	0.32	28.0				N/A	N/A	
C11	0.75	0.90	20.0	0.25	0.28	12.0				N/A	N/A	
D11	0.75	1.08	44.0	0.25	0.35	40.0				N/A	N/A	
E11	0.75	1.07	42.7	0.25	0.34	36.0				N/A	N/A	
F11	0.75	1.10	46.7	0.25	0.36	44.0				N/A	N/A	
G11	0.75	0.75	0.0	0.25	0.23	8.0				N/A	N/A	
H11	0.75	0.81	8.0	0.25	0.25	0.0				N/A	N/A	
Average	0.75	0.95	26.50	0.25	0.30	23.00						
Std. Dev.		0.13	17.54		0.05	16.25						
%Avg/Std. Dev		13.86	66.17		15.78	70.64						
A12	0.25	0.33	32.0	0.50	0.63	26.0	0.25	0.31	24.0	N/A	N/A	
B12	0.25	0.26	4.0	0.50	0.52	4.0	0.25	0.28	12.0	N/A	N/A	
C12	0.25	0.43	72.0	0.50	0.80	60.0	0.25	0.41	64.0	N/A	N/A	
D12	0.25	0.34	36.0	0.50	0.60	20.0	0.25	0.30	20.0	N/A	N/A	
E12	0.25	0.33	32.0	0.50	0.62	24.0	0.25	0.32	28.0	N/A	N/A	
F12	0.25	0.32	28.0	0.50	0.63	26.0	0.25	0.30	20.0	N/A	N/A	
G12	0.25	0.35	40.0	0.50	0.67	34.0	0.25	0.32	28.0	N/A	N/A	

H12	0.25	0.32	28.0	0.50	0.72	44.0	0.25	0.28	12.0	N/A	N/A
Average	0.25	0.34	34.00	0.50	0.65	29.75	0.25	0.32	26.00		
Std. Dev.		0.05	18.76		0.08	16.71		0.04	16.56		
%Avg/Std. Dev		14.00	55.18		12.88	56.18		13.14	63.70	NiCuNiPt	

Table 1.10 Laser Assisted Membrane Introduction Mass Spectroscopy (LAMIMS) and Micro-Xray Fluorescence (μ -XRF) analysis of samples with Ni as last adsorption from a 3 component (Pt, Cu and Ni), 3 step (4 adsorptions and 3 transfers), 96 wellplate library; synthesized according to the column only directed sorting algorithm. Eight replicates are represented by a two or three digit sample well identifier; alphabet (A through H) followed by a number (1 through 12). The eight alphabet code indicates order of addition of elements (Pt, Cu and Ni) from solutions in 2% HCl. LAMIMS analysis was carried out under a mixture of H₂ (50 ml/min) and MCH (0.02ml/min). The laser was switched to 55% peak power and held at each bead for 40 seconds, resulting in a power input of 550J. The LAMIMS area and height were normalized to 1wt% Pt on γ -alumina [20a]. N/A denotes no signal.

Sample	Pt Target	Pt XRF	% Dif Pt	Ni Target	Ni XRF	% Dif Ni	Cu Target	Cu XRF	% Dif Cu	Normalized LAMIMS Area	Normalized LAMIMS Height
Well											
A1				1	1.39	39.0				N/A	N/A
B1				1	1.21	21.0				N/A	N/A
C1				1	1.17	17.0				0.22	0.25
D1	NiNiNiNi			1	1.28	28.0				0.32	0.27
E1				1	1.24	24.0				0.29	0.22
F1				1	1.42	42.0				0.41	0.37
G1				1	1.24	24.0				N/A	N/A
H1				1	1.18	18.0				N/A	N/A
Average				1	1.27	26.63				0.31	0.28
Std. Dev.					0.09	9.29				0.08	0.07
%Avg/Std. Dev					7.34	34.88				24.89	23.54

A2				0.25	0.33	32.0	0.75	1.02	36.0	N/A	N/A	
B2	CuCuCuNi			0.25	0.3	20.0	0.75	0.93	24.0	0.28	0.26	
C2				0.25	0.33	32.0	0.75	1.02	36.0	0.31	0.28	
D2				0.25	0.31	24.0	0.75	0.96	28.0	0.24	0.18	
E2				0.25	0.29	16.0	0.75	0.85	13.3	0.32	0.28	
F2				0.25	0.34	36.0	0.75	0.99	32.0	0.40	0.34	
G2				0.25	0.38	52.0	0.75	1.14	52.0	N/A	N/A	
H2				0.25	0.36	44.0	0.75	1.06	41.3	N/A	N/A	
Average				0.25	0.33	32.00	0.75	1.00	32.83	0.31	0.27	
Std. Dev.					0.03	12.09		0.09	11.60	0.06	0.06	
%Avg/Std. Dev	CuCuCuNi				9.16	37.80		8.73	35.33	18.92	21.03	
A3				0.5	0.63	26.0	0.5	0.65	30.0	N/A	N/A	
B3				0.5	0.58	16.0	0.5	0.59	18.0	0.18	0.14	
C3	CuCuNiNi			0.5	0.65	30.0	0.5	0.58	16.0	0.23	0.20	
D3				0.5	0.64	28.0	0.5	0.64	28.0	0.25	0.21	
E3				0.5	0.65	30.0	0.5	0.66	32.0	0.32	0.27	
F3				0.5	0.56	12.0	0.5	0.56	12.0	0.38	0.32	
G3				0.5	0.68	36.0	0.5	0.68	36.0	N/A	N/A	
H3				0.5	0.69	38.0	0.5	0.65	30.0	N/A	N/A	
Average				0.5	0.64	27.00	0.50	0.63	25.25	0.27	0.23	
Std. Dev.					0.05	9.01	0.00	0.04	8.68	0.08	0.07	
%Avg/Std. Dev					7.09	33.36	0.00	6.93	34.38	29.12	30.29	
A4		0.5	0.52	4.0	0.25	0.3	20.0	0.25	0.32	28.0	N/A	N/A
B4		0.5	0.51	2.0	0.25	0.3	20.0	0.25	0.31	24.0	0.19	0.18
C4		0.5	0.58	16.0	0.25	0.34	36.0	0.25	0.32	28.0	0.42	0.39
D4		0.5	0.66	32.0	0.25	0.33	32.0	0.25	0.32	28.0	0.46	0.46
E4		0.5	0.57	14.0	0.25	0.31	24.0	0.25	0.29	16.0	0.33	0.29
F4		0.5	0.63	26.0	0.25	0.31	24.0	0.25	0.31	24.0	N/A	N/A
G4		0.5	0.73	46.0	0.25	0.4	60.0	0.25	0.4	60.0	N/A	N/A

H4	0.5	0.65	30.0	0.25	0.34	36.0	0.25	0.34	36.0	N/A	N/A	
Average	0.50	0.61	21.25	0.25	0.33	31.50	0.25	0.33	30.50	0.35	0.33	
Std. Dev.		0.08	15.00		0.03	13.26		0.03	13.17	0.12	0.12	
%Avg/Std. Dev	PtPtCuNi	12.37	70.60		10.08	42.08		10.09	43.18	34.22	37.20	
A5	CuNiNiNi			0.75	0.83	10.7	0.25	0.29	16.0	N/A	N/A	
B5				0.75	0.88	17.3	0.25	0.31	24.0	0.12	0.08	
C5				0.75	0.95	26.7	0.25	0.34	36.0	0.24	0.20	
D5				0.75	0.92	22.7	0.25	0.34	36.0	0.24	0.21	
E5				0.75	1.13	50.7	0.25	0.39	56.0	0.27	0.24	
F5				0.75	1	33.3	0.25	0.34	36.0	N/A	N/A	
G5	CuNiNiNi			0.75	0.98	30.7	0.25	0.34	36.0	N/A	N/A	
H5				0.75	1.03	37.3	0.25	0.36	44.0	N/A	N/A	
Average				0.75	0.97	28.67	0.25	0.34	35.50	0.22	0.18	
Std. Dev.					0.09	12.41		0.03	11.99	0.07	0.07	
%Avg/Std. Dev					9.64	43.28		8.85	33.77	31.49	38.09	
A6		0.25	0.34	36.0	0.25	0.28	12.0	0.5	0.56	12.0	N/A	N/A
B6		0.25	0.31	24.0	0.25	0.29	16.0	0.5	0.58	16.0	0.14	0.09
C6		0.25	0.37	48.0	0.25	0.34	36.0	0.5	0.71	42.0	0.23	0.18
D6		0.25	0.37	48.0	0.25	0.36	44.0	0.5	0.7	40.0	0.36	0.28
E6		0.25	0.26	4.0	0.25	0.3	20.0	0.5	0.59	18.0	0.31	0.22
F6		0.25	0.36	44.0	0.25	0.38	52.0	0.5	0.74	48.0	N/A	N/A
G6		0.25	0.31	24.0	0.25	0.34	36.0	0.5	0.69	38.0	N/A	N/A
H6		0.25	0.39	56.0	0.25	0.36	44.0	0.5	0.71	42.0	N/A	N/A
Average		0.25	0.34	35.50	0.25	0.33	32.50	0.50	0.66	32.00	0.26	0.19
Std. Dev.			0.04	17.16		0.04	14.73		0.07	14.18	0.10	0.08
%Avg/Std. Dev	PtCuCuNi	12.67	48.35		11.11	45.31		10.74	44.32	37.81	40.41	
A7		0.25	0.38	52.0	0.5	0.52	4.0	0.25	0.39	56.0	N/A	N/A
B7		0.25	0.33	32.0	0.5	0.67	34.0	0.25	0.37	48.0	0.25	0.22

C7	0.25	0.42	68.0	0.5	0.68	36.0	0.25	0.4	60.0	0.81	0.91
D7	0.25	0.37	48.0	0.5	0.67	34.0	0.25	0.35	40.0	0.32	0.29
E7	0.25	0.37	48.0	0.5	0.75	50.0	0.25	0.4	60.0	0.28	0.25
F7	0.25	0.28	12.0	0.5	0.59	18.0	0.25	0.31	24.0	0.57	0.53
G7	0.25	0.3	20.0	0.5	0.6	20.0	0.25	0.31	24.0	N/A	N/A
H7	0.25	0.3	20.0	0.5	0.64	28.0	0.25	0.31	24.0	N/A	N/A
Average	0.25	0.34	37.50	0.50	0.64	28.00	0.25	0.36	42.00	0.44	0.44
Std. Dev.		0.05	19.47		0.07	13.94		0.04	16.28	0.24	0.29
%Avg/Std. Dev	PtCuNiNi	14.16	51.92		10.89	49.78		11.47	38.77	53.87	65.85
A8	0.25	0.36	44.0	0.5	0.66	32.0	0.25	0.33	32.0	N/A	N/A
B8	0.25	0.33	32.0	0.5	0.65	30.0	0.25	0.34	36.0	0.24	0.19
C8	0.25	0.32	28.0	0.5	0.71	42.0	0.25	0.37	48.0	0.46	0.45
D8	0.25	0.32	28.0	0.5	0.62	24.0	0.25	0.31	24.0	0.35	0.34
E8	0.25	0.3	20.0	0.5	0.62	24.0	0.25	0.32	28.0	0.24	0.18
F8	0.25	0.45	80.0	0.5	0.83	66.0	0.25	0.42	68.0	N/A	N/A
G8	0.25	0.38	52.0	0.5	0.7	40.0	0.25	0.31	24.0	N/A	N/A
H8	0.25	0.3	20.0	0.5	0.68	36.0	0.25	0.3	20.0	N/A	N/A
Average	0.25	0.35	38.00	0.50	0.68	36.75	0.25	0.34	35.00	0.32	0.29
Std. Dev.		0.05	20.28		0.07	13.56		0.04	15.96	0.11	0.13
%Avg/Std. Dev	NiPtCuNi	14.70	53.38		9.92	36.90		11.83	45.61	33.12	44.27
A9	0.25	0.43	72.0	0.75	1	33.3				N/A	N/A
B9	0.25	0.24	4.0	0.75	1.08	44.0				0.34	0.25
C9	0.25	0.38	52.0	0.75	1.01	34.7				0.42	0.36
D9	0.25	0.3	20.0	0.75	0.93	24.0				0.44	0.41
E9	0.25	0.34	36.0	0.75	1.09	45.3				0.17	0.15
F9	0.25	0.26	4.0	0.75	0.89	18.7				N/A	N/A
G9	0.25	0.43	72.0	0.75	1.14	52.0				N/A	N/A
H9	0.25	0.25	0.0	0.75	0.95	26.7				N/A	N/A
Average	0.25	0.33	32.50	0.75	1.01	34.83				0.34	0.29

Std. Dev.		0.08	30.12		0.09	11.57	Plate 2			0.12	0.12	
%Avg/Std. Dev	PtNiNiNi	23.81	92.67		8.58	33.21				35.45	39.97	
A10				0.5	0.55	10.0	0.5	0.57	14.0	N/A	N/A	
B10				0.5	0.71	42.0	0.5	0.7	40.0	0.33	0.35	
C10	NiCuCuNi			0.5	0.68	36.0	0.5	0.71	42.0	0.31	0.29	
D10				0.5	0.6	20.0	0.5	0.62	24.0	0.47	0.46	
E10				0.5	0.67	34.0	0.5	0.64	28.0	0.21	0.20	
F10				0.5	0.64	28.0	0.5	0.63	26.0	N/A	N/A	
G10				0.5	0.7	40.0	0.5	0.69	38.0	N/A	N/A	
H10				0.5	0.62	24.0	0.5	0.51	2.0	N/A	N/A	
Average	NiCuCuNi			0.50	0.65	29.25	0.50	0.63	26.75	0.33	0.33	
Std. Dev.					0.05	10.90		0.07	13.73	0.10	0.11	
%Avg/Std. Dev					8.43	37.26		10.83	51.33	31.37	32.64	
A11				0.75	0.88	17.3	0.25	0.31	24.0	N/A	N/A	
B11				0.75	1.06	41.3	0.25	0.36	44.0	0.32	0.35	
C11				0.75	0.93	24.0	0.25	0.33	32.0	0.32	0.26	
D11	NiCuNiNi			0.75	0.93	24.0	0.25	0.32	28.0	0.54	0.54	
E11				0.75	0.91	21.3	0.25	0.31	24.0	0.46	0.44	
F11				0.75	0.99	32.0	0.25	0.34	36.0	N/A	N/A	
G11				0.75	0.92	22.7	0.25	0.31	24.0	N/A	N/A	
H11				0.75	0.99	32.0	0.25	0.32	28.0	N/A	N/A	
Average				0.75	0.95	26.83	0.25	0.33	30.00	0.41	0.40	
Std. Dev.					0.06	7.72		0.02	7.09	0.11	0.12	
%Avg/Std. Dev					6.09	28.78		5.45	23.64	26.81	30.44	
A12		0.25	0.38	52.0	0.25	0.35	40.0	0.5	0.7	40.0	N/A	N/A
B12		0.25	0.39	56.0	0.25	0.37	48.0	0.5	0.72	44.0	0.27	0.22
C12		0.25	0.29	16.0	0.25	0.31	24.0	0.5	0.61	22.0	0.29	0.27
D12		0.25	0.41	64.0	0.25	0.37	48.0	0.5	0.75	50.0	0.65	0.62

E12	0.25	0.29	16.0	0.25	0.3	20.0	0.5	0.59	18.0	0.46	0.40
F12	0.25	0.29	16.0	0.25	0.29	16.0	0.5	0.57	14.0	N/A	N/A
G12	0.25	0.37	48.0	0.25	0.34	36.0	0.5	0.7	40.0	N/A	N/A
H12	0.25	0.31	24.0	0.25	0.29	16.0	0.5	0.6	20.0	N/A	N/A
Average	0.25	0.34	36.50	0.25	0.33	31.00	0.50	0.66	31.00	0.42	0.38
Std. Dev.		0.05	20.45		0.03	13.65		0.07	13.90	0.18	0.18
%Avg/Std. Dev	CuPtCuNi	14.98	56.01		10.42	44.03		10.61	44.83	42.06	47.53

Table 1.11 Laser Assisted Membrane Introduction Mass Spectroscopy (LAMIMS) and Micro-Xray Fluorescence (μ -XRF) analysis of samples with Cu as last adsorption from a 3 component (Pt, Cu and Ni), 3 step (4 adsorptions and 3 transfers), 96 wellplate library synthesized according to the column only directed sorting algorithm. Eight replicates are represented by a two or three digit sample well identifier; alphabet (A through H) followed by a number (1 through 12). The eight alphabet code indicates order of addition of elements (Pt, Cu and Ni) from solutions in 2% HCl. LAMIMS analysis was carried out under a mixture of H₂ (50 ml/min) and MCH (0.02ml/min). The laser was switched to 55% peak power and held at each bead for 40 seconds, resulting in a power input of 550J. The LAMIMS area and height were normalized to 1wt% Pt on γ -alumina [20a]. N/A denotes no signal.

Sample	Pt Target	Pt XRF	% Dif Pt	Ni Target	Ni XRF	% Dif Ni	Cu Target	Cu XRF	% Dif Cu	Normalized LAMIMS Area	Normalized LAMIMS Height
Well											
A1							1.00	1.26	26.0	0.046	0.052
B1				CuCuCuCu			1.00	1.13	13.0	0.005	0.024
C1							1.00	1.36	36.0	0.005	0.021
D1							1.00	1.19	19.0	0.006	0.032
E1							1.00	1.08	8.0	0.020	0.024
F1							1.00	1.33	33.0	0.000	0.010
G1							1.00	1.21	21.0	0.025	0.027

H1								1.00	1.21	21.0	N/A	N/A
Average								1.00	1.22	22.13	0.02	0.03
Std. Dev.									0.09	9.42	0.02	0.01
%Avg/Std. Dev									7.71	42.57	106.48	47.41
A2	0.75	0.75	0.0	PtPtPtCu				0.25	0.29	16.0	0.169	0.194
B2	0.75	0.78	4.0					0.25	0.27	8.0	0.203	0.223
C2	0.75	0.94	25.3					0.25	0.32	28.0	0.265	0.284
D2	0.75	0.96	28.0					0.25	0.32	28.0	0.174	0.192
E2	0.75	0.86	14.7					0.25	0.21	16.0	0.259	0.282
F2	0.75	0.99	32.0					0.25	0.32	28.0	0.275	0.283
G2	0.75	0.93	24.0					0.25	0.32	28.0	0.288	0.274
H2	0.75	0.94	25.3					0.25	0.33	32.0	N/A	N/A
Average	0.75	0.89	19.17					0.25	0.30	23.00	0.23	0.25
Std. Dev.		0.09	11.71						0.04	8.49	0.05	0.04
%Avg/Std. Dev		9.83	61.09	PtPtPtCu					13.65	36.89	21.44	17.25
A3	0.50	0.58	16.0	PtPtCuCu				0.50	0.59	18.0	0.002	0.022
B3	0.50	0.49	2.0					0.50	0.52	4.0	0.062	0.079
C3	0.50	0.53	6.0					0.50	0.55	10.0	0.034	0.057
D3	0.50	0.56	12.0					0.50	0.54	8.0	0.052	0.061
E3	0.50	0.57	14.0					0.50	0.56	12.0	0.048	0.061
F3	0.50	0.57	14.0					0.50	0.58	16.0	0.044	0.053
G3	0.50	0.62	24.0					0.50	0.65	30.0	N/A	N/A
H3	0.50	0.57	14.0					0.50	0.62	24.0	N/A	N/A
Average	0.50	0.56	12.75					0.50	0.58	15.25	0.04	0.06
Std. Dev.		0.04	6.58						0.04	8.61	0.02	0.02
%Avg/Std. Dev		6.76	51.64						7.47	56.49	52.03	33.78
A4	0.25	0.29	16.0	0.50	0.57	14.0	0.25	0.30	20.0	0.042	0.049	

B4	0.25	0.29	16.0	0.50	0.57	14.0	0.25	0.32	28.0	0.064	0.083
C4	0.25	0.30	20.0	0.50	0.56	12.0	0.25	0.29	16.0	0.049	0.072
D4	0.25	0.28	12.0	0.50	0.59	18.0	0.25	0.32	28.0	0.071	0.090
E4	0.25	0.34	36.0	0.50	0.64	28.0	0.25	0.34	36.0	0.033	0.044
F4	0.25	0.32	28.0	0.50	0.62	24.0	0.25	0.31	24.0	0.029	0.038
G4	0.25	0.34	36.0	0.50	0.62	24.0	0.25	0.33	32.0	N/A	N/A
H4	0.25	0.33	32.0	0.50	0.71	42.0	0.25	0.37	48.0	N/A	N/A
Average	0.25	0.31	24.50	0.50	0.61	22.00	0.25	0.32	29.00	0.05	0.06
Std. Dev.		0.02	9.67		0.05	9.91		0.02	9.97	0.02	0.02
%Avg/Std. Dev		7.76	39.45	NiNiPtCu	8.13	45.06		7.73	34.38	34.88	34.52
A5	0.25	0.29	16.0				0.75	0.88	17.3	0.022	0.031
B5	0.25	0.33	32.0				0.75	0.87	16.0	0.062	0.080
C5	0.25	0.33	32.0	PtCuCuCu			0.75	0.91	21.3	0.054	0.055
D5	0.25	0.33	32.0				0.75	0.90	20.0	0.088	0.089
E5	0.25	0.32	28.0				0.75	0.89	18.7	0.015	0.024
F5	0.25	0.29	16.0				0.75	0.86	14.7	0.020	0.031
G5	0.25	0.29	16.0				0.75	0.81	8.0	N/A	N/A
H5	0.25	0.32	28.0				0.75	0.91	21.3	N/A	N/A
Average	0.25	0.31	25.00				0.75	0.88	17.17	0.04	0.05
Std. Dev.		0.02	7.63					0.03	4.42	0.03	0.03
%Avg/Std. Dev		6.11	30.54	PtCuCuCu				3.77	25.74	67.01	53.77
A6	0.50	0.60	20.0	0.25	0.28	12.0	0.25	0.29	16.0	0.028	0.033
B6	0.50	0.60	20.0	0.25	0.29	16.0	0.25	0.30	20.0	0.070	0.084
C6	0.50	0.59	18.0	0.25	0.29	16.0	0.25	0.28	12.0	0.144	0.178
D6	0.50	0.56	12.0	0.25	0.27	8.0	0.25	0.29	16.0	0.115	0.127
E6	0.50	0.55	10.0	0.25	0.28	12.0	0.25	0.25	0.0	0.084	0.105
F6	0.50	0.63	26.0	0.25	0.32	28.0	0.25	0.31	24.0	0.082	0.085
G6	0.50	0.57	14.0	0.25	0.29	16.0	0.25	0.28	12.0	N/A	N/A
H6	0.50	0.66	32.0	0.25	0.34	36.0	0.25	0.35	40.0	N/A	N/A

Average	0.50	0.60	19.00	0.25	0.30	18.00	0.25	0.29	17.50	0.09	0.10
Std. Dev.		0.04	7.33		0.02	9.32		0.03	11.50	0.04	0.05
%Avg/Std. Dev		6.16	38.57	NiPtPtCu	7.90	51.78		9.79	65.72	45.70	47.25
A7	0.25	0.32	28.0	0.25	0.32	28.0	0.50	0.63	26.0	0.013	0.026
B7	0.25	0.29	16.0	0.25	0.29	16.0	0.50	0.57	14.0	0.023	0.030
C7	0.25	0.36	44.0	0.25	0.34	36.0	0.50	0.65	30.0	0.000	0.010
D7	0.25	0.34	36.0	0.25	0.33	32.0	0.50	0.52	4.0	N/A	0.007
E7	0.25	0.32	28.0	0.25	0.28	12.0	0.50	0.51	2.0	0.010	0.014
F7	0.25	0.33	32.0	0.25	0.31	24.0	0.50	0.62	24.0	N/A	0.002
G7	0.25	0.34	36.0	0.25	0.33	32.0	0.50	0.69	38.0	N/A	N/A
H7	0.25	0.39	56.0	0.25	0.34	36.0	0.50	0.71	42.0	N/A	N/A
Average	0.25	0.34	34.50	0.25	0.32	27.00	0.50	0.61	22.50	0.01	0.01
Std. Dev.		0.03	11.89	NiPtCuCu	0.02	9.01		0.07	14.76	0.01	0.01
%Avg/Std. Dev		8.84	34.47		7.09	33.36		12.05	65.62	80.17	75.14
A8	0.25	0.26	4.0	0.25	0.26	4.0	0.50	0.57	14.0	N/A	N/A
B8	0.25	0.33	32.0	0.25	0.32	28.0	0.50	0.55	10.0	0.009	0.020
C8	0.25	0.29	16.0	0.25	0.31	24.0	0.50	0.64	28.0	0.031	0.028
D8	0.25	0.29	16.0	0.25	0.28	12.0	0.50	0.55	10.0	N/A	0.007
E8	0.25	0.28	12.0	0.25	0.28	12.0	0.50	0.59	18.0	0.009	0.011
F8	0.25	0.34	36.0	0.25	0.32	28.0	0.50	0.67	34.0	N/A	0.009
G8	0.25	0.32	28.0	0.25	0.29	16.0	0.50	0.60	20.0	0.021	0.032
H8	0.25	0.34	36.0	0.25	0.31	24.0	0.50	0.65	30.0	N/A	N/A
Average	0.25	0.31	22.50	0.25	0.30		0.50	0.60	20.50	0.02	0.02
Std. Dev.		0.03	12.08		0.02			0.05	9.24	0.01	0.01
%Avg/Std. Dev		9.86	53.70	CuNiPtCu	7.43			7.67	45.09	61.18	61.12
A9	NiCuCuCu			0.25	0.33	32.0	0.75	0.95	26.7	N/A	N/A
B9				0.25	0.27	8.0	0.75	0.77	2.7	0.012	0.019

C9				0.25	0.33	32.0	0.75	1.02	36.0	0.021	0.018	
D9				0.25	0.32	28.0	0.75	0.98	30.7	0.003	0.014	
E9				0.25	0.28	12.0	0.75	0.83	10.7	0.015	0.012	
F9				0.25	0.29	16.0	0.75	0.90	20.0	0.002	0.009	
G9				0.25	0.30	20.0	0.75	0.83	10.7	0.010	0.019	
H9				0.25	0.33	32.0	0.75	0.89	18.7	N/A	N/A	
Average				0.25	0.31	22.50	0.75	0.90	19.50	0.01	0.02	
Std. Dev.					0.02	9.78		0.08	11.27	0.01	0.00	
%Avg/Std. Dev					7.99	43.48		9.43	57.78	66.98	27.12	
A10	0.50	0.59	18.0					0.50	0.61	22.0	N/A	N/A
B10	0.50	0.60	20.0					0.50	0.60	20.0	0.030	0.030
C10	0.50	0.56	12.0					0.50	0.57	14.0	0.019	0.026
D10	0.50	0.59	18.0	CuPtPtCu				0.50	0.62	24.0	0.027	0.026
E10	0.50	0.49	2.0					0.50	0.51	2.0	0.017	0.017
F10	0.50	0.60	20.0					0.50	0.59	18.0	0.003	0.013
G10	0.50	0.61	22.0					0.50	0.62	24.0	0.019	0.021
H10	0.50	0.62	24.0					0.50	0.60	20.0	N/A	N/A
Average	0.50	0.58	17.00					0.50	0.59	18.00	0.02	0.02
Std. Dev.		0.04	7.01	CuPtPtCu					0.04	7.25	0.01	0.01
%Avg/Std. Dev		7.09	41.24						6.14	40.28	48.50	28.55
A11	0.25	0.32	28.0					0.75	0.86	14.7	N/A	N/A
B11	0.25	0.29	16.0	CuPtCuCu				0.75	0.85	13.3	0.055	0.059
C11	0.25	0.30	20.0					0.75	0.92	22.7	0.021	0.029
D11	0.25	0.30	20.0					0.75	0.93	24.0	0.060	0.059
E11	0.25	0.28	12.0					0.75	0.87	16.0	0.017	0.023
F11	0.25	0.29	16.0					0.75	0.87	16.0	0.016	0.027
G11	0.25	0.28	12.0					0.75	0.87	16.0	0.011	0.017
H11	0.25	0.41	64.0					0.75	1.28	70.7	N/A	N/A
Average	0.25	0.31	23.50					0.75	0.93	24.17	0.03	0.04

Std. Dev.	0.04	17.16						0.14	19.17	0.02	0.02
%Avg/Std. Dev	13.90	73.03						15.44	79.32	71.37	52.08
A12	0.50	0.69	38.0	0.25	0.32	28.0	0.25	0.34	36.0	N/A	N/A
B12	0.50	0.69	38.0	0.25	0.37	48.0	0.25	0.36	44.0	0.013	0.017
C12	0.50	0.65	30.0	0.25	0.33	32.0	0.25	0.35	40.0	0.061	0.068
D12	0.50	0.68	36.0	0.25	0.33	32.0	0.25	0.33	32.0	0.019	0.020
E12	0.50	0.67	34.0	0.25	0.33	32.0	0.25	0.34	36.0	0.056	0.063
F12	0.50	0.62	24.0	0.25	0.30	20.0	0.25	0.32	28.0	0.062	0.064
G12	0.50	0.67	34.0	0.25	0.33	32.0	0.25	0.34	36.0	0.012	0.020
H12	0.50	0.67	34.0	0.25	0.33	32.0	0.25	0.32	28.0	N/A	N/A
Average	0.50	0.67	33.50	0.25	0.33	32.00	0.25	0.34	35.00	0.04	0.04
Std. Dev.		0.02	4.63		0.02	7.71		0.01	5.55	0.03	0.03
%Avg/Std. Dev		3.47	13.82	PtNiPtCu	5.84	24.09		4.11	15.87	67.08	60.26

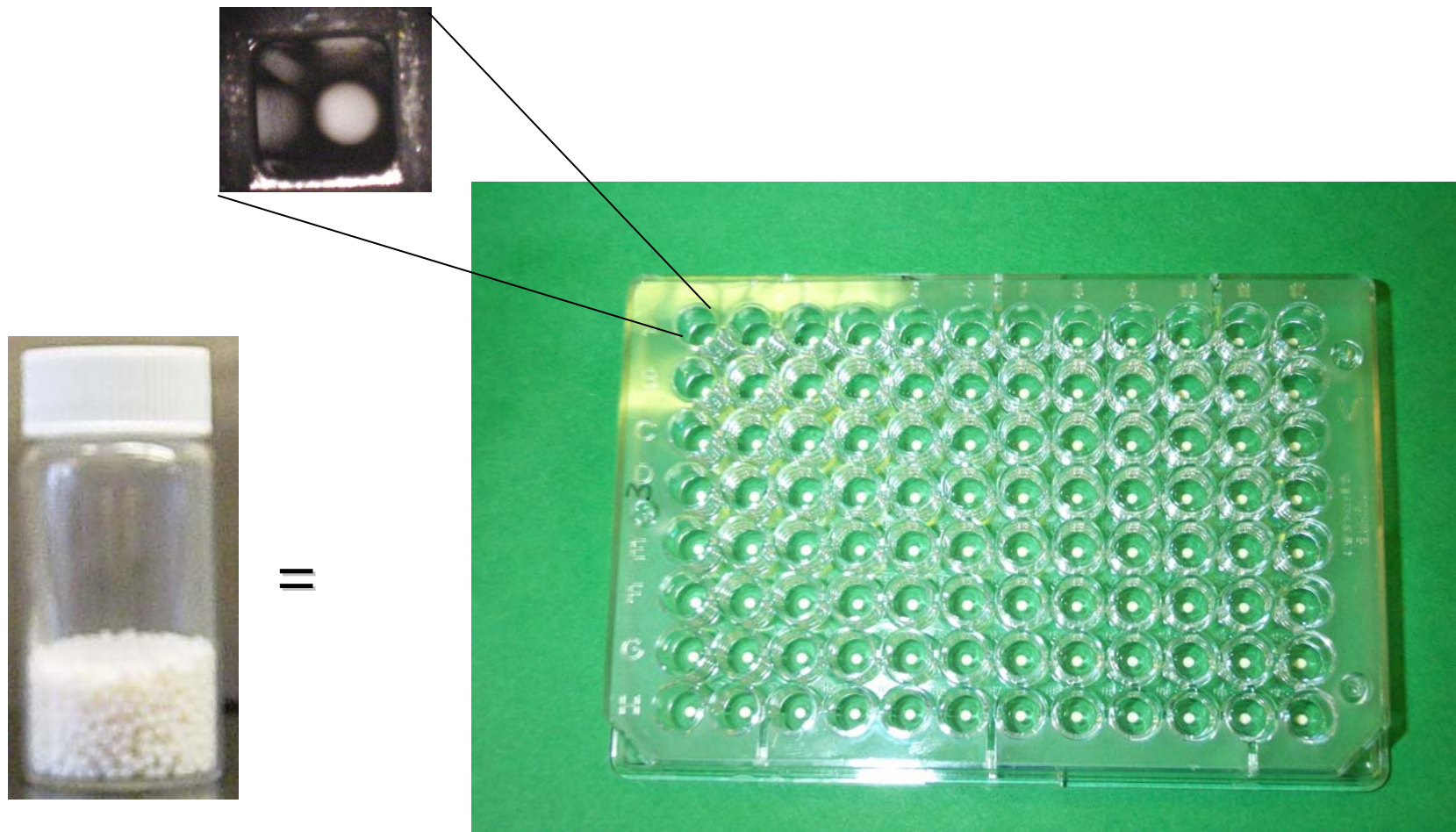


Figure 1.1 Schematic illustrating the advantage of replacing beads in vials by beads in well plates, potentially solving the mixing and tagging problems. Note the wells in each wellplate are indexed by their rows and columns and each wellplate is indexed by a unique identifier.

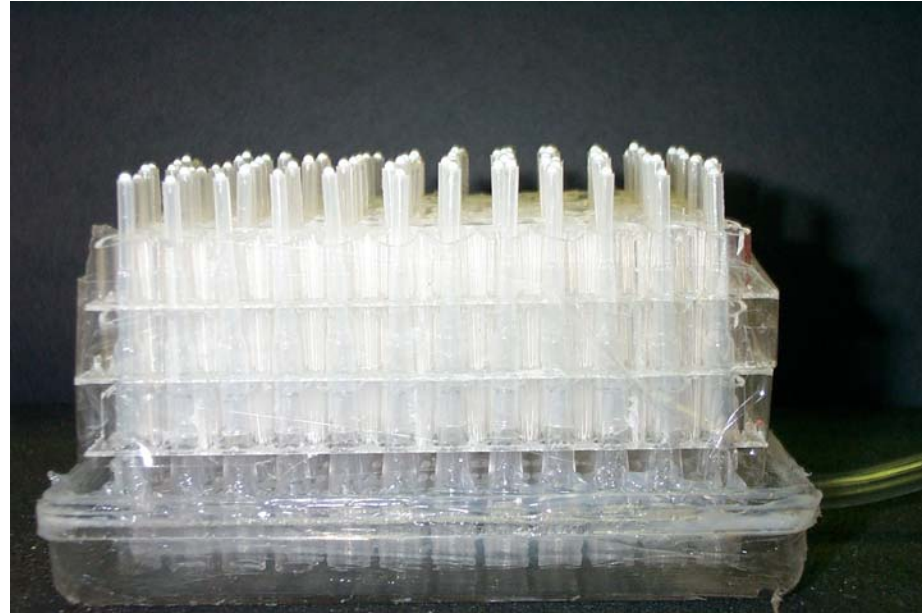


Figure 1.2a Home built device for transferring beads across rows and columns



Figure 1.2b A modified home made device for sorting beads along rows



Figure 1.2c Homemade Multipipette delivering solutions of 0-20 μ l

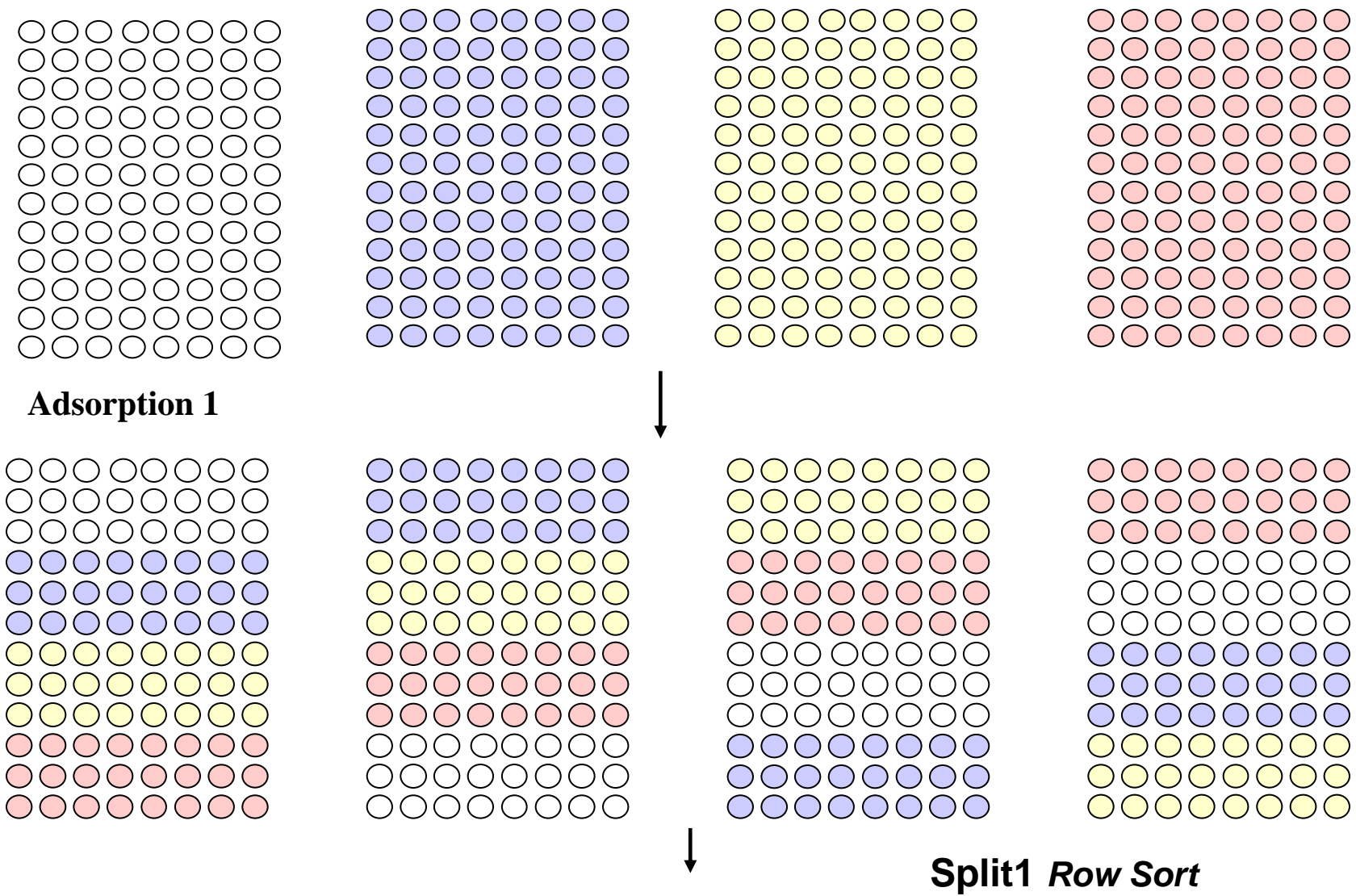
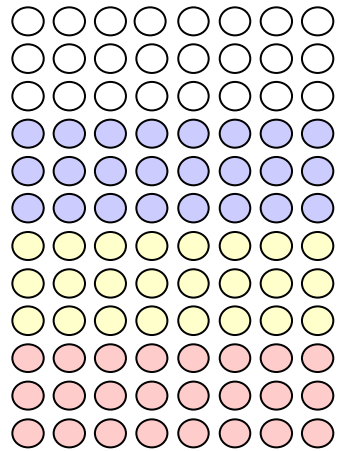
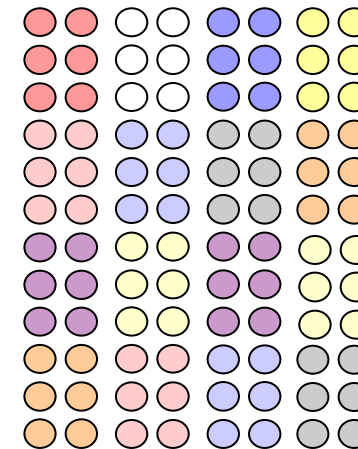
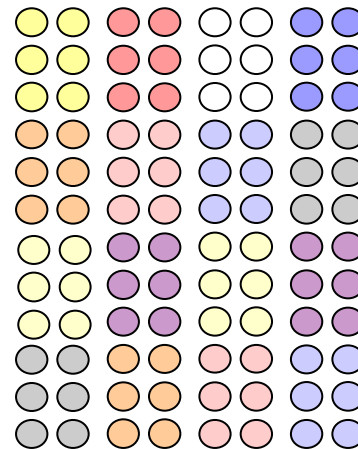
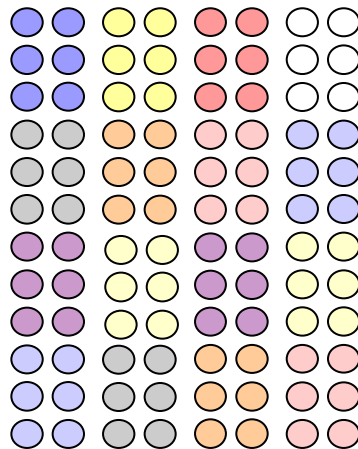
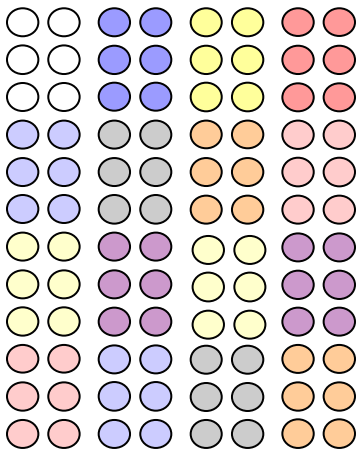
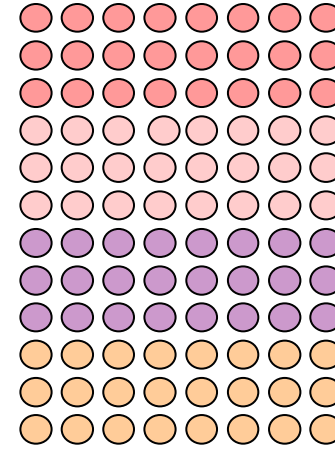
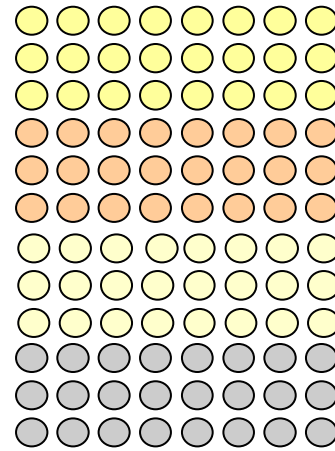
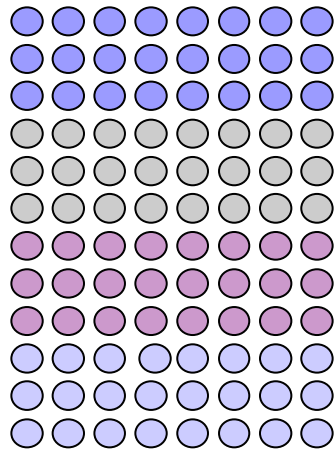


Figure 1.3a Color simulation of first adsorption and first row transfer (first split) of a four component-four step split pool library 57



Adsorption 2



Split 2 Column Sort

Figure 1.3b Color simulation of second adsorption and first column transfer (second split) of a four component-four step split pool library

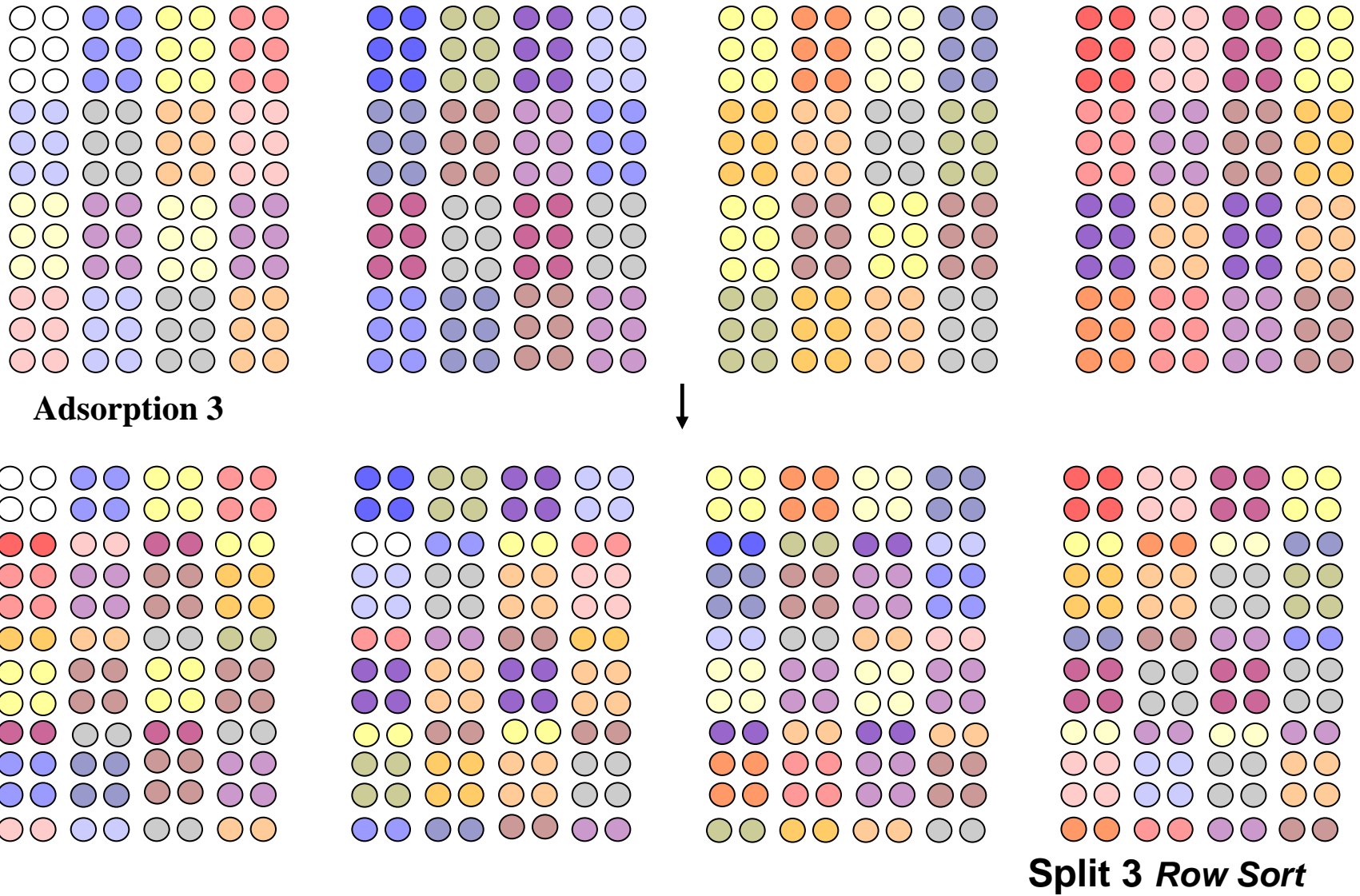


Figure 1.3c Color simulation of third adsorption and second row transfer (third split) of a four component-four step split pool library

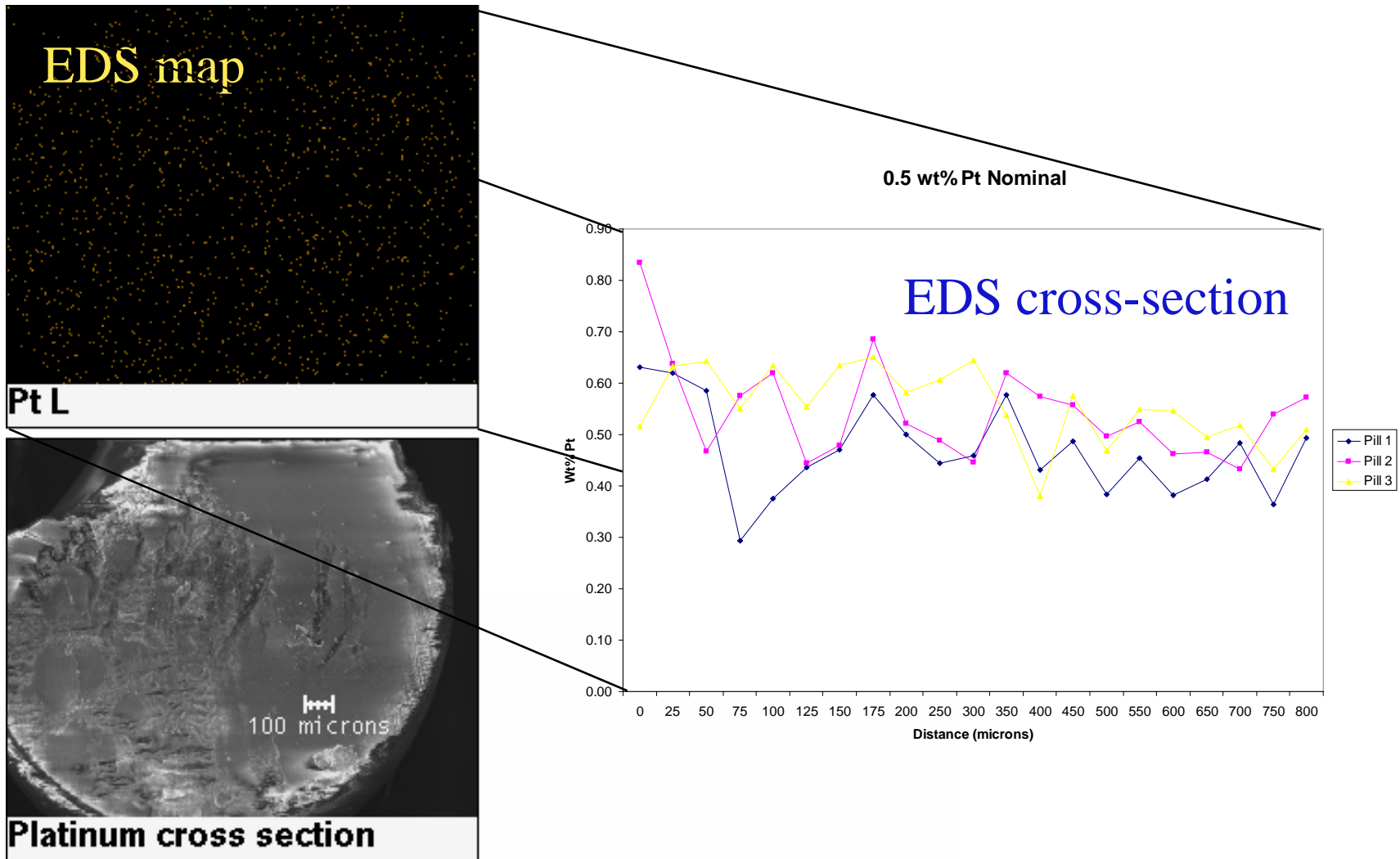


Figure 1.4a Schematic of Energy Dispersive X-ray Spectroscopy (EDS) as a function of position. Each bright spot on the EDS map of Pt L line varied between 3-4 μm .

0.2 wt% Pt Nominal

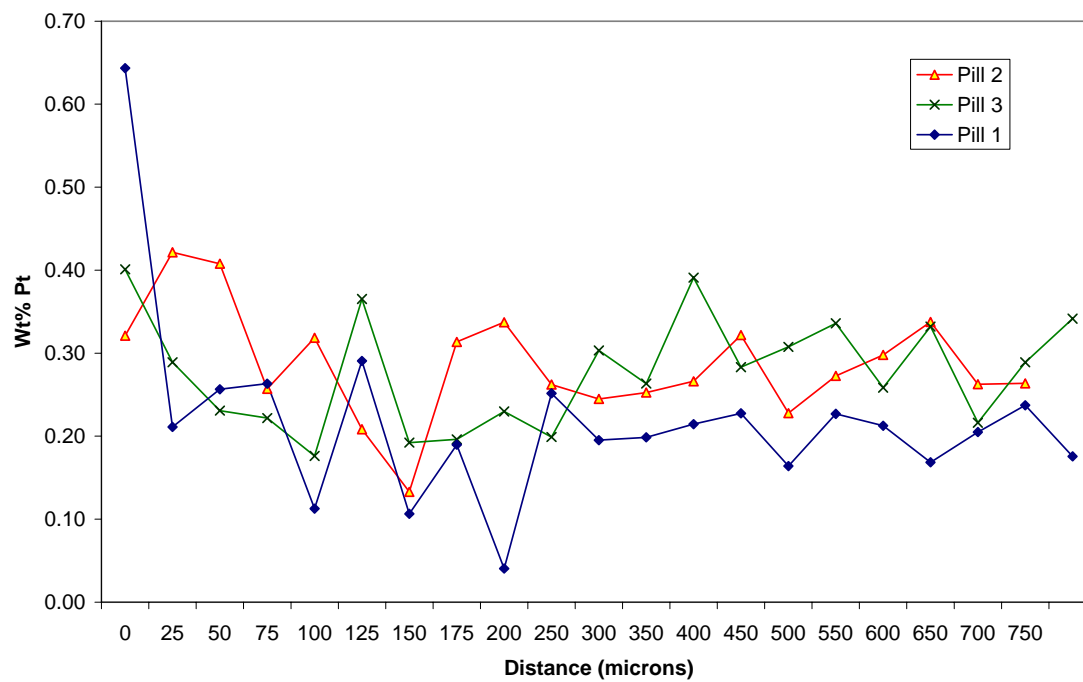


Figure 1.4b Energy Dispersive X-ray Spectroscopy (EDS) as a function of position (0.2 wt% Pt on γ -alumina)

1.0 wt% Pt Nominal

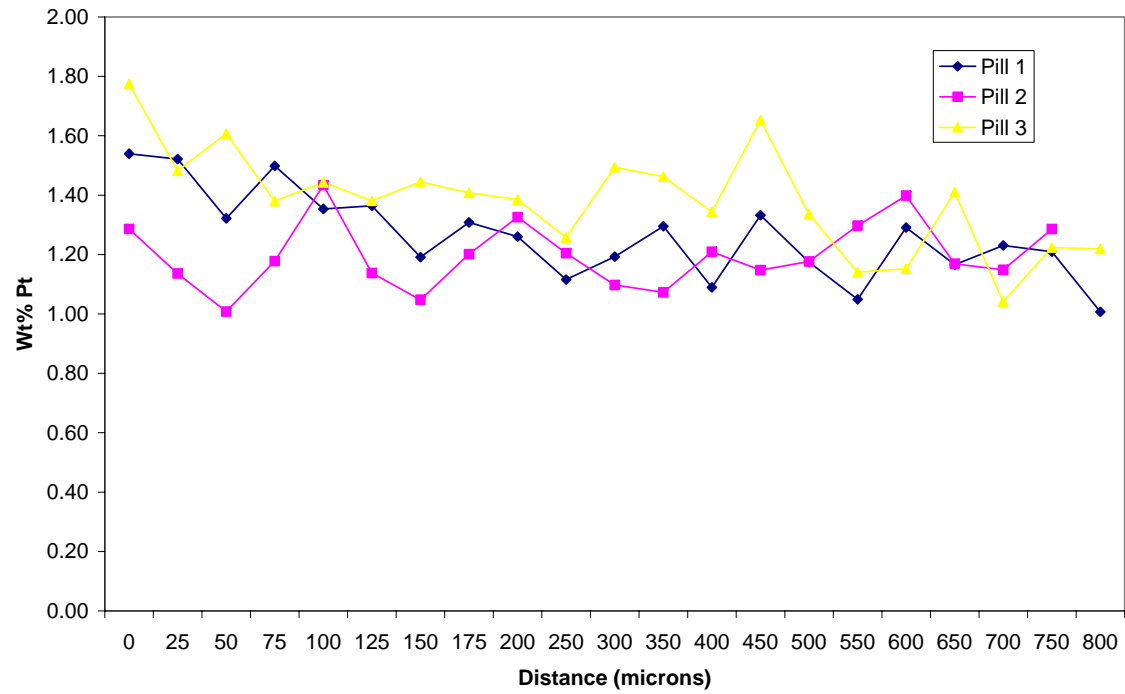


Figure 1.4c Energy Dispersive X-ray Spectroscopy (EDS) as a function of position (1 wt% Pt on γ -alumina)

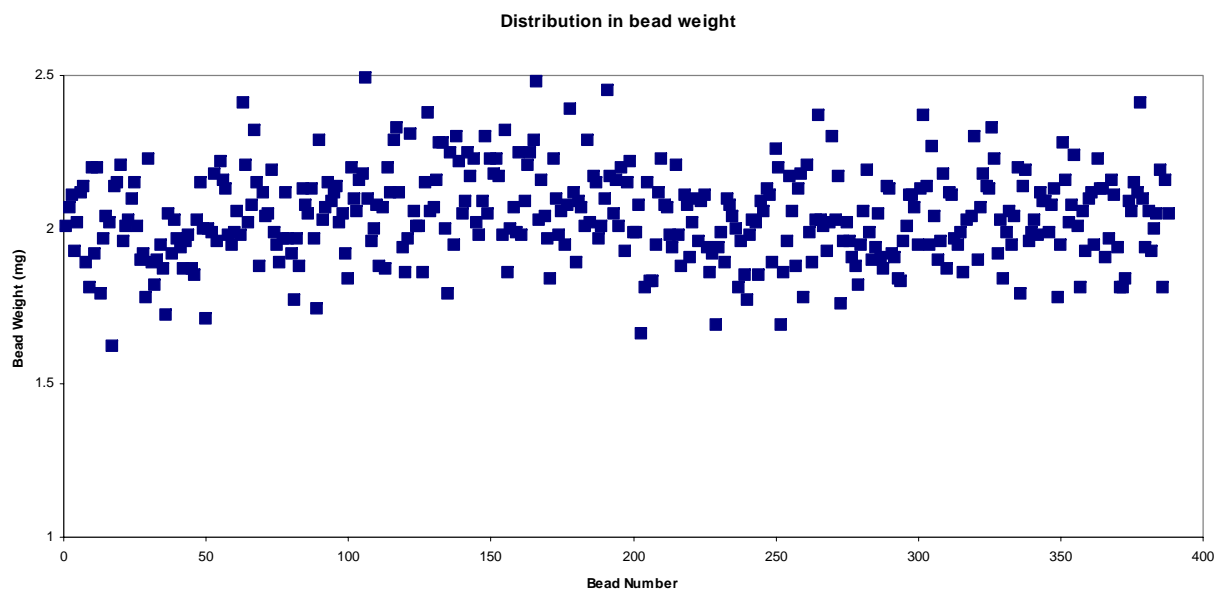


Figure 1.5 Bead weight (mg) versus bead number

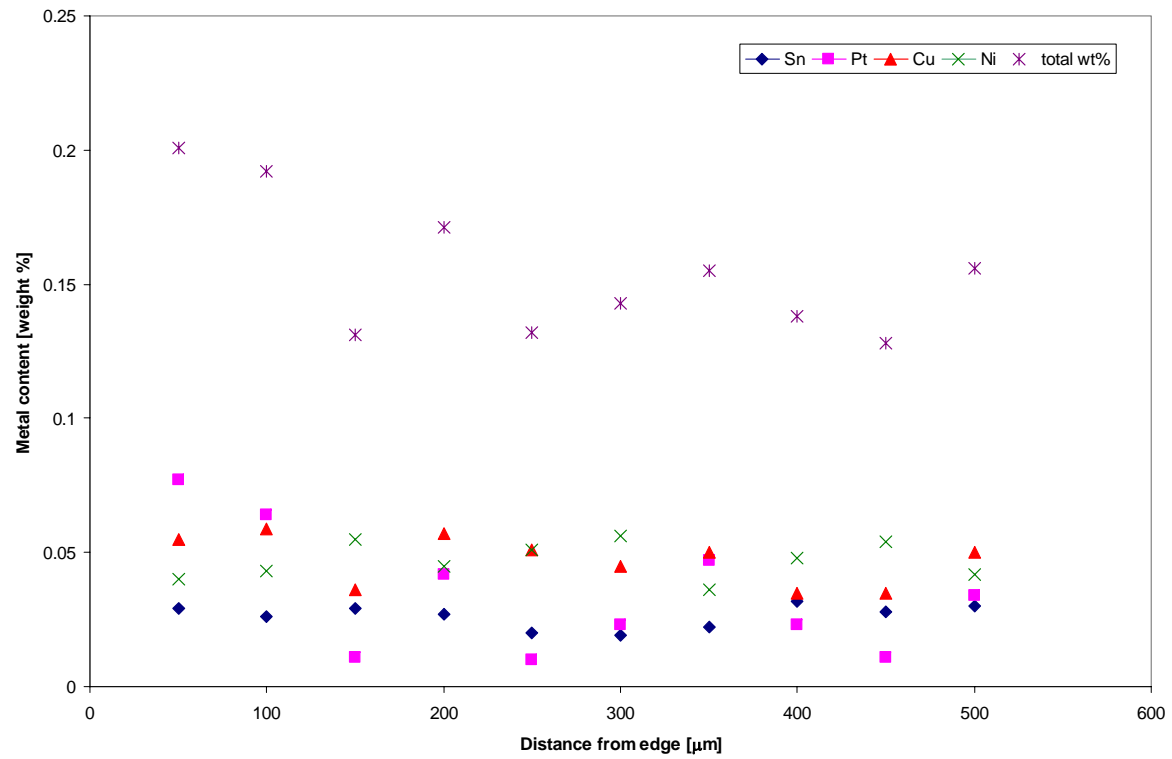


Figure 1.6a Electron Probe Microanalysis (EPMA) of $Pt_{0.05}Ni_{0.05}Cu_{0.1}Sn_{0.05}$. Subscripts indicate metal content in weight%

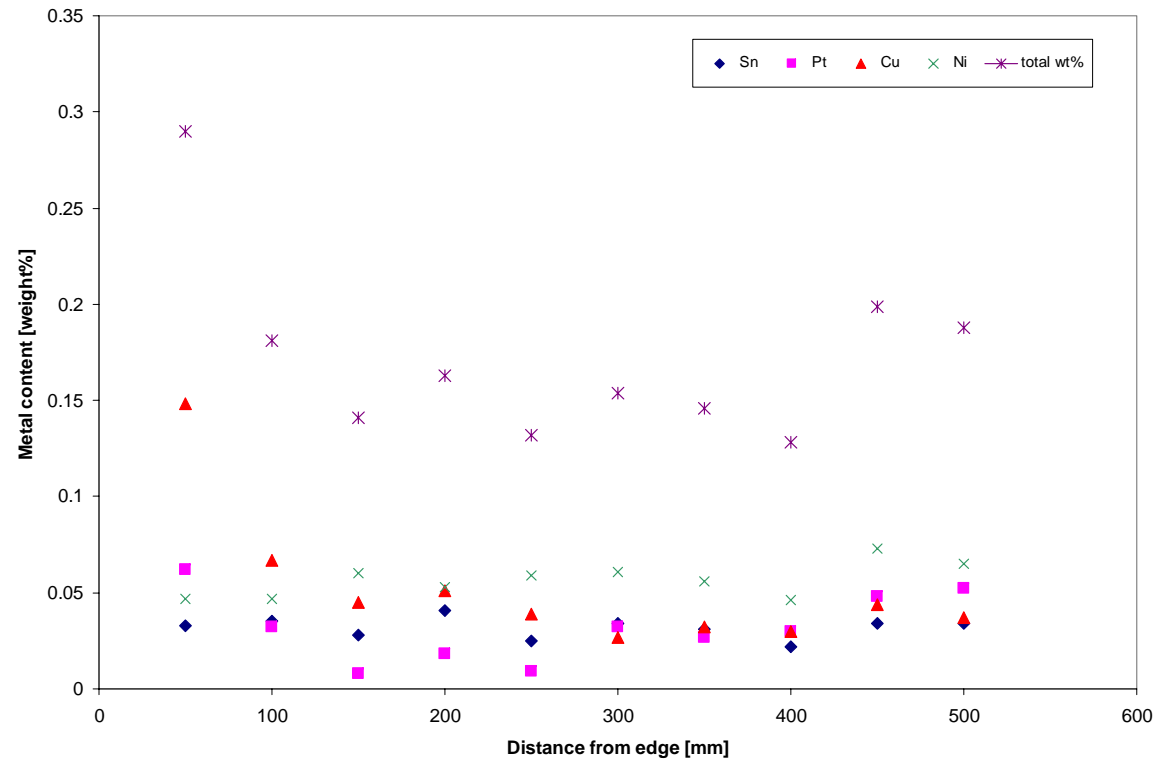


Figure 1.6b Electron Probe Microanalysis of $\text{Pt}_{0.1}\text{Ni}_{0.05}\text{Cu}_{0.05}\text{Sn}_{0.05}$. Subscripts indicate metal content in weight%

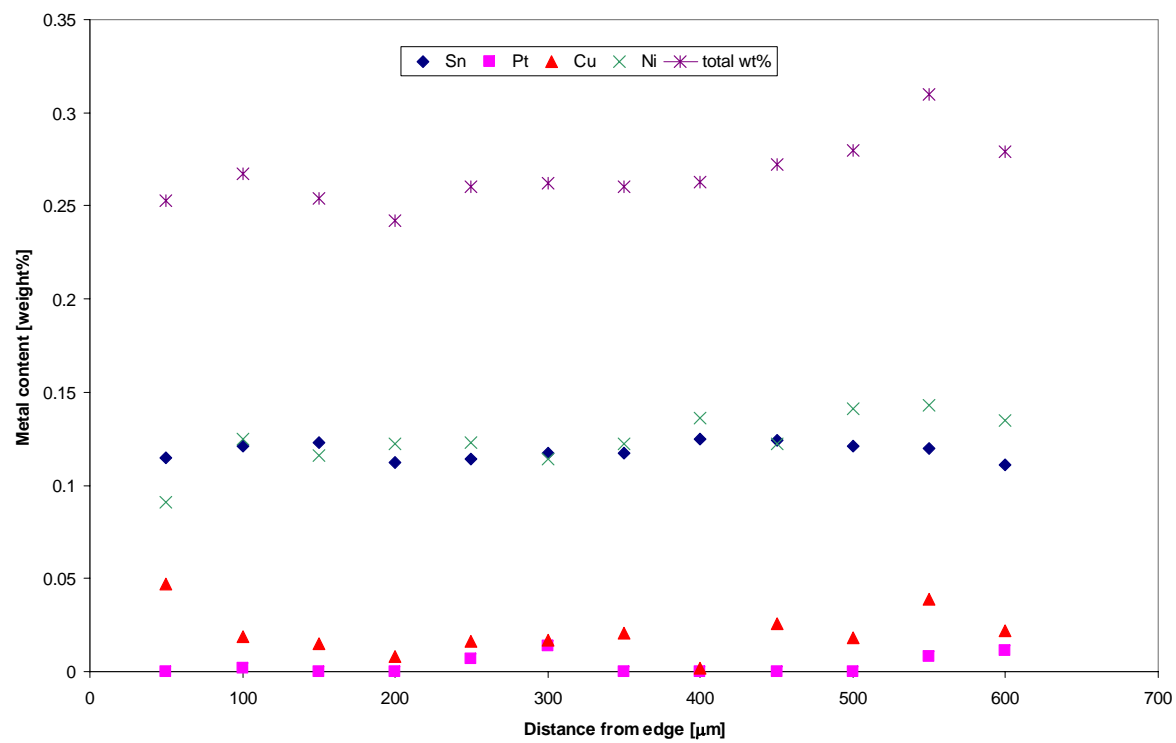


Figure 1.6c Electron probe Microanalysis of $\text{Ni}_{0.15}\text{Sn}_{0.1}$. Subscripts indicate metal content in weight%

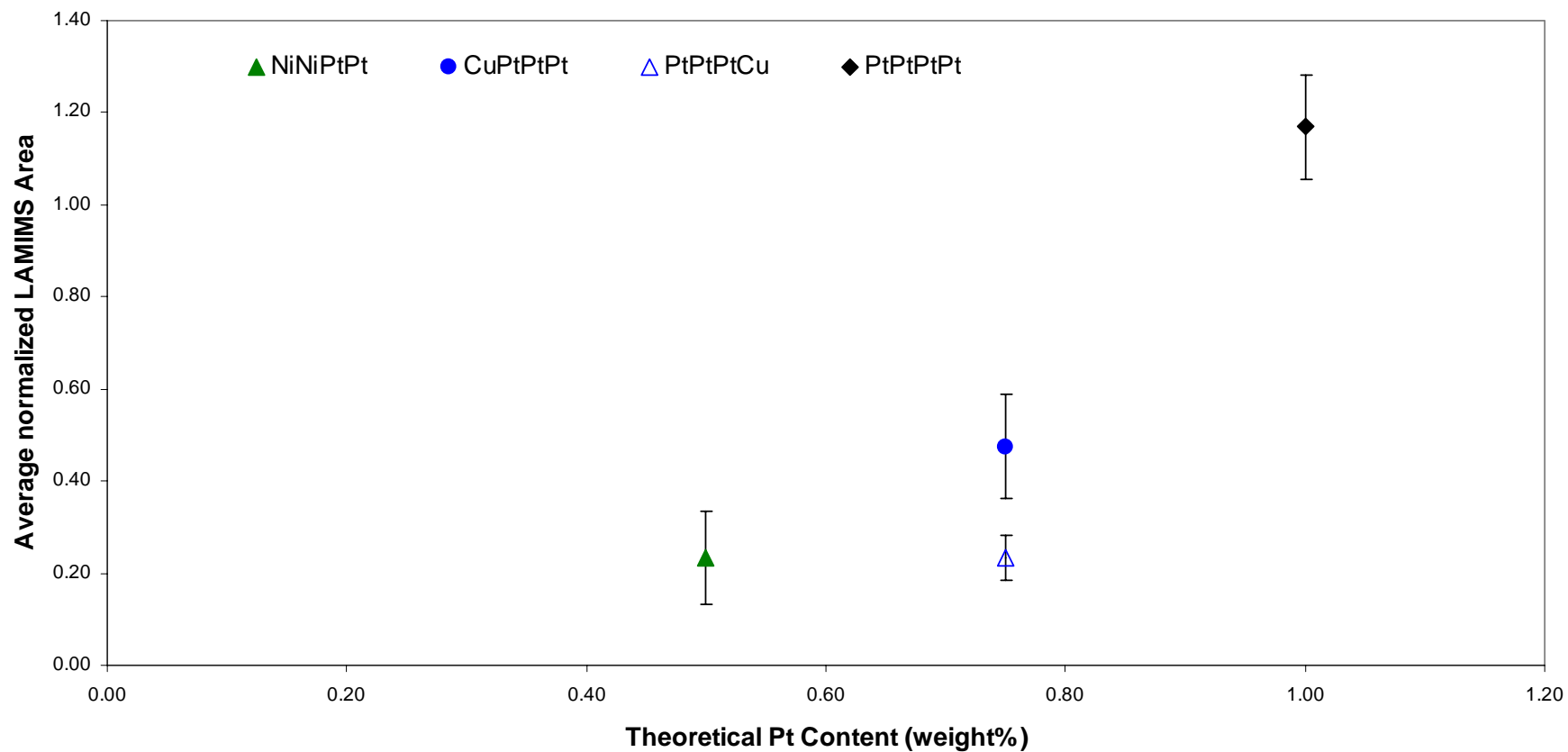


Figure 1.7a Average normalized Laser Assisted Membrane Introduction Mass Spectrometry (LAMIMS) area vs. theoretical Pt content (weight%) for three samples with Pt as last adsorption and one with Cu as last adsorption. Error bars represent standard deviation in normalized LAMIMS area. Order of addition is represented by a four element code following green closed triangles (NiNiNiNi), blue closed circles (CuPtPtPt), blue open triangles (PtPtPtCu) and black closed diamonds (PtPtPtPt).

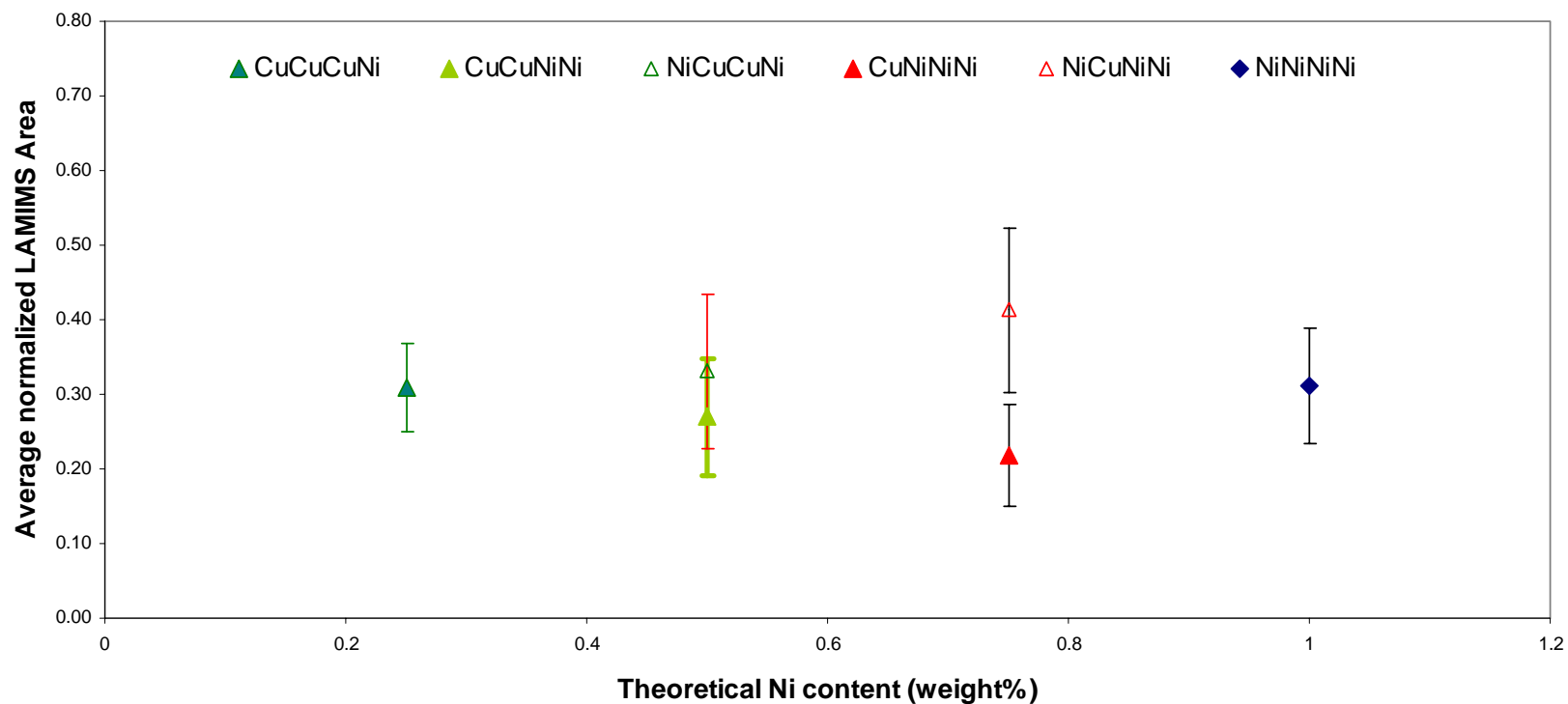


Figure 1.7b Average normalized Laser Assisted Membrane Introduction Mass Spectrometry (LAMIMS) area vs. theoretical Ni content (weight%) for six samples with Ni as last adsorption. Error bars represent standard deviation in normalized LAMIMS area. Order of addition is represented by a four element code following blue closed triangles (CuCuCuNi), open green triangles (NiCuCuNi), green closed triangles (CuCuNiNi), open red triangles (NiCuNiNi), closed red triangles (CuNiNiNi) and blue closed diamonds (NiNiNiNi).

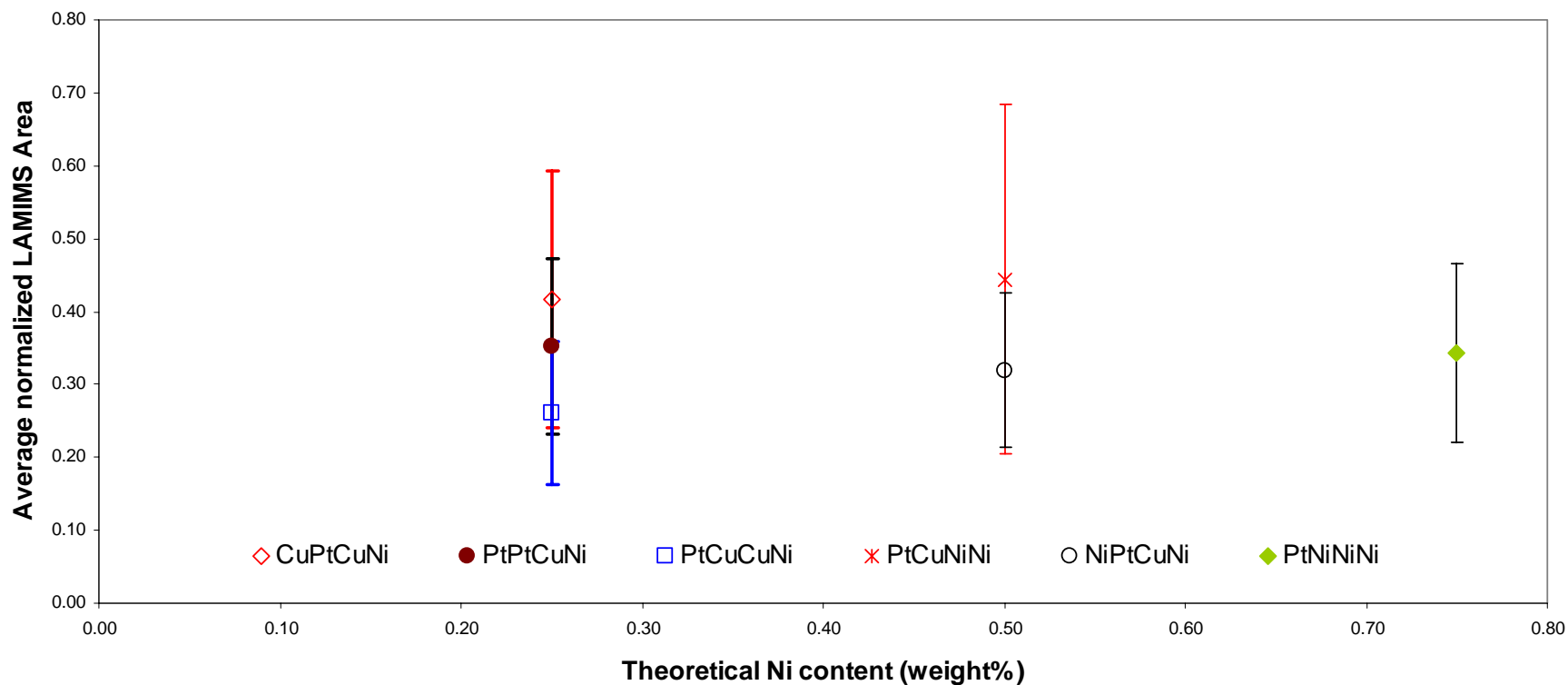


Figure 1.7c Average normalized Laser Assisted Membrane Introduction Mass Spectrometry (LAMIMS) area vs. theoretical Ni content (weight%) for six samples with Ni as last adsorption. Error bars represent standard deviation in normalized LAMIMS area. Order of addition is represented by a four element code following red open diamonds triangles (CuPtCuNi), closed red circles (PtPtCuNi), open blue squares (PtCuCuNi), red asterisk (PtCuNiNi), open black circles (NiPtCuNi) and green closed diamonds (PtNiNiNi).

Chapter 2 Studies on electrocatalysts and fuel cells

Introduction

This chapter focuses on investigations on fuel cells. This chapter illustrates some of the characterization, half cell and fuel cell tests typically followed during the search for electrocatalysts. The purpose is to outline some of the experimental protocols enroute to reliable, reproducible testing of electrocatalysts in actual fuel cells, logical reasons for our choices and to analyze transport effects with physical scaling criteria rather than numerical curve fitting or simulation.

This effort involved a large number of people over the years with sporadic collaborations. The initial work in our lab focused on searching for new catalysts by combinatorial methods and testing promising candidates in small (5cm²) fuel cells. The fuels investigated included hydrogen, methanol and reformat gas (a mixture of CO and H₂) and O₂ as the oxidizer. The experimental section of this chapter describes attempts in pursuing this approach. Primarily, I was involved in testing electrocatalysts in fuel cells by setting up a fuel cell testing station briefly described on page 86, and in testing methanol tolerant catalysts in a modified three-electrode cell discussed on page 94 and characterizing them. I also attempted the synthesis of electrocatalysts for methanol and reformat gas electro-oxidation but the catalysts I prepared yielded no current in fuel cell tests.

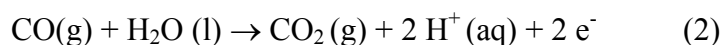
Background

Fuel cells are electrochemical engines that are being studied as possible sources of clean power. One of the claims from an environmental standpoint is that most fuel cell prototypes emit almost no pollutants as compared to internal combustion engines, which is valid assuming we have clean fuel sources. Applications envisioned for fuel cells include automobile power, portable electronics and on-site power generation.

A cross-sectional view of a solid polymer electrolyte fuel cell is shown in Figure 2.1a. The cell consists of two catalyst layers (about 10 μm thick) separated by a proton exchange membrane (usually Nafion® about 50-175 μm thick). The catalyst membrane assembly is known as Membrane Electrode Assembly (MEA). The fuel used is a liquid (methanol) or a gas (H_2 , H_2+CO or natural gas). The oxidant used is usually air or oxygen. The catalysts used in these cells are usually Pt or Pt alloy clusters dispersed on carbon. The fuel is oxidized on the anode and oxidant reduced at the cathode and power drawn across the cell. Figure 2.1b shows a single cell. To meet the power requirements for automobiles, portable electronics or on-site power generation, many such cells are connected in series or parallel to build up voltage and current. Conceptual advances in porous electrodes by Cahan, Justi, Westphal, DeLevie and Wagner [1-5] and practical advances in fabricating porous electrodes and reducing catalyst loading and thickness by Srinivasan, initially at Texas A&M and later at Los Alamos National Laboratory [21, 68] and Wilson and Gottesfeld [10] made large advances to turn an electrochemical vision to commercial reality and was used effectively by Dyer [78]. The hope of using alcohols as fuels has prompted re-examination and application of concepts in $\text{H}_2\text{-O}_2$ cells.

Non-predictive models for reformate gas electro-oxidation

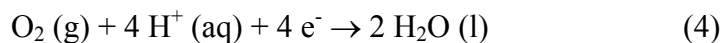
The most common anode reaction for PEM fuel cells is the oxidation of hydrogen (1), often accompanied by oxidation of CO (2) if hydrogen is produced by reforming an oxygenated hydrocarbon fuel.



The hydrogen oxidation reaction is kinetically facile at Pt-catalyzed electrodes and takes place at values close to equilibrium defined by reaction (1) i.e., 0-10mV. In feeds containing reformed oxygenated carbons, reaction (1) is inhibited by the adsorption of CO, resulting in losses of about 250 mV. A second anode reaction that occurs in direct methanol fuel cells (DMFC's) is the oxidation of methanol (3), a six-electron reaction, mechanistically complex and resulting in a loss of about 300 mV.



The cathode reaction in PEM fuel cells is the reduction of oxygen to water (4), a four-electron process and also a source of large voltage losses (~ 300 mV)



The total cell voltage is the difference between the cathode and the anode potential (assuming no resistance losses at the membrane). An ideal fuel cell operates at 1.23V. Voltage losses on the cathode due to oxygen reduction kinetics lower the operating voltage to 0.8V, at practical current densities of about 100 mA cm^{-2} . Anode losses due to CO in the fuel or due to sluggish kinetics of alcohol electro-oxidation reduce the operating voltage to 0.55 V. Resistance losses of 50 mV due to the membrane, lower the operating voltage to 0.5V, at temperatures between 60-80°C. Figures 2.2 and 2.3 schematically illustrate the above concepts.

The metal of choice during early studies on electrocatalysis was Pt [21-24, 27-33]. Pure Pt was considered to be a poor catalyst for oxidizing methanol completely to CO_2 due to the formation of adsorbed intermediates (CO , $\text{C}_x\text{H}_y\text{O}$) following seminal work by Bagotsky [32] and Breiter [31] and confirmed in experiments that followed in the 1990s [27-33]. Studies with adatoms and alloying elements such as Ru and Sn with Pt [24,27b], showed that methanol oxidizes at lower voltages compared to pure Pt and several models have been proposed to explain this effect, drawing parallels from developments in heterogeneous catalysis [24,27,50]. One of the models, the bifunctional mechanism [26,27], proposes that oxophilic elements, such as Ru that alloy or physically contact Pt clusters, adsorb water needed in reaction (2) more efficiently. This model has found experimental evidence in many studies on well defined bulk alloys [28] and some studies on working electrocatalysts [24,25,33]. A second model argues the case for a ligand effect, proposing that the d-band occupancy of Pt is changed by alloying elements such as Ru although this model is phenomenological [33]. A third model proposed by Rolison et al. [34] argues that elements such as Ru do not alloy with Pt, but provide a mixed-conductor hydrous oxide phase that improves the contact with Pt and the polymer membrane. This last model has not found support in recent in-situ and ex-situ fuel cell studies on synchrotron sources [63].

Taken together, these models provided us with candidates (Pt, Ru, Sn, W, and Mo) for a parallel search of combinations of metals during the initial phases of this work.

Combinatorial approaches towards electrocatalyst discovery

The combinatorial approach to discovery of electrocatalysts can be traced to the work of Sandstede [14]. Like Mittasch [13], he had no access to robotics or sophisticated synthetic equipment, relying instead on intuition and prior research at Batelle in the early 1900s. A seminal study by Sandstede and co-workers that overlapped the development of the bifunctional model in the 1970s gave a few pointers in the choice of metals as possible candidates including Ru, Os, Sn, W, and Mo. Sandstede and co-workers also mapped out single elements, binaries, ternaries as a function of potential at an appreciable current density ($\sim 100 \text{ mA cm}^{-2}$) in a serial manner i.e., one composition at a time in three-electrode cells. Using studies based on metallic sheets and high surface area powders synthesized by the Raney method, Sandstede and co-workers identified Os as a candidate element having comparable activity as Pt, with no prescription about phases, solubility or stability. An often ignored work from Shell Labs [24] identified electrocatalysts containing Pt-Ru with small amounts of lanthanum in the 1960s and 70s after exhaustive search of the periodic table, limiting themselves to binaries and ternaries. This kind of approach can be traced to the work of Arico et al. in the 1990s [35]. Arico et al. [35] extended the search of combinations of elements to quaternaries and identified Sn and W co-precipitated with Pt and Ru as a promising composition based on studies in three-electrode cells using methanol in sulfuric acid as the electrolyte, and on actual fuel cells.

The work of Reddington et al. [17] demonstrated an indirect optical detection of electrochemical half-cell reactions and was the first high throughput screening method applied to fuel cell catalysts. The word “high throughput” in this work referred to simultaneous evaluation of 220 combinations of 4 elements and the screening method used was onset of fluorescence. The optical technique is indirect i.e., the evaluation of activity (current) of a given electrocatalyst is measured indirectly by the onset of fluorescence at a given electrode potential. The electrode potential serves to correlate with the energetics of a given reaction, and the idea was to look for onset of fluorescence at lower electrode potentials. This method was originally developed to search for improved DMFC anode catalysts and claimed an improved quaternary catalyst

containing Os and Ir in addition to Pt and Ru compared to a commercial Pt-Ru 50-50 at % catalyst from Johnson Matthey. The search followed the reasoning by Ley et al. [15] that adding Os to Pt-Ru enhanced the catalytic activity of Pt-Ru towards methanol oxidation based on the oxophilic mechanism. The results of the initial papers were very surprising for the following reasons:

- a) Concentration dependence for electro-oxidation of methanol in fuel cell tests, which is highly unusual in the history of oxidation of organic alcohols [18].
- b) Claims of enhancement over a commercial catalyst [17].
- c) Claims of discovery of compositions with open circuit potentials between 150-220 mV; Pt₃₇Ru₄₃Os₁₄Ir₆ with open circuit potential of about 220mV, Pt₅₁Ru₃₃Os₁₀Ir₆ with open circuit potential of about 200mV, Pt₄₇Ru₂₉Os₂₀Ir₄ with open circuit potential of about 150mV, lower than 250-300mV that is characteristic of state of the art catalysts and of Pt₅₀Ru₅₀ in the same study [18].

A closer analysis of the original work [15,16] that laid the original basis of combinatorial searches in our lab, revealed negative currents in the potential window of interest (0 to 450 mV) as shown in Figure 2.4a. These negative currents indicate cathodic reduction or background cathodic reactions, possibly due to secondary reaction, not due to methanol electro-oxidation (a reaction involving anodic oxidation and positive currents in the potential window of interest). If we assume that the potentiostat in the work was configured to indicate that anodic currents were held negative and assuming that the data collected at potentials positive of 450mV were collected during the same run, our original assumption about configuring the potentiostat is moot. The concentration dependence claims [18] have not been independently verified to date, nor was the cathode potential [18] checked to account for cathodic polarization contributing to the fuel cell curves shown in Figure 2.4b. The pseudo-reference electrode was assumed to be stable without verification, despite earlier mention in the literature of drifts in the pseudo reference electrodes [10] and recent re-verification of this phenomenon [67]. The catalysts used in the work [17,18] were synthesized by Dr. Sarangapani, a co-author of the paper, and there are no clear statements, either in the reviews of Mallouk and Smotkin [47a] and Smotkin and Diaz-Morales [47b], or in the Ph. D. theses of Reddington [72] or Gurau [18b] or in the papers themselves [17,18a], if the samples used in fuel cell tests [17,18,72] were checked to see if the optical screening

experiments correlated with fuel cell tests. As the catalysts were not checked by the optical screening experiments (valid in the absence of documented evidence), the hypothesis inherent in [17, 18] that combinatorial screening experiments translate to realistic correlations in fuel cell tests or point out to compositions that might be active in fuel cells are not substantiated by these papers and theses. Enhancement of activity of home made catalysts compared to commercial catalysts is found in the literature [70] often without adequate justification or testing under rigorous conditions. A typical claim is in the paper by Reetz et al. [70b], I quote from page 7419, “These electrocatalysts, which are of the Smotkin/Mallouk type, are more efficient than commercial Pt/Ru-based catalysts because they show an unusually high resistance to CO poisoning”. Analysis of fuel cell polarization curves in the kinetic window i.e., (0.9-0.7V) and 0-100 mA cm⁻² does not warrant their conclusion. Using current-voltage behavior at high current density i.e. 200 mA cm⁻² and above, is not enough evidence to claim “high resistance to CO poisoning”. To justify claims of poisoning, experiments that account for H₂ and CO utilization are required and this paper does not address those.

The reviews by Smotkin *et al.* [47a and 47b] and a paper by Lei *et al.* [66] argue that “concentration-dependent current–voltage curves together with CD₃OH and CH₃OD kinetic isotope data have shown unambiguously that C–H bond activation becomes a kinetically comparable effect within the fuel cell relevant potential regime for two high-performance mixed metal catalysts (PtRu and PtRuOsIr). At potentials above 0.4V, C–H activation becomes the dominant barrier to methanol oxidation.” Parsons [83], Damjanovic and Bockris [53, 57, 71] analyzed steady state rotating disk electrodes and transient stationary electrodes to elucidate mechanisms which explicitly account for the concentration of product(s) and intermediates. They also analyzed diagnostic criteria for reaction mechanisms based on the pseudoequilibrium approximation, stoichiometry and based on number of electrons before and after a clearly defined rate determining step following Vetter [84]. The work by Smotkin and Diaz-Morales [47b] and Lei et al. [66] was unclear on the mass transport normalization and on the choice of the concentration of product(s) and intermediates or on the clear definition of a rate determining step i.e., clearly define the first, second or third proton attached directly to the carbon or the hydrogen that is part of the –OH group in methanol. Their analysis does not clearly mention if they followed the steady state or pseudoequilibrium approximation or delineate diagnostic criteria that

supported their arguments. Therefore, conclusions based on unsubstantiated normalizations and analysis of raw polarization curves in [66], do not argue for a change in mechanism or support the claim by Smotkin and Diaz-Morales [47b] and Lei et al. [66] that “Ir substantially improves the performance of PtRuOs as a DMFC anode”. It is also not clear to the author of the current chapter that the currents observed during the experiments [17, 18] were the result of faradaic methanol electrooxidation; and not due to oxidation of any of the metals or metal oxides present in the samples to higher oxidation states, as illustrated in the work of DiSalvo and co-workers [74]. Unless the data are reproduced and the observed current correlated to faradaic methanol electro-oxidation, the claims in [17, 18, 47 and 66] are moot. I also question the relevance of dropping 400 mV on the anode, when I would like to operate close to equilibrium i.e., 20mV or at worst operate by dropping 250mV at open circuit and 62mV per decade of current on the anode, with state of art catalysts.

The optical detection scheme discussed in the above papers [17, 18] has been applied to search for improved catalysts for regenerative fuel cells [42, 51] and electrochemical glucose oxidation [51c] using 715 combinations of 5 elements. A ternary catalyst containing Pt, Ru and Ir was identified for regenerative fuel cells [42, 51] based on studies on a three-electrode gas diffusion cell shown in Figure 2.10, without explicit estimation of flowrates of the oxidizer. Non-linear regression and curve fitting was used to delineate kinetic and transport limited currents without explicit analytical expression for limiting currents. Thus a mathematical model served to delineate kinetic currents for a physical system whose flow rate was never estimated.

Schmidt *et al.* [65, 69] studied the difference in limiting current densities as a function of Nafion film thickness surrounding the catalyst using the Koutecky-Levich plot under RDE conditions for a unique catalyst; Pt on carbon. They found that sum of kinetic current corrected for Nafion film thickness decreased by a factor of four (40 to 10 mA cm⁻²), nonlinearly for an increase in Nafion film thickness by a factor of 32 (125 nm to 4μm), with a decrease in corrected kinetic current by a factor of two over a narrow range of thickness (500 to 125nm). They concluded that film thickness correction for diffusion was negligible at thickness less than 500 nm using H₂ as the reactant though the corrected kinetic current differed by a factor of 2 with thickness over this range. Schmidt *et al.* [65, 69] followed mathematical formalism documented by Bard *et al.* [6],

treating polymer films on modified electrodes as films in series and added a correction factor explicitly accounting for kinetic current based on modeling the Nafion film as a Nernst type diffusion layer. They then assumed a linear variation in concentration with distance with little theoretical justification. Assuming this linear approximation was valid, they estimated the total current as “ $1/i = (1/i_l + 1/i_k + 1/i_f)$,” where, i_f the film current, was modeled as a product of diffusion coefficient times solubility of the reactant in the film multiplied by total number of electrons and Faraday’s constant, divided by thickness of the film. They calculated a permeability (product of diffusion coefficient and the solubility) of H_2 in the film as $7.8 \cdot 10^{-12} \text{ molcm}^{-1}\text{s}^{-1}$ based on a non-linear fit of data over the entire range of thickness. The calculated product of diffusion coefficient times solubility of the reactant in the film was a factor of 100 lower than the theoretical product of diffusivity ($3.7 \cdot 10^{-5} \text{ cm}^2\text{s}^{-1}$) and solubility ($7.14 \cdot 10^{-6} \text{ molcm}^{-3}$) of H_2 in H_2SO_4 [8]. Schmidt’s [65, 69] study showed that the Nafion film thickness presented a larger barrier to estimating transport effects than considerations of hydrodynamics at the catalyst alone, confirming the earlier theoretical and experimental work by Durand [38, 39], Ozil [39] and Watanabe [11]. A plausible explanation for the difference in estimated and theoretical permeability of protons was in the variation in proton self diffusion co-efficient in Nafion using Pulse-Field Gradient NMR by Slade *et al.* [64]. Slade *et al.* [64] found the proton self diffusion co-efficient in Nafion to vary between 10^{-6} and $10^{-7} \text{ cm}^2\text{s}^{-1}$ for acid pre-treated membranes and about $10^{-8} \text{ cm}^2\text{s}^{-1}$ for membranes treated in deionized water at 298 K. Interestingly, the oxygen diffusion co-efficients are in the same range as that of protons in Nafion (values between 10^{-6} and $10^{-7} \text{ cm}^2\text{s}^{-1}$) at similar solubilities ($7.14 \cdot 10^{-6} \text{ molcm}^{-3}$), though the experimental and theoretical values for diffusion of oxygen were on the same order of magnitude as documented by Parthasarathy *et al.* [45], Zook *et al.* [12] and reconfirmed by Holdcroft *et al.* [46].

Based on the permeability of H_2 in the film, we can estimate that the error in neglecting Nafion thickness would roughly scale as the ratio of permeability of reactant in the film versus permeability of the same in solution, assuming the film/solution interface has no resistance to the measurement. The author of this chapter believes that the film current approximation is more physically realistic than neglecting the same. Parthasarathy’s *et al.* [45] work found that Nafion films block access to catalyst sites and a linear correlation with bare electrodes was unwarranted.

Further, Schmidt *et al.* [65, 69] found that the sum of the inverse kinetic ($1/i_k$) and inverse film thickness ($1/i_f$), was on the order of 20-40 mA cm⁻².

Every *et al.* [81] estimated the methanol diffusion coefficients in Nafion 117, and found it to increase from 2.9×10^{-6} to 4.0×10^{-6} cm² s⁻¹ in the concentration range between 0.5-8M methanol. They found upon increasing the methanol concentration, Nafion 117 showed a steady increase in mass and experimentally determined that for Nafion, water and methanol are partitioned equally within the membrane, i.e. the methanol concentration within the membrane was the same as in solution. They estimated a solubility of 1 molcm⁻³ for methanol and found that the permeability of methanol in Nafion 117 scaled as its diffusivity, confirming work by Cussler [82]. Based on the permeability of methanol in the film, the error in neglecting Nafion thickness would roughly scale as the ratio of diffusivity of methanol in the film versus diffusivity of the same in solution, assuming the film/solution interface has no resistance to the measurement. Further, it is unclear to the author of this chapter if the approximation by Schmidt *et al.* [65, 69] of a linear variation in concentration of methanol with distance in the Nafion film would be valid following Every's [81] documented swelling of Nafion in methanol i.e., the swelling phenomenon calls for a more realistic model at the membrane/electrode interface, perhaps following advances in polymer-solvent theory by Duda [85].

Assuming that the concentration of oxygen in the work on regenerative fuel cells [42, 51] was sufficiently high i.e., data were not transport limited by flux of oxygen to the catalyst surface, the work does not address the issue of Nafion film thickness or estimate the magnitude of the same in their cell or correct for Nafion film thickness in treating mass transfer. Assuming that the thickness of Nafion was the same for every catalyst tested in 3-electrode cells, the correction does not explicitly account for film thickness in estimating corrected kinetic current. Thus, the results in this paper [42, 51] do not quantify mass transfer in their cell and cannot be used to draw any conclusions about intrinsic electrocatalytic activity. In addition, there was no physical explanation, justifying ignoring the Nafion film thickness and the approximations used.

A binary catalyst containing Pt and Pb was identified for the electrochemical oxidation of glucose [51c], based on three-electrode tests, wherein screening experiments were carried out on unsupported catalysts printed onto carbon paper and bulk electrode tests on carbon supported

electrocatalysts. The supported electrocatalysts used in the glucose experiments were not checked by optical screening to see if the optical screening experiments correlated with bulk catalyst tests in three-electrode cells. Thus, it is also not clear if optical screening experiments correlated with bulk catalyst tests in three-electrode cells. The use of two transient techniques in-situ, cyclic voltammetry and rotating electrode studies, makes it unclear to determine if both Pt and Pb are required in electrocatalysts operating on treated carbon and if there is a change in mechanism when Pb is added to Pt on treated carbon electrocatalysts. Pb is known to dissolve at 400mV [80] and the data on glucose oxidation [51] is not enough evidence to justify any claims of “poisoning” effects, “acceptable stability” or “inhibition of adsorption of oxidation products” [51]. There were no data presented in this work to correlate the catalytic effect based on linear sweep voltammetry at slow scan rates or chronoamperometry at selected potentials. Both these preliminary claims [42, 51] have not been demonstrated on working fuel cells or real sensors.

Since the publication of the optical detection method, many research groups have searched for electrocatalysts by the combinatorial route relying on claims of greater accuracy and speed [54, 55]. In the designs described in references [54, 55], 64 individually addressable electrode pads, were fabricated using lithographic techniques on an insulating quartz wafer. The electrode pads provided electrical contacts to the catalytic electrode materials to be deposited thereon, interfacing the materials library and a multichannel potentiostat/galvanostat. The combinatorial library was synthesized using rf-magnetron sputtering and electrocatalysts evaluated using chronoamperometry [54] and cyclic voltammetry [55]. No in-situ fuel cell or battery tests were reported to back up any of the claims. Notable exceptions to using combinatorial methods to increase speed and accuracy are in coupling scanning electrochemical microscopy (SECM) with combinatorial methods by Hillier *et al.* [73] and Fernandez *et al.* [19]. However, these preliminary experiments [19, 73] have not been tested in actual fuel cells at the time of writing this thesis. In addition, Fernandez *et al.* [19] studied screening experiments (SECM) on unsupported catalysts printed onto glassy carbon and rotating disk electrode (RDE) tests on carbon supported electrocatalysts and the correlation between these and fuel cell tests is unclear. However, this work [19] was the first step towards correlating screening experiments (SECM) with bulk catalyst tested by rotating disk electrode studies and conceptually and experimentally addressed mass transfer issues with in-situ (SECM) and ex-situ (RDE) studies. It would be of

scientific interest to see if this work [19] ties up conceptual advances in porous electrode theory [1-5] or test approximations inherent in RDE analysis decoupling hydrodynamics and electrodics [52, 53, 57].

To try to match the fuel cell architecture shown in Figures 2.1 and 2.2, Liu and Smotkin [20] described a parallel testing device that contained 25 individually addressable electrodes. The fuel or oxidizer was introduced through flow fields, and the catalyst/MEA layer was fabricated in the same manner as in fuel cells. Hydrogen was run at the common cathode in order to provide a large area, non-polarizable reference/counter electrode. The authors then tested this cell using the same catalyst (Johnson Matthey PtRu) and loading (1.6 mg cm^{-2}) at 25 spots addressed by the electrodes with 10 ml min^{-1} of 0.5 M methanol at $60 \text{ }^\circ\text{C}$. The individual catalysts were prepared as inks and applied to ELAT carbon, which was cut into disks and hot-pressed into the Nafion membrane. The authors then corrected I-V plots in their data using curve fitting. I quote from page 53 and 54 of Liu and Smotkin [20] “The limiting currents are used to obtain the kinetic currents by mass transfer correcting the raw data according to the following equation $1/i = (1/i_l + 1/i_k)$ ” and “Fig. 9 shows mass transfer corrected the I-V plots. The curves overlap as expected since all electrodes are of the same material and the same loading. This control experiment confirms that depletion of the anode flow field reactant stream is negligible.” Thus, 25 catalysts were “ranked” based on mass transport corrected currents with no explicit analytical expression for limiting currents. The quoted statement has not been backed up with precise quantitative arguments. The work of Liu and Smotkin [20] also does not address the issue of Nafion film thickness or estimate the magnitude of the same in their cell or correct for Nafion film thickness to correct for mass transfer following Schmidt *et al.* [65, 69]. Thus, the results in this paper [20] do not quantify mass transfer in their cell and cannot be used to draw any conclusions about “ranking”. In addition, there was no physical explanation, justifying ignoring the Nafion film thickness and the approximations used.

Liu and Smotkin [20] then tested their cell with a Nafion membrane using four different catalysts for methanol oxidation under the same conditions described above. Four catalysts were “ranked” based on mass transport corrected currents with no explicit analytical expression for limiting currents or as described above, the correction or estimate for Nafion film thickness is absent in

the analysis as is the explanation for neglecting the same. However, when the catalyst composition changed in the array, visual inspection of the “ranking” per catalyst spot varied, possibly due to inhomogeneous flow distribution or subtle transport effects at each electrocatalyst. The word “ranking” deserves some explanation in this context, as the text of the author’s paper is unclear in this regard. The authors used the electrode potential (with respect to a large counter quasi-steady state reference electrode) as the basis for distinguishing the activity of each catalyst (measured in terms of current) and picked the potential window of interest (0.3-0.4V) to the fuel of interest, in this case 0.5 M methanol at 10 ml min⁻¹. Without explicit analytical expressions for each unique electrocatalyst, the authors also argue, I quote from page 54 of Liu and Smotkin [20] “We do not mass transport correct the data of Fig. 10 because the control experiments (Figs. 8 and 9) indicate that mass transport corrections are not needed within the fuel cell regime (i.e. less than 0.5 V).” when Figures 8 and 9 were for a unique electrocatalyst and Fig. 10 shows four different electrocatalysts. Both quoted statements have not been backed up with precise quantitative arguments. As described above, the correction or estimate for Nafion film thickness is absent in the analysis as is an explanation for neglecting the same. Thus, the results in this paper [20] do not quantify mass transfer in their cell and cannot be used to draw any conclusions about “ranking”. In addition, the cell has not been tested in a galvanic mode i.e., methanol as fuel and air or oxygen as the oxidizer to draw any conclusions regarding their applicability in working fuel cells.

During the course of our combinatorial experiments prior to summer 2002, we postulated that some of the problems we had experienced with candidates identified using the optical techniques not translating to working catalysts in fuel cells, were due to the mis-match between the cell geometry in optical experiments with cell designs currently employed in fuel cells. We also postulated that the difference might be due to change in flow patterns and flow rates used in the different experiments. The optical technique is indirect i.e., the evaluation of activity (i.e., current) of a given electrocatalyst is measured indirectly by the onset of fluorescence at a given electrode potential. The experiment was performed with catalysts deposited on large arrays (serving as the working electrode), with a dynamic hydrogen reference electrode and platinum gauze running along the length and breadth of the cell as the counter electrode. To check to see if the optical method qualitatively distinguishes catalysts without reference to orientation and

position in the array, Reddington [72] synthesized identical ternary compositions, rotated 120° to each other and found that the qualitative fluorescence was correlative i.e., orientation and position was not a variable in the experiment involving unsupported electrocatalysts and methanol as the fuel. To see if this held true in supported electrocatalysts, Chan [41] used a commercial catalyst (Johnson Matthey Pt-Ru/C) deposited onto 715 different positions using 100ppm CO in H_2 as the fuel at the same flow rate used in fuel cell tests for comparison (70 ml min^{-1}). Fluorescence was observed at the same potential (100 mV) on all the spots, indicating IR drop, position of the catalysts on the array and position of the reference electrode were not variables in qualitative screening experiments. The test was repeated for two commercial catalysts and these catalysts were tested in fuel cells with very good correlation for the set of catalysts. The optical method suffers from an important drawback that the onset potential in fluorescence does not result in the same onset potential in three-electrode or fuel cell tests. For example in tests involving Johnson Matthey Pt-Ru/C in 100ppm CO in H_2 , fluorescence onset is at 100mV and onset potential in electrochemical and fuel cell tests is on the order of 250 mV. Thus, the test is qualitative at best and serves as a comparison.

To try and quantify the variables involved in optical screening and other electrochemical techniques used in our experiments (rotating disk, linear sweep voltammetry) and quasi-fuel cell tests employed by researchers at the Illinois Institute of Technology, Nuvant Systems and the University of Puerto Rico, Chan et al. [40,41] compared the activity of six anode electrocatalysts prepared by different synthetic methods. Six catalysts were “ranked” by three methods (array fuel cell, linear sweep voltammetry and quasi- steady state fuel cell) with most of the testing done in a “double blind” manner i.e., the author of this chapter held the identities of the catalysts secret prior to testing. The word “rank” deserves some attention here. Ranking in the optical screening experiments referred to the electrode potential (with respect to a traditional reference electrode – saturated calomel) as the basis for distinguishing the activity of each catalyst (measured qualitatively in terms of observed fluorescence) for the fuel of interest, in this case 0.5M methanol at quasi-quiescent conditions. The word “quasi-quiescent” refers to ambient conditions, not taking into account free convection. The position of the reference electrode in the optical screening experiments was not a variable, and the counter electrode was a high surface area platinum gauze electrode running along the length and breadth of the cell. The optical

screening experiments were compared to Linear Sweep Voltammetry in a 3- electrode cell (done at Penn State) and to tests done by authors at the Illinois Institute of Technology, Nuvant Systems and the University of Puerto Rico who used an array fuel cell [20] and a quasi- fuel cell test. The latter authors used the electrode potential (with respect to a large counter quasi-steady state reference and counter electrode) as the basis for distinguishing the activity of each catalyst (measured in terms of current) and picked the potential window of interest (0.3-0.4V) to the fuel of interest, in this case 0.5 M methanol at 10 ml min^{-1} in an array cell [20] and a quasi-fuel cell operating with one anode catalyst and a large counter quasi-steady state reference and counter electrode (cathode). The word “quasi-fuel cell” is used to denote adopting the fuel cell geometry but running the cell in an electrolytic mode, feeding methanol at the anode and H_2 at the cathode.

Chan et al. [40, 41] concluded that the optical method correctly ranked catalysts into “high” and “low” activity categories, but it did not differentiate among the best catalysts. The word “high activity” refers to the lower onset potential i.e., 260 mV and “low activity” corresponds to higher onset potentials i.e., 290 mV in optical screening experiments. The optical screening experiments served to illustrate our observation that the test is qualitative at best while evaluating electrocatalysts. We can therefore legitimately argue that the technique will have limited application when applied broadly to different problems in electrocatalysis. Linear sweep voltammetry correlated well with quasi-fuel cell testing, at the relevant temperature, $60 \text{ }^\circ\text{C}$. Chan et al. [40,41] concluded that the most reliable high throughput method was to obtain anode polarization curves using a 25-working electrode array cell [20] or disk electrode linear sweep voltammetry under conditions that match those of quasi fuel cell i.e., nominally the same potential (in this case 350 mV) and same fuel concentration (0.5M methanol). The experiments have not been run in a traditional fuel cell mode i.e., with methanol as the fuel and oxygen or air as the oxidizer, to check to see if any of the methods used in this study validate the hypothesis inherent in [17,18, 20], that combinatorial screening experiments translate to realistic correlations in fuel cell tests. The results of this study [40] remain to be validated by independent research groups using the same battery of techniques. To add more quantitative information and insight, it would be of scientific interest to study the effect of the different techniques using well-defined metal cluster systems i.e., metal clusters with known interatomic spacing and degree of alloying, such as those used by DiSalvo and co-workers [74].

Fuel cell tests and combinatorial screening experiments rarely correlated despite these controls. The authors still use wrong arguments; I quote from Chan et al. [40], “Optical screening data have not always correlated well with fuel cell testing of new catalysts.” despite no prior data in any of the publications [15-18, 42, 51] where this correlation holds. I know of two instances to date, described in the experimental section of this thesis and in Benny Chan’s PhD thesis [41] based on fuel cell experiments done by me and optical screening experiments done by Benny Chan [41], where this correlation holds.

Experimental Section

Optical Screening Experiments Three catalysts were evaluated by optical screening (Johnson Matthey PtRu, Etek PtRu, Johnson Matthey Pt, PtRu) using optical screening experiments were carried out as described by Chan [41]. Johnson Matthey PtRu fluoresced at 135 mV, Etek PtRu at 140mV and Johnson Matthey Pt at 200mV. Of these, Johnson Matthey PtRu and Johnson Matthey Pt were evaluated in fuel cell tests.

Synthesis of home made materials Three materials were synthesized based on the procedure developed in our labs using H₂ in Argon as the reducing gas and evaluated in fuel cells as potential electrocatalysts. The nominal compositions were Au₁Pt_{0.5}Ir₁ (reduced by a mixture of H₂ 76 sccm in Argon 240 sccm), Ir₂Pt₁Au_{0.5} (reduced by a mixture of H₂ 408 sccm and Argon 100 sccm) and Pt_{0.5} Au_{0.5} (reduced by a mixture of H₂ 81 sccm and Argon 280 sccm) on XC72R carbon. The choice of the metals was based on papers by Michael Weaver [75] based on studies on CO chemical and electrochemical oxidation. Prior to adsorption of the metals, 100 mg of the carbon was mixed with 100 ml H₂O and 1 ml concentrated HNO₃ was added. The carbon was air-dried overnight and metal salts (HAuCl₄, H₂PtCl₆ and H₂IrCl₆) were added in one step i.e., metal salts dissolved in water and added. The carbon was air dried for 2 hours at ambient temperature and the materials were reduced at 200°C by ramping the temperature at 2°C /minute to 200°C and cooling down to ambient at 5°C /min. None of these compositions gave any current in actual fuel cell tests. I attempted synthesizing Pt₅₀Ru₅₀ three times using the Bonneman method described by Gotz and Wendt [76]. Attempted scale up resulted in very little sample for

fuel cell or electrochemical tests. Email contact with Dr. Gotz confirmed that the method was of limited utility in fuel cell experiments.

Electrocatalysts were purchased from Etek Inc. and Johnson Matthey Inc. and were typically Pt or Pt-Ru clusters supported on carbon. To compare these to catalysts made in house and to adapt carbon supported electrocatalysts in a combinatorial format, various heat treatments to the carbon (XC-72 and XC-72R) were investigated. This included heating the carbon, treating with sulfanilic acid [41, 42, 51] or a combination of both. Five catalysts with nominal composition (Pt-Ru 50-50 at%) were prepared on the treated carbons, to try and arrest variables involved in combinatorial screening. Of these, two catalysts synthesized by Dr. Guoying Chen, now at the University of California Berkeley (Hydrophilic Pt-Ru and XC72R PtRu) based on heat treated or chemically treated carbon displayed current voltage characteristics comparable to commercial catalysts in a H_2/O_2 cell. None of the carbon treatments resulted in a material that had any activity in fuel cell tests based on 100ppm $CO + H_2/O_2$, to be classified as an electrocatalyst.

Characterization of electrocatalysts All carbon supported catalysts and carbons tested in fuel cells were characterized by X-ray Photoelectron Spectroscopy (XPS) by irradiating the sample with monochromatic soft X-rays (Mg K alpha 1253.6 eV) Kratos Analytical XSAM 800 pci. The chalcogenide catalysts were analyzed by Kratos Analytical Axis Ultra using monochromatic aluminum X-rays (1486.6 eV). The samples were mounted on double-sided adhesive tape and analyzed as received. XPS quantification was performed by applying the appropriate relative sensitivity factors (RSF) for the Kratos instrument to the integrated peak areas. The RSFs took into consideration the x-ray cross section and the transmission function of the spectrometer. The approximate sampling depth under these conditions was 25Å. The pore diameter of the carbon powder (XC-72 and XC-72R) was analyzed using Chloromethane as the probe molecule based on the procedure developed by Mariwala and Foley [56], to account for long adsorption equilibration times using N_2 in a conventional porosimeter. Surface areas determined by N_2 physisorption using the Brunauer-Emmett-Teller (BET) method for the carbons (XC-72 and XC-72R).

Fuel Cell Tests

Synthesis of Membrane Electrode Assemblies (MEA) Membrane electrode assemblies are layers containing a proton conducting polymer membrane sandwiched between cathode and anode electrocatalysts dispersed on a gas distributor (typically carbon cloth or paper). Nafion 117™ from Dupont was cut into 6 cm² strips and boiled in 50% by volume of 30% H₂O₂, followed by DI water, followed by concentrated H₂SO₄ and DI water at 80 °C for 1 hour each. This chemical treatment was carried out 3 times and the membranes were stored in distilled DI water prior to use. Catalyst inks were prepared using the method developed by Wilson [10]. 100mg of commercial catalyst (Pt/C or Pt-Ru/C, Johnson Matthey Inc.) was mixed with 0.4g DI water and 762μl of 15% Nafion solution (Aldrich) in a 4ml vial and stirred for 2 days. Catalyst inks were dispersed onto carbon cloth (5 cm² geometric area, A-7 ELAT® from E-Tek) by painting the ink contained in vials using a hair brush till a desired loading (0.5mg Pt/ cm²) was achieved. The cloth was dried at 120 °C for 1hr between each coat. To assemble the final MEA, anode and cathode carbon cloths were hot-pressed at 120 °C at 88 kg cm⁻² (based on MEA geometric area) for 5 minutes in a heated Carver press. This involved sandwiching Nafion between the two carbon cloths, followed by cool-down to room temperature. During the hot-press step, the MEA was held between Aluminum plates and teflonized fiber glass (McMaster Carr). The MEA was sandwiched between graphite blocks (Poco Graphite Inc., Decatur, Texas) containing interdigitated flowfields that function both as a current collector and gas distributor at 2 Newton-meter torque. A Pressurex® sensor (Sensor Products Inc., East Hanover, NJ) was used to check for uniform pressure throughout the MEA.

Fuel cell testing of electrocatalysts for the reformate gas reaction Testing was carried out by placing the fuel cell assembly in a modified Lynntech test stand (Lynntech Industries, College Station, TX) that consisted of a gas distributor manifold, a humidifier and a loadbank. H₂ or H₂/CO (70 sccm) and O₂ (150 sccm) were humidified enroute to the fuel cell by mixing the gases with a controlled flow of water (0.3ml/min.) in a humidifier at 160 °C (*Note*: sccm refers to standard cubic centimeter /min). The inlet temperatures at the anode and cathode were typically 10 °C above the cell temperature under these conditions and checked by thermocouples at the fuel cell inlet. The fuel cell was heat traced to ensure uniform external temperature on the graphite plates. Prior to collecting fuel cell current-voltage curves, the MEA was held at 0.6V

(cell voltage) overnight at the temperature of operation by passing 70 sccm of H₂ at the anode and 150 sccm of O₂ at the cathode. This is referred to as the conditioning voltage in the fuel cell literature and the time referred to as conditioning time. Fuel cell current-voltage curves were collected by controlling the current through a loadbank, and data was recorded after the potential stabilized by tracking the potential and current with time for at least 30 minutes. The protocol was followed to minimize the effect of transients on current-voltage measurements.

Results and Discussion

Pore diameter analysis

Figure 2.9 indicated that the carbons (XC-72 and XC-72R) used in the study had a broad pore diameter distribution in the micropore (5-20 Å) and mesopore range (greater than 20 Å), with about 50% of the pore volume in the mesopore range. Surface areas determined by N₂ physisorption using the Brunauer-Emmett-Teller (BET) method for XC-72 and XC-72R was 250 m²/g.

XPS analysis of Carbons

All samples contained greater than 90 atomic% carbon. The C 1s spectra contained features characteristic of graphitic or amorphous carbon. The samples contained varying quantities of sulfur. All samples contained reduced sulfur species, possibly elemental sulfur and/or an unknown sulfide. Two samples, sulfanilic acid treated XC72R and XC72 [51], contained relatively large quantities of oxidized sulfur (sulfonate or sulfate). These same samples also contained measurable amounts of Na⁺ (possibly as Na₂SO₄). Little or no oxidized sulfur was observed on the other samples.

XPS analysis of Pt or Pt-Ru supported on Carbon

Species observed on the catalyst surfaces included a mixture of reduced (metallic) and oxidized Ru as well as C-C and small quantities of oxygen-containing functional groups. Platinum was present on every surface as a metal, and oxidized platinum species could not be definitively identified on any sample. Carbon was excluded because of concern that random amounts of

signal would be generated from the adhesive tape the samples were mounted on. There was major spectral interference between the C 1s and Ru 3d spectra. Analysis of standards of Ru, Pt and Ir powders did not aid in determining these peak positions.

Choice of conditioning voltage

The choice of conditioning voltage has received some attention in the fuel cell literature. Issues have been raised as to Ru dissolution at very positive anode potentials, choice of support material etc. [77] based on the perspective of the researcher, with almost little universal agreement on many of the issues. The only conclusive study, in the opinion of the author exists for Pt-Ru clusters used as anodes for direct methanol fuel cells in the work of Zelenay et al. [77c] who found that Ru crosses over to the cathode from the anode resulting in a loss in cell voltage between 40 and 200 mV. Our experiments involved H₂ or H₂/100ppm CO as the fuel and we sought to use 0.6V assuming that the drop in voltage was on the cathode side. Attempts to test this hypothesis using a pseudo reference electrode were unsuccessful leading to more questions as to their placement in the fuel cell geometry [10,67] than solving the problem i.e., delineating anode and cathode potentials. The author has yet to see a clear set of experiments in the literature that clearly delineate anode and cathode potentials in a fuel cell geometry under the conditions relevant to optimizing the power and energy density of these cells.

Applicability of Faraday's law and choice of conditioning voltage

To check to see if Faraday's law applied at steady state in the experiments, a water balance at steady state was carried out based on inlet and outlet water flow rates at the anode and cathode. Assuming that the membrane transported between 6-7 $\mu\text{l min}^{-1}$, based on a water balance, the agreement was quantitative, i.e., under the conditions of high stoichiometry and the flow rates of fuel and oxidizer, production of water was in agreement with the coulombs of charge. The open circuit voltage in the tests was typically around 1V. At the conditioning voltage of 0.6V, currents of about 2.3 A were observed at the end of the conditioning period i.e., overnight. The run-to-run reproducibility was 5% in terms of currents. Conditioning at 0.5V or 0.4V in some experiments did not change the observed current-voltage behavior in tests involving H₂ or H₂/100 ppm CO as the fuel with O₂ as the oxidizer.

Transport effects at the electrocatalyst surface during fuel cell runs

Figures 2.2 and 2.3 qualitatively illustrated the operating regimes in a fuel cell. To quantify the results, we analyzed terms in currents and potentials by relating concepts from heterogeneous catalysis and electrode kinetics, without resorting to curve fitting and simulation. The approach was tailored towards physical insight based on observables and empirical knowledge gained from experience. We used scaling criteria, as the pore diameter analysis described above indicated a broad pore diameter distribution and we found it difficult to conclusively argue the case for structure-property relationships. We also could not conceptually or experimentally separate the effects due to metal clusters adsorbed onto various pore diameters and the difference between molecules that stayed adsorbed and probably participated in electron and proton transfer and the ones that freely moved around i.e., we could not conclusively argue for a case for a linear relation between the concentration term in the left and right hand side of Fick's second law. The electrocatalysts were also were mixed with Nafion and annealed, prior to fuel cell tests. We therefore could not use models assuming bare catalyst sites that quantify transport effects based on thickness and variation in proton diffusion co-efficient i.e., the formalisms due to Bard *et al.* [6] and analysis by Schmidt *et al.* [65,69] did not help add physical insight to the author of this chapter. Therefore, I chose a very simple model described below that was insightful in suggesting areas for improvement and useful in separating transport and intrinsic kinetics.

The simplest model accounting for effects of internal and external transport to a catalyst surface was discussed by Weisz [44]. The model carries explicit and implicit guidelines to avoid transport effects in kinetic measurements. For kinetically demanding non-trivial reactions, Weisz introduced a criterion to estimate the maximum length between two “active” sites or surfaces distance L apart based on Fick's law as

$$\left[\frac{dN}{dt} \right]_{\max} = \left[\frac{D^* B_{eq}}{L} \right] \quad (5)$$

where,

$(dN/dt)_{\max}$ is the maximum rate of reaction in $\text{mol cm}^{-2} \text{s}^{-1}$

D is the diffusion co-efficient of species of interest $\text{cm}^2 \text{s}^{-1}$

B_{eq} is the equilibrium concentration of the species (mol cm^{-3}) at each site L (cm)

The elegant aspect of this simple expression is that it relates a kinetic parameter (rate of the reaction) to concentration and transport parameters (B_{eq} & D) with distance (L). Equation (5) can be treated as a reformulation of Fick's law with rate of reaction between two surfaces distance L apart replacing flux. This expression has found use in many areas of chemical and biological science [44] as a test to determine diffusion effects in chemical and biological systems.

To apply the criterion to electrocatalysis, we multiplied both sides of equation (5) by Faraday's constant and total number of electrons n , and derived

$$\frac{[D * B_{eq} * nF]}{L} = \left(\left[\frac{dN}{dt} \right]_{\max} * nF \right) \quad (6)$$

$$= \text{Current Density in A cm}^{-2}$$

Assuming that the diffusion co-efficient is invariant with applied potential and the concentration of the redox species is uniform throughout the membrane electrode assembly, we can solve for L . L represents the maximum distance two sites can be apart to prevent diffusional limitations. Equation (6) thus ties concepts from heterogeneous catalysis and electrode kinetics. We then ask what equation (6) would mean to a practical engineer. A practical engineer would design his system in such a way to capture maximum rate by operating his cell to maximize a given B_{eq} and minimize L . In the opinion of the author, this approach is routinely followed in optimizing electrocatalyst thickness empirically i.e., the fuel cell literature abounds with terms such as effect of catalyst loading, catalyst layer thickness etc. without recognizing useful basic concepts.

Our approach was comparison of different electrocatalysts and not optimizing fuel cells for maximum power. We sought to avoid effects of transport limitation by comparison at small current densities ($0\text{-}100 \text{ mA cm}^{-2}$) and potentials ($50\text{-}100 \text{ mV}$ deviation from rest). To avoid the effect of external flux on the electrocatalyst surface, the experiments were run at theoretical maximum currents of 7 Amps on the anode and 40 Amps on the cathode based on inlet flow rate. This resulted in a stoichiometry of 10 on the anode and 40 on the cathode on a 1 Amp basis, according to equations (1), (2) and (4). The maximum current observed in the fuel cell runs were 4.5 Amps (runs with H_2 and O_2) and 2.5 Amps in (runs with H_2 containing 100ppmCO),

indicating we were not limited by external transport of fuel and oxidizer to the electrocatalyst surface.

Figures 2.5 and 2.6 show the results of fuel cell test on commercial and two home made catalysts. The y-axis in these plots is cell voltage and the x-axis indicates current (in Amps) or current density ($A\text{ cm}^{-2}$), normalized to geometric area of the MEAs. In the absence of CO, the figures indicate similar activity. During the course of the experiments, fuel cell current-voltage curves were collected by controlling the current through a load bank and data were recorded after the potential stabilized by tracking the potential and current with time for at least 30 minutes. This suggests that we were at steady state during data collection.

We estimated a molecule:site by treating every site as equal strength and checking to see for external flux effects. Using a Pt/C surface area of $100\text{ m}^2/\text{g}$ and of Pt-Ru/C surface area of $70\text{ m}^2/\text{g}$ at the catalyst loading used in the above runs (0.5 mg cm^{-2}), we found a molecule:site of 200 for the runs with Pt/C and 280 with Pt-Ru/C for runs in H_2/O_2 . A good rule of thumb is to maintain a molecule:site of 100 [50]. Increasing flowrates beyond 70 sccm on the anode (H_2 flow rate) and 150 sccm on the cathode (O_2 flow rate), had no effect on the current-voltage curves, confirming that external flux was not an issue under the conditions of the experiments as shown in Figure 2.7. This satisfied the Koros-Nowak [49] and Madon-Boudart [48] tests in heterogeneous catalysis.

To check the effect of reproducibility between runs and in runs with H_2 and 100ppm CO as the fuel on the anode and O_2 on the cathode, Figure 2.7 shows an increased current-voltage at an increased flow rate of 140 sccm on the anode. This flowrate indicates the upper limit to compare catalysts using 100 ppm CO / H_2 as the fuel. Introduction of CO resulted in complete poisoning of home made catalysts, as illustrated in Figure 2.8.

Slade et al. [64] measured the proton self diffusion co-efficient in Nafion using Pulse-Field Gradient NMR and found the value to vary between 10^{-6} and $10^{-7}\text{ cm}^2\text{s}^{-1}$ for acid pre-treated membranes and about $10^{-8}\text{ cm}^2\text{s}^{-1}$ for membranes treated in deionized water at 298 K. These values increased to $10^{-7}\text{ cm}^2\text{s}^{-1}$ or higher at temperatures greater than $60\text{ }^\circ\text{C}$. Assuming sites on a given MEA were as far as $0.10\text{ }\mu\text{m}$ apart (worst case scenario) and a diffusion co-efficient of 10^{-8}

$\text{cm}^2 \text{ s}^{-1}$ and the experimental conditions described above, we calculated the maximum current density to be 37.8 A cm^{-2} for a 2-electron transfer (anode) and 75.7 A cm^{-2} for a 4-electron transfer (cathode) using Equation (6) (*Note*: This analysis assumes a smaller diffusion coefficient as the membranes were pre-treated in conc. H_2SO_4 and deionized water in this study). This term is referred to limiting current density in electrode kinetics. The maximum currents observed in this study, were about 2.5% of this value (based on the lower anode limiting current). Assuming that the concentration dropped by a factor of 10 through the catalyst layer or the diffusion co-efficient dropped by a factor of 10, the maximum observed currents were lower than 25% of theoretical. We sought to avoid effects of transport limitation by comparison at small current densities ($0\text{-}100 \text{ mA cm}^{-2}$) and potentials (50-100 mV deviation from rest) and the current density ($0\text{-}100 \text{ mA cm}^{-2}$) represents 0.02% of theoretical limiting current. Bockris [53] and Bard [52] suggest that the effects of limiting currents can be neglected when the currents of interest are less than 1% of limiting value. The analysis above suggests that the conditions of catalyst comparison are in a regime relevant to neglecting internal transport losses, based on a particle size of 3-4nm [65, 69]. The analysis also holds at separation distance as large as 100nm and assuming sites of equal strength and a deviation in reactant concentration by a factor of 10 or a change in diffusion co-efficient by a factor of 100.

Correlation between Optical screening and fuel cell test for two commercial catalysts

Figure 2.5 shows the results of fuel cell tests for a large range of catalysts including catalysts evaluated by optical screening (Johnson Matthey PtRu and Johnson Matthey Pt). We observed from results shown in Figure 2.5 that the optical screening method correctly predicted the trends for qualitatively ranking fuel cell electrocatalysts under the conditions used in the fuel cell tests.

Note on tests with home made materials

The same figure also shows results for two catalysts (Hydrophilic Pt-Ru and XC-72R PtRu) showing activity comparable to commercial catalysts in a H_2/O_2 feed. We failed to detect any current during fuel cell tests in $70 \text{ ml min}^{-1} \text{ H}_2$ in $\text{Au}_1\text{Pt}_{0.5}\text{Ir}_1$, $\text{Ir}_2\text{Pt}_1\text{Au}_{0.5}$ and $\text{Pt}_{0.5} \text{ Au}_{0.5}$ on XC72R carbon. We failed to detect any current during fuel cell tests in $70 \text{ ml min}^{-1} \text{ H}_2/100\text{ppmCO}$ in Hydrophilic Pt-Ru on XC72, PtRu on XC-72R, $\text{Au}_1\text{Pt}_{0.5}\text{Ir}_1$, $\text{Ir}_2\text{Pt}_1\text{Au}_{0.5}$ and $\text{Pt}_{0.5} \text{ Au}_{0.5}$ on XC72R carbon. As an illustration, Figure 2.8 shows that introduction of CO resulted in complete poisoning of home made catalysts (XC-72R PtRu).

Methanol tolerant cathode electrocatalysts

Methanol-tolerant, non-noble metal catalysts were first discovered about 15 years ago by Alonso-Vante and coworkers [60]. These materials are interesting from the viewpoint of their methanol-tolerance i.e., they retain their ability to reduce oxygen in a methanol environment. These could potentially function as cathodes in multipass direct methanol fuel cells if their activity could be increased to provide about 100 mA cm^{-2} of current at 0.85 V (cathode potential). Literature on these systems was very limited in the early 1990s, and they seemed an interesting problem for combinatorial exploration [60, 61]. The most active of these materials contained ruthenium and selenium doped with molybdenum. These ruthenium-rich compositions were originally formulated as Chevrel phases [60,61] or M_2X ($M = \text{Ru}$ or Mo , $X=\text{Se}$) compounds and later as $\text{Ru}/\text{Ru}_x\text{Se}_y\text{C}_v\text{O}_w$, in which the active $\text{Ru}_x\text{Se}_y\text{C}_v\text{O}_w$ phase was supported on Ru clusters [61,62]. These materials were examined by the fluorescent screening method [17, 36] using Phloxine B as the indicator. Ru-W-Sn-Se-Mo combinations were printed onto Toray carbon paper using aqueous glycerol inks (solutions of $\text{RuCl}_3 \cdot x\text{H}_2\text{O}$, SeO_2 , Na_2WO_4 , SnCl_4 , and Na_2MoO_4) and then reduced with hydrogen gas at 250°C . Active compositions in 645-member arrays were found in the Ru-rich regions of the Ru-Sn-Se ternary and Ru-Mo-Sn-Se quaternary regions. Physical characterization of the most active composition, $\text{Ru}_{7.0}\text{Sn}_{1.0}\text{Se}_{1.0}$, by powder x-ray diffraction, gas adsorption, and x-ray photoelectron spectroscopy revealed that the predominant crystalline phase was hexagonal close-packed (hcp) ruthenium and showed a surface mostly covered with oxide, consistent with recent studies by Tributsch, et al. [61]. Preliminary MEA testing of carbon-supported catalysts prepared by the same method showed that they are poor catalysts, relative to Pt metal [36]. As the synthetic method used to prepare these catalysts [36] was chosen to be compatible with ink-jet printing, we chose more sophisticated synthetic routes, based on organometallic precursors, adapting the preparative methods discussed by Tributsch [62].

Synthesis of chalcogenide catalysts using organometallic precursors The chalcogenide catalysts in this study were prepared by Jennifer Blough, now a graduate student at the University of California, Berkeley. Molybdenum carbonyl ($\text{Mo}(\text{CO})_6$), Ruthenium carbonyl ($\text{Ru}_3(\text{CO})_{12}$) and tetrapropyl tin ($\text{Sn}(\text{n-propyl})_4$) were purchased from Strem Chemicals.

Selenium powder and p-xylene from Aldrich and Carbon XC-72 from Cabot were used as received. In a typical synthesis, 300 mg $\text{Ru}_3(\text{CO})_{12}$, 15.871 mg Se powder, 1.50 g of XC-72 Carbon, and 53.2 μl $\text{Sn}(\text{n-propyl})_4$, were added to 200 ml p-xylene in a 500 ml, 3 neck, round bottom flask. The flask was clamped to an oil bath heated to reflux (120°C) with stirring for 20 hrs after purging with argon. The particles were washed with acetone and filtered (Whatman 100, 350 nm average pore diameter) to remove excess p-xylene. The catalysts were dried overnight at $60\text{--}80^\circ\text{C}$. Two compositions, picked from screening experiments described above [36], $\text{Ru}_7\text{Sn}_1\text{Se}_1$ and $\text{Ru}_3\text{Mo}_{0.08}\text{Se}_2$ on XC-72 carbon were compared in three-electrode experiments described below.

Characterization of electrocatalysts

XPS analysis of chalcogenides

The chalcogenide catalysts were analyzed by Kratos Analytical Axis Ultra using monochromatic aluminum X-rays (1486.6 eV). The samples were mounted on double-sided adhesive tape and analyzed as received. XPS quantification was performed by applying the appropriate relative sensitivity factors (RSFS) for the Kratos instrument to the integrated peak areas. These RSFs take into consideration the x-ray cross section and the transmission function of the spectrometer. The approximate sampling depth under these conditions is 25\AA . Species observed on the surfaces before electrochemical tests included metallic Ru, Ru oxides (RuO_2 and/or RuO_3), Sn^{4+} , C-C, metallic Se or a selenide, SeO_2 and on samples with Molybdenum MoO_x and metallic Mo. Sn was absent or below detection limits in XPS test post electrochemical tests.

Half cell testing of catalysts for methanol tolerant cathode electrocatalysts

Catalyst inks for testing in gas diffusion electrodes were prepared by the method of Wilson and Gottesfeld [10] and were painted onto Teflon-coated Toray carbon discs (metal loadings were $0.8\text{--}0.9\text{ mg/cm}^2$). The electrodes were then heated under Ar at 120°C for 1 h. The painted electrode discs were then assembled as the working electrode of a three-electrode cell with Pt gauze as the counter electrode and RHE as the reference electrode. A 0.5 M H_2SO_4 solution was used as the electrolyte. For oxygen reduction experiments, oxygen was introduced from the back of the Teflon-coated Toray carbon working electrode at 70 sccm, using a piece of carbon cloth to

diffuse the gas flow, with a back-pressure of an inch of water (equal to the height of the electrolyte in the cell) (*Note*: sccm refers to standard cubic centimeter / min). The cell used in these experiments is shown in Figure 2.10. All electrode areas were approximately 2.45 cm². Voltammetric studies were carried out using a BAS 100B/W potentiostat. All potentials are reported vs. RHE, and temperatures were controlled to an accuracy of $\pm 0.1^\circ\text{C}$ using an Omega temperature controller.

Results and discussion

To avoid the effect of external flux on the electrocatalyst surface, the experiments were run at a theoretical current 20 A based on inlet flow rate. This results in a stoichiometry of 20 on the cathode on a 1 A basis, according to equation (4). Current-voltage curves were collected by changing the potential using a potentiostat and measuring the current. The data was recorded after the current stabilized by tracking the potential and current with time for at least 30 minutes. This suggests that we are at steady state during data collection. The maximum current observed in the half cell runs were 0.4 A (in O₂), indicating we were not limited by external transport of O₂ to the electrocatalyst surface. We also estimated a molecule:site by treating every site as equal strength and checking to see for external flux effects. Using a catalyst surface area of 100 m²/g and at the catalyst loading used in the above runs (0.8-0.9 mg cm⁻²), we get a molecule:site of 100 during the experiments.

Figure 2.11 show the results of half cell tests on catalysts made by the organometallic route at flow rates free from external transport effects. The y-axis in these plots is cell voltage and the x-axis indicates current (Amps) or current density (A mg⁻¹), normalized to mass loading of the catalysts (2.5 cm² geometric area). The currents are negative indicating a cathodic reaction. From Figure 2.11, it was evident that Ru₇Sn₁Se₁ had lower activity (defined here as lower current at every electrode potential) compared to Ru₃Mo_{0.08}Se₂. The experiments suggested that compositions suggested by combinatorial screening experiments [36] do not translate to realistic correlations with testing of electrocatalysts in the half cell environment. Assuming sites on a given electrocatalyst layer are as far as 0.10 μm apart and a diffusion co-efficient of $10^{-8} \text{ cm}^2 \text{ s}^{-1}$

and the experimental conditions described above, we calculate the maximum current density using (5) to be 75.7 A cm^{-2} for a 4-electron transfer (cathode) using Equation (6). This term is referred to limiting current density in electrode kinetics. The maximum currents observed in this study were about 0.2% of the above value. Assuming that the concentration drops by a factor of 10 in the electrocatalyst layer or the diffusion co-efficient drops by a factor of 10, the observed currents were about 2% of the theoretical value. Comparing the catalysts at practical voltage drop of 50-100 mV, where the applied potential-current relation can be linearly approximated [53], we observed that none of the combinatorial leads [36] translated to electrocatalysts in the half cell environment.

We currently postulate that Sn in $\text{Ru}_7\text{Sn}_1\text{Se}_1$ (based on absence of Sn from XPS analysis) is unstable and probably leaches out at the positive potentials used in this experiment (0.4V and above) consistent with the literature available on electrodisolution of Sn from fuel cell anodes [33, 79]. Another reason that the experiments in this section do not translate to realistic correlations suggested by combinatorial screening experiments is perhaps the choice of synthetic methods used in screening (reduction of metal chlorides in H_2) [36], versus using organometallic precursors in xylene used in the current study.

Conclusions

This section described attempts to search for catalysts using a combinatorial technique developed in our laboratory. During the search for improved anode electrocatalysts for reformat gas electro-oxidation and methanol-tolerant, non-noble metal cathode catalysts; we followed the procedures outlined in references [15-18, 66]. Despite the efforts outlined in this work and in references [40-42], our experiments yielded no insight or leads in the search for electrocatalysts. This chapter is the first (in the author's opinion) that tries to bridge many of the scattered attempts at testing electrocatalysts in fuel cells with correlations in optical screening and explaining choice of experiments using simple arguments from thermodynamics and mass transfer. I have also argued in the literature review section that the theses and papers [18b, 51c, 72] bear no evidence that the samples used in fuel cell tests [17,18,72] or 3electrode experiments

[51c] were checked to see if the optical screening experiments correlated with fuel cell or 3electrode tests respectively. The 3electrode gas diffusion experiments on regenerative electrocatalysts based on combinatorial screening experiments [51a and 51b] suggests new compositions but is not conclusive. The experimental section of this thesis and that of Benny Chan [41] are the only two known to the author where correlations between optical screening experiments and fuel cell tests are clear.

To date, there has been no new electrocatalyst discovered using combinatorial searches that operate in working fuel cells. At the time of writing this thesis, it seems unlikely to the author that optical screening or other combinatorial methods will lead to discovery of better electrocatalysts in operating fuel cells.

References

1. Bockris J. O'M and Cahan B. D., *J. Chem. Phys.*, **1969**, *50*, 1307.
2. Justi E., "A Solar Hydrogen Energy System", Plenum Press, NY, **1987**, p1-323.
3. Westphal A., *German Patent 22393*, 1980.
4. J.O'M. Bockris and Shahed U. M. Khan, "Surface Electrochemistry", p 861-925, Plenum Press, NY, **1993**.
5. De Levie, R., *Advances in Electrochemistry and Electrochemical Engineering*, **1967**, *6*, 329-97.
6. A. J. Bard and L. R. Faulkner, "Electrochemical methods: fundamentals and applications", *2nd ed.*, John Wiley, NY, **2001**, p608-623.
7. Adcock, P. A., Brosha, E. L., Garzon, F. H., Uribe, F. A., *Mat. Res. Soc. Symp. Proc.*, **2003**, *756*, 365.
8. Gasteiger, H.A., Markovic, N., Ross, P.N. Jr, *J. Phys .Chem.*, **1995**, *99*, 8290.
9. Handbook of heterogeneous catalysis, *Vol. 4*, Ed. by G Ertl, H Knözinger, and J Weitkamp, VCH, Weinheim, **1997**, p1801-1900.
10. (a) Wilson, M. S., Gottesfeld, S., *J. E. Soc.*, **1992**, *139(2)*, L28; (b) Wilson, M. S., Valerio, J. A. and Gottesfeld, S., *Electrochimica Acta*, **1995**, *40(3)*, 355.
11. Watanabe, M.; Igrashi, H., Yosioka, K., *Electrochim. Acta*, **1995**, *40*, 329.

12. Zook, L. A., Leddy, J., *Proceedings - Electrochemical Society*, **1999**, 99-5(*New Directions in Electroanalytical Chemistry II*), 217-225.
13. Mittasch A., *Advances in Catalysis*, Academic Press Inc., NY, **1950**, 2, 81.
14. Sandstede, G., "From electrocatalysts to fuel cells", Sandstede, G., ed., University of Washington Press, Seattle, WA, **1972**, p43-79.
15. a) Ley, K. L.; Liu, R.; Pu, C.; Fan, Q.; Leyarovska, N.; Segre, C.; Smotkin, E. S., *J.E. Soc.*, **1997**, *144*, 1543. b) Liu, R., Ph.D thesis, Illinois Institute of Technology, Chicago, IL, **1998**.
16. a) Liu, R.; Triantafillou, K.; Li, L.; Cong, P.; Smith, C.; Smotkin, E. S., *J. E. Soc.*, **1997**, *144*, L148; b) Liu, R.; Triantafillou, K.; Li, L.; Cong, P.; Smith, C.; Smotkin, E. S., *J. E. Soc.*, **1997**, *144*, 2942.
17. Reddington, E.; Sapienza, A.; Gurau, B.; Viswanathan, R.; Sarangapani, S.; Smotkin, E. S.; Mallouk, T. E., *Science*, **1998**, *280*, 1735.
18. a) Gurau, B., Viswanathan, R., Lafrenz, T. J., Liu, R., Ley, K. L., Smotkin, E.S., Reddington, E., Sapienza, A., Chan, B. C., Mallouk, T. E., and Sarangapani, S., *J. Phys. Chem. B.*, **1998**, *102*, 9997; b) Bogdan, G., Ph. D. thesis, Illinois Institute of Technology, Chicago, IL, **2002**.
19. Fernandez, J. L.; Walsh, D. A.; Bard, A. J., *JACS*, **2005**, *127(1)*, 357-365.
20. Liu, R.; Smotkin, E. S., *J. Electroanal. Chem.*, **2002**, *535*, 49.
21. Srinivasan, S., Ticianelli, E.A., Derouin, C. R., Redondo, A., *J.Power Sources*, **1988**, *22*, 359.
22. Bockris, J.O'M.; Wroblowa, H., *J. Electroanal.Chem.*, **1964**, *7*, 428;(b) Dahms, H.; Bockris, J.O'M., *J. E.. Soc.*, **1964**, *111*, 728.
23. Janssen, M.M.P.; Moolhuysen, J., *Electrochim. Acta*, **1976**, *21*, 869.
24. (a) Andrew, M. R.; McNicol, B. D.; Short, R. T.; Drury, J. S., *J. Appl. Electrochem.*, **1977**, *7(2)*, 153; (b) McNicol, B. D.; Short, R. T., *Journal of Electroanalytical Chemistry and Interfacial Electrochemistry*, **1977**, *81(2)*, 249; (c) McNicol, B. D.; Short, R. T., *Journal of Electroanalytical Chemistry and Interfacial Electrochemistry*, **1978**, *92(1)*, 115; (d) Lowde, D. R.; Williams, J. O.; Attwood, P. A.; Bird, R. J.; McNicol, B. D.; Short, R. T., *Journal of the Chemical Society, Faraday Transactions I: Physical Chemistry in Condensed Phases*, **1979**, *75(10)*, 2312.
25. (a) Kadirgan, F.; Bedeb, B.; Leger, J., Lamy, C., *J. Electroanal.Chem.*, **1981**, *125*, 89; (b) Lamy, C., *Electrochim. Acta*, **1984**, *29*, 1584; (c) Lamy, C., Lima, V. LeRhun A., Delime, F.,

- Coutanceau C. and Léger, J.-M., *Journal of Power Sources*, **2002**, *105*(2), 283; (d) Dubau, L.; Hahn, F.; Coutanceau, C.; Leger, J.-M.; Lamy, C., *J. Electroanal.Chem.*, **2003**, *554-555*, 407; (e) Dubau, L.; Coutanceau, C.; Garnier, E.; Leger, J.-M.; Lamy, C., *J. Appl. Electrochem.*, **2003**, *33*(5), 419.
26. (a) Watanabe, M.; Furuuchi, Y.; Motoo, S., *J. Electroanal.Chem.*, **1985**, *191*, 367; (b) Shibata, M.; Motoo, S.; *J. Electroanal.Chem.*,**1986**, *209*, 151; (c) Watanabe, M.; Uchida, M.; Motoo, S. J., *J. Electroanal.Chem.*, **1987**, *229*, 395.
27. (a) Sinfelt J., *Bimetallic Catalysts: Discoveries, Concepts and Applications*, John Wiley and Sons, NY, **1983**; (b) P. N. Ross Jr., in *Electrocatalysis*, J. Lipkowski and P. N. Ross, Editors, p. 43, Wiley-VCH, NY, **1998**.
28. (a) Gasteiger, H.A.; Markovic, N.; Ross, P.N. Jr.; Cairns, E.J., *J. Phys. Chem.*, **1994**, *98*, 617; (b) Gasteiger, H.A.; Markovic, N.; Ross, P.N. Jr.; Cairns, E.J., *J. E. Soc.*, **1994**, *141*, 1795; (c) Gasteiger, H.A.; Markovic, N.; Ross, P.N. Jr.; Cairns, E.J., *Electrochimica Acta*, **1994**, *39*, 1825.
29. Parsons, R., T. Vandernoot, T., *J. Electroanal. Chem.*,**1998**, *257*, 9.
30. (a) Frelink, T., Visscher, W., and van Veen, J.A.R., *Surf. Sci.*, **1995**, *335*, 353; b)Frelink, T., Visscher, W., and van Veen, J.A.R., *Langmuir*, **1996**, *12*, 3702; c) Frelink, T., Visscher, W., and van Veen, J.A.R., Cox, A. P., *Electrochim. Acta.*, **1995**, *40*, 1537.
31. (a) Breiter, M., *J. Electroanal. Chem.*,**1967**, *14*, 407; (b) Breiter, M., *J. Electroanal. Chem.*,**1967**, *15*, 221.
32. Bagotsky and Skundin, *Chemical Power Sources*, Academic Press, NY, **1980**.
33. (a) Jarvi, T.D. and Stuve, E.M., in *Electrocatalysis*, J. Lipkowski and P. N. Ross, Ed., p. 75, Wiley-VCH, NY,1998; (b)Madden, T. H. and Stuve, E. M., *J. E. Soc.*, **2003**, *150*(11), E571.
34. Long, J. W., Stroud, R. M., Swider-Lyons, K. E., and Rolison, D. R., *J. Phys. Chem. B*, **2000**, *104*, 9772.
35. (a) Arico, A. S.; Poltarzewski, Z.; Kim, H.; Morana, A.; Giordano, N.; Antonucci, V., *J. Power Sources*, **1995**, *55*, 159; (b) Arico, A. S.; Creti, P.; Giordano, N.; Antonucci, V.; Antonucci, P. L.; Chuvilin, A., *J. Appl. Electrochem.*, **1996**, *26*(9), 959.
36. a) Yu, J.-S., Sapienza, A., Reddington, E., Kim, B. Y., Chan, B. C., Chen, G., Schaak, R. E., Egan, G. L., Mallouk, T. E., Liu, R., and Smotkin, E. S., unpublished results.;b) Reddington, E.,

- Yu, J.-S., Sapienza, A., Chan, B. C., Gurau, B., Viswanathan, R., Liu, R., Smotkin, E. S., Sarangapani, S., and Mallouk, T. E., in *Advanced Catalytic Materials*, Lednor, P. W.; Nakagi, D. A.; Thompson, L. T., Eds., *MRS Symp. Proc.*, **1999**, 549, 231.
37. a) Weisz, P. B.; Frilette, V. J., *J. Phys. Chem.*, **1960**, 64, 382.; b) Weisz, P. B., *IECR*, **1995**, 34(8), 2692.
38. Kabbabi, A.; Gloaguen, F.; Andolfatto, F.; Durand, R., *J. Electroanal. Chem.*, **1994**, 373(1-2), 251-54.
39. a) Bultel, Y.; Ozil, P.; Durand, R., *J. Appl. Electrochem.*, **1999**, 29(9), 1025-1033.; b) Antoine, O.; Bultel, Y.; Durand, R.; Ozil, P., *Electrochimica Acta*, **1998**, 43(24), 3681-3691.; c) Bultel, Y.; Ozil, P.; Durand, R., *Electrochimica Acta*, **1998**, 43(9), 1077-1087.
40. Chan, B. C., Liu, R., Jambunathan, K., Zhang, H., Chen, G., Mallouk, T. E., and Smotkin, E. S., *J. E. Soc.*, **2005**, 152, A594.
- 41 Chan, B. C., Ph.D. thesis, The Pennsylvania State University, **2003**.
42. Chen, G., Ph.D. thesis, The Pennsylvania State University, **2002**.
44. (a) Weisz, P. B., "Polyfunctional Heterogeneous Catalysis", *Advances in Catalysis*, Academic Press Inc., New York, NY, **1962**, 13, 137; (b) Weisz, P. B., *Science*, **1973**, 4072(179), 433.
45. a) Parthasarathy, A.; Srinivasan, S.; Appleby, A. J.; Martin, C. R., *J. E. Soc.*, **1992**, 139(10), 2856-62.; b) Parthasarathy, A.; Dave, B.; Srinivasan, S.; Appleby, A. J.; Martin, C. R., *J. E. Soc.*, **1992**, 139(6), 1634-41.; c) Parthasarathy, A.; Srinivasan, S.; Appleby, A. J.; Martin, C. R., *J. E. Soc.*, **1992**, 139(1-2), 101-21.; d) Parthasarathy, A.; Srinivasan, S.; Appleby, A. J.; Martin, C. R., *J. E. Soc.*, **1991**, 138(4), 916-21.
46. a) Xie, Z.; Holdcroft, S., *J. Electroanal. Chem.*, **2004**, 568(1-2), 247-260.; b) Navessin, T.; Holdcroft, S.; Wang, Q.; Song, D.; Liu, Z.; Eikerling, M.; Horsfall, J.; Lovell, K.V., *J. Electroanal. Chem.*, **2004**, 567(1), 111-122.; c) Beattie, P. D.; Basura, V. I.; Holdcroft, S., *J. Electroanal. Chem.*, **1999**, 468(2), 180-192.; d) Basura, V. I.; Beattie, P. D.; Holdcroft, S., *J. Electroanal. Chem.*, **1998**, 458(1-2), 1-5.
47. a) Mallouk T. E. and Smotkin, E. S., "Combinatorial Catalyst Development Methods", *Handbook of Fuel Cells - Fundamentals, Technology and Applications*, Vielstich, W., Lamm, A., and Gasteiger, H., Eds., *Volume 2, Part 3*, pp 334-347, John Wiley & Sons, Ltd, Chichester,

- 2003**; b) Smotkin, E. S. and Diaz-Morales, R. R., *Annual Review of Materials Research*, **2003**, 33, 557.
48. Madon R. J. and Boudart M, *I & EC Fundamentals*, **1982**, 21, 438.
49. Koros R. M. and Nowak E. J., *Chem. Engg. Sci.*, **1967**, 22, 469.
50. Boudart, M. and Djega–Mariadassou, “Kinetics of heterogeneous catalytic reactions”, Princeton University Press, Princeton, **1984**.
51. a) Chen, G., Delafuente, D. A, Sarangapani, S., and Mallouk, T. E., *Catal. Today*, **2001**, 67, 341.; (b) Chen, G., Bare, S. R., and Mallouk, T. E., *J. E. Soc.*, **2002**, 149, A1092; c) Sun, Y., Buck, H., and Mallouk, T. E., *Anal. Chem.*, **2001**, 73, 1599.
52. A. J. Bard and L. R. Faulkner, “Electrochemical methods: fundamentals and applications”, *2nd ed.*, Chapter 3, John Wiley, NY, **2001**.
53. J.O'M. Bockris and A. K.N. Reddy, “Modern electrochemistry”, *2nd ed.*, Vol. 2B, pages 1246-1257, Plenum Press, NY, **1998**.
54. (a) Gorer, S. A., *World Patent Application*, WO 00/54346, **September 2000**; (b) Strasser, P., Gorer, S. A., and Devenney, M., in International Symposium on Fuel Cells for Vehicles, Yamamoto, O., Ed., p. 153, Nagoya, **November 2000**, Electrochemical Society of Japan; (c) Strasser, P., Gorer, S. A., and Devenney, M., *Proc. Electrochem. Soc.*, **2001**, 2001-4 (Direct Methanol Fuel Cells), 191.
55. (a) Warren, C. J., Haushalter, R. C., and Matsiev, L., *U.S. Pat. 6,187,164*, **2001**.; (b) Sullivan, M. G., Utomo, H., Fagan, P. J., and Ward, M D., *Anal. Chem.*, **1999**, 71, 4369.;(c) Peter, S.; Fan, Q.; Devenney, M.; Weinberg, W. H.; Liu, P.; Norskov, J. K, *J. Phys. Chem. B*, **2003**, 107(40), 11013-11021. (d) Fleischauer, M. D.; Hatchard, T. D.; Rockwell, G. P.; Toppole, J. M.; Trussler, S.; Jericho, S. K.; Jericho, M. H.; Dahn, J. R., *J. E. Soc.* **2003**, 150(11), A1465.
56. Mariwala, R. K. and Foley, H. S., *IECR*, **1994**, 33, 2314.
57. J.O'M. Bockris and Shahed U. M. Khan, “Surface Electrochemistry”, Plenum Press, NY, **1993**, p 211-394.
58. Yi, J. S. and Van Nguyen, T., *J. E. Soc.*, **1999**, 146(1), 38.
59. Alonso-Vante, N. and H. Tributsch, *Nature*, **1986**, 323, 486.
60. Alonso-Vante, N., Jeagerman, W., Tributsch, H., Honle, W., and Yvon, K., *JACS*, **1987**, 109, 3251.

61. (a) Alonso-Vante, N., Giersig, M., and Tributsch, H., *J. E. Soc.*, **1991**, 138, 639.;(b) Alonso-Vante, N., Schubert, B., and Tributsch, H., *J. Catal.*, **1988**, 112, 384.; (c) Alonso-Vante, N., Schubert, B., and Tributsch, H., *Mat. Chem. Phys.*, **1989**, 22, 281.; (d) Alonso-Vante, N., Tributsch, H., and Solorza-Feria, O., *Electrochim. Acta*, **1995**, 40, 567.
62. Tributsch, H., Bron, M., Hilgendorff, M., Schulenburg, H., Dorbandt, I., Eyert, V., Bodganoff, P., and Fiechter, S., *J. Appl. Electrochem.*, **2001**, 31, 739.
63. (a) McBreen, J.; Mukerjee, S., *J. Electrochem. Soc.*, **1995**, 142(10), 3399; (b) Maniguet, S.; Mathew, R. J.; Russell, A. E., *J. Phys. Chem. B*, **2000**, 104, 1998; (c) O'Grady, W. E.; Hagans, P. L.; Pandya, K. I.; Maricle, D. L., *Langmuir*, **2001**, 17, 3047; (d) Russell, A. E.; Maniguet, S.; Mathew, R. J.; Yao, J.; Roberts, M. A.; Thompsett, D., *J. Power Sources*, **2001**, 96, 226; (e) Viswanathan, R.; Hou, G.; Liu, R.; Bare, S. R.; Modica, F.; Mickelson, G.; Segre, C. U.; Leyarovska, N.; Smotkin, E. S., *J. Phys. Chem. B.*, **2002**, 106(13); 3458.
64. Slade R. C. T., Barker J. and Strange J. H., *Solid State Ionics*, **1989**, 35, 11.
65. Schmidt, T. J.; Noeske, M.; Gasteiger, H. A.; Behm, R. J.; Britz, P.; Bonnemann, H., *J. E. Soc.*, **1998**, 145(3), 925-931.
66. Lei, H.-W.; Sanghyuk, S.; Gurau, B.; Workie, B.; Liu, R.; Smotkin, E. S., *Electrochimica Acta*, **2002**, 47(18), 2913.
67. Liu, Z.; Wainright, J. S.; Huang, W.; Savinell, R. F., *Electrochimica Acta*, **2004**, 49(6), 923.
68. J.O'M. Bockris and S. Srinivasan, "Fuel Cells", Mc-Graw Hill, NY, **1969**, p 179.
69. Schmidt, T. J.; Gasteiger, H. A.; Stab, G. D.; Urban, P. M.; Kolb, D. M.; Behm, R. J., *J. E. Soc.*, **1998**, 145(7), 2354-2358.
70. a) Reetz, M. T., Lopez, M., Grünert, W., Vogel, W., and Mahlendorf, F., *J. Phys. Chem B.*, **2003**, 107(30), 7414; b) Choi, W. C.; Kim, J. D.; Woo, S.I, *Catal. Today*, **2002**, 74(3-4), 235.; c) Chai, G. S.; Yoon, S. B.; Yu, J.-S.; Choi, J.-H.; Sung, Y.-E., *J. Phys. Chem.B.*, **2004**, 108(22), 7074.
71. Damjanovic, A., Genshaw, M. A., and Bockris, J. O'M., *J. Chem. Phys.*, **1966**, 45, 4057.
72. Reddington, E., PhD thesis, The Pennsylvania State University, **1999**.
73. a) Shrisudersan, J.; Hillier, A.C., *Langmuir*, **2001**, 17(25), 7857-7864.; b) Shrisudersan, J.; Hillier, A.C., *J. Phys. Chem. B*, **2003**, 107(22), 5221-5230.;c) Shrisudersan, J.; Hillier, A.C., *J. Combi. Chem.*, **2004**, 6(1), 27-31.; d) Shrisudersan, J.; Hillier, A.C., *Materials Research Society*

Symposium Proceedings, **2004**, 804 (*Combinatorial and Artificial Intelligence Methods in Materials Science II*), 171-179.

74. Casado, R. E.; Volpe, D. J., Alden, L., Lind, C., Downie, C.; Vazquez, A. T.; Angelo, A. C. D.; DiSalvo, F. J.; Abruna, H. D.; *JACS*, **2004**, *126*(12), 4043.

75. a) Edens, G. J.; Hamelin, A.; Weaver, M. J., *J. Phys. Chem.*, **1996**, *100*(6), 2322.; b) Zou, S.; Weaver, M. J., *J. Phys. Chem.*, **1996**, *100*(10), 4237; c) Gomez, R.; Weaver, M. J., *J. Phys. Chem.*, **1998**, *102*(19), 3754.; d) Gomez, R.; Weaver, M. J., *Langmuir*, **1998**, *14*(9), 2525.; d) Mrozek, M. F.; Luo, H.; Weaver, M. J., *Langmuir*, **2000**, *16*(22), 8463.

76. a) Gotz, M.; Fuess, H.; Roth, C.; Fischer, A.; Wendt, H., *GDCh-Monographie*, **1999**, *18* (*Metalle in der Elektrochemie*), 227.; b) Goetz, M.; Wendt, H., *J. Appl. Electrochem.*, **2001**, *31*(7), 811.; c) Gotz, M.; Wendt, H., *Institution of Chemical Engineers Symposium Series*, **1999**, *145* (*Electrochemical Engineering*), 31.

77. a) Thomas, S. C.; Xiaoming, R.; Gottesfeld, S.; Zelenay, P., *Electrochimica Acta*, **2002**, *47*(22-23), 3741.; b) Dinh, H. N.; Ren, X.; Garzon, F. H.; Zelenay, Piotr; Gottesfeld, S., *J. Electroanal. Chem.*, **2000**, *491*(1-2), 222.; c) Piel, P.; Eickes, C.; Brosha, E. Garzon, F.; Zelenay, P., *J. E. Soc.*, **2004**, *151*(12), A2053.

78. Dyer C., *Nature*, **1990**, *343*, 547.

79. a) Bae, I. T.; Takeshi, S.; Scherson, D. A., *J. Electroanal. Chem.*, **1991**, 297, 185; b) Sobkowski, J.; Franaszczak, K.; Piasecki, A., *J. Electroanal. Chem.*, **1985**, *196*, 145.

80. a) Moskovskikh, L. A.; Pnev, V. V.; Zakharov, M. S., *Zhurnal Analiticheskoi Khimii*, **1973**, *28*(9), 1669.; b) Sakamoto, M.; Takamura, K., *Bioelectrochem. Bioener.*, **1982**, *9*, 571.

81. a) Every, H. A.; Hickner, M. A.; McGrath, J. E.; Zawodzinski, T.A., *J. Memb.Sci.*, **2005**, *250*(1-2), 183-188.; b) Every, H.A.; Zawodzinski, T. A., Jr., *Pre-Print Archive - American Institute of Chemical Engineers, [Spring National Meeting], New Orleans, LA, United States*, **2002**, 2456-2464.

82. a) Pivovar, B. S.; Smyrl, W. H.; Cussler, E. L., *J. E. Soc.*, **2005**, *152*(1), A53-A60.; b) Libby, B.; Smyrl, W. H.; Cussler, E. L., *Electrochem. and Solid-State Lett.*, **2001**, *4*(12), A197-A199.

83. Parsons, R., *Trans. Faraday. Soc.*, **1951**, *47*, 1332.

84. Vetter, K., *Electrochemische Kinetik*, 2nd Ed., Springer-Verlag, Frankfurt, **1961**.

85. Vrentas, J. S., and Duda J. L., *Journal of Applied Polymer Science*, **1980**, *25*, 1297.

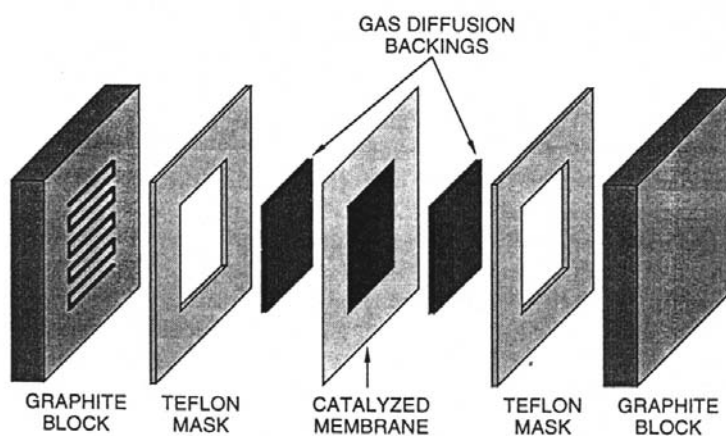


Figure 2.1a Cross-sectional view of a solid polymer electrolyte fuel cell

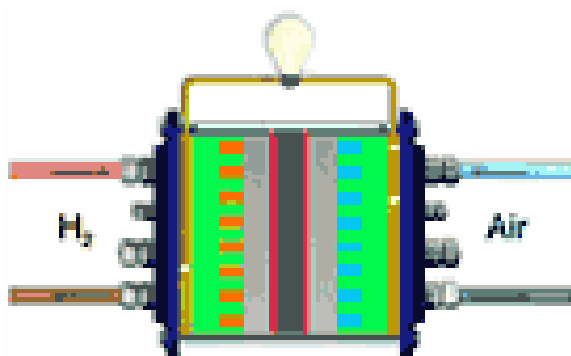


Figure 2.1b Assembled polymer electrolyte fuel cell. Ribs indicate flow fields that contact the membrane electrode assembly.

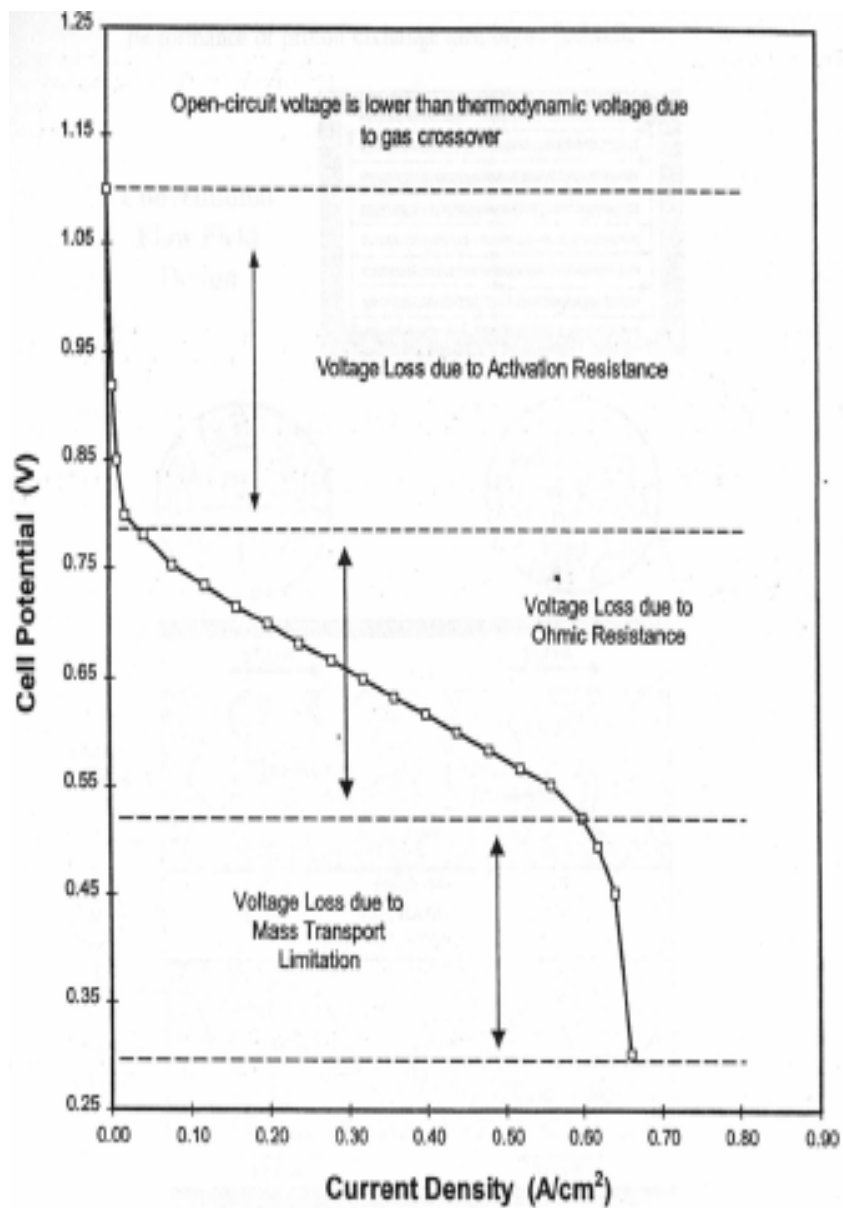


Figure 2.2 Schematic of kinetic, ohmic and mass transport control in fuel cell curves[58]. Current density values are shown for illustration purposes. Absolute values of current density and potential vary depending on each system.

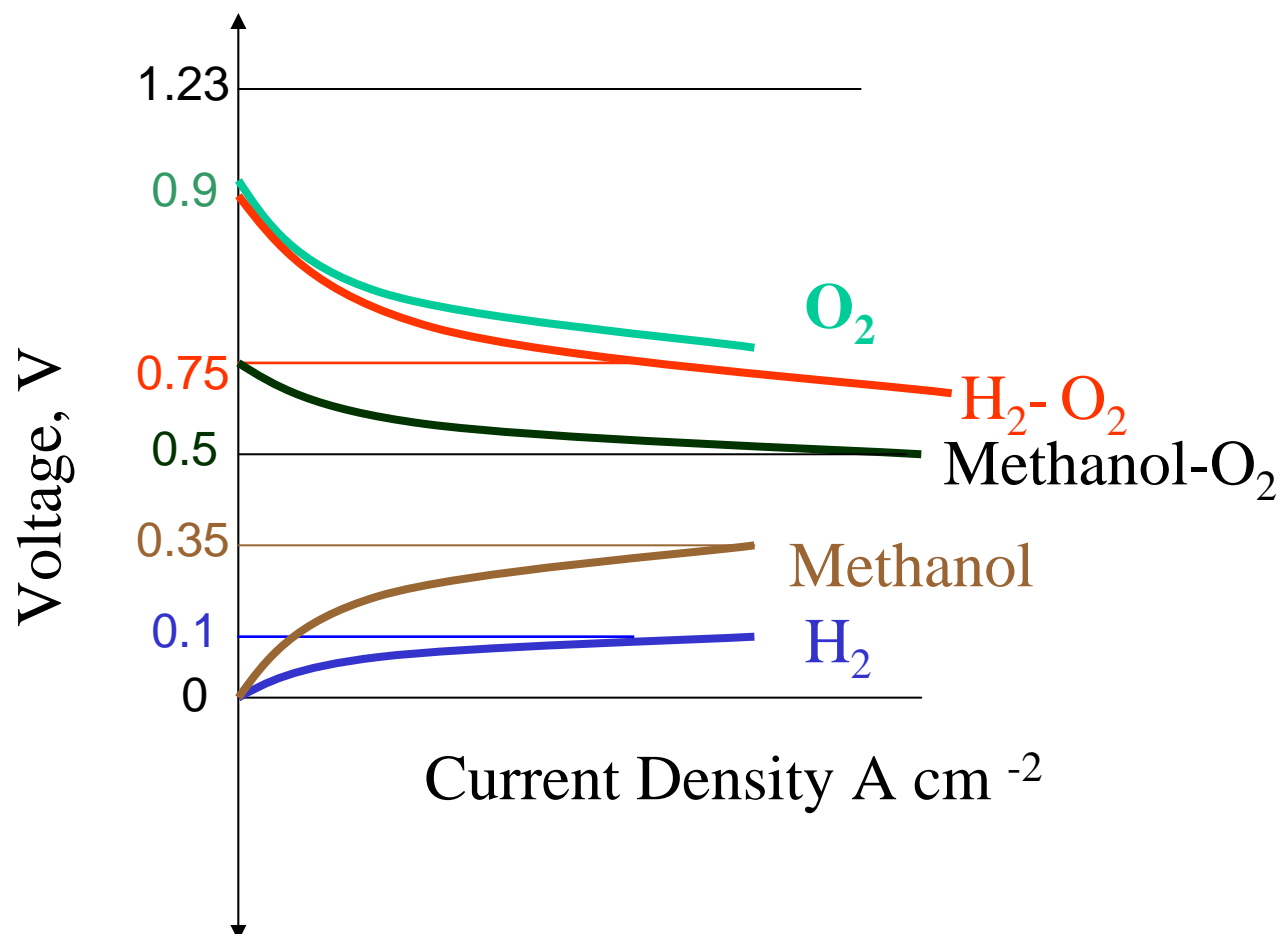


Figure 2.3 Schematic of voltage losses in anode and cathode due to various fuels, correcting for resistance losses due to the polymer membrane. Cathodic currents are not explicitly shown. The cathode potential is shown as a function of current density

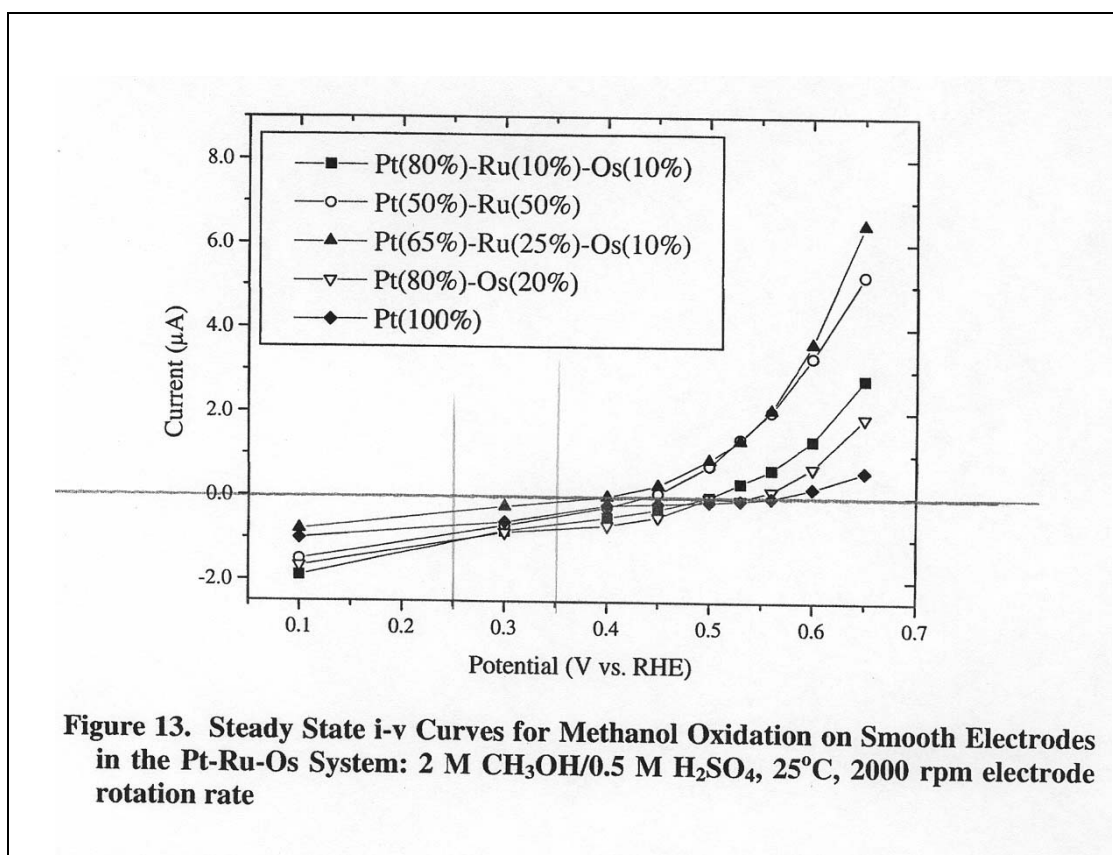


Figure 2.4a Horizontal and vertical lines drawn for illustration of negative currents at relevant potentials from Ley et al.[15].

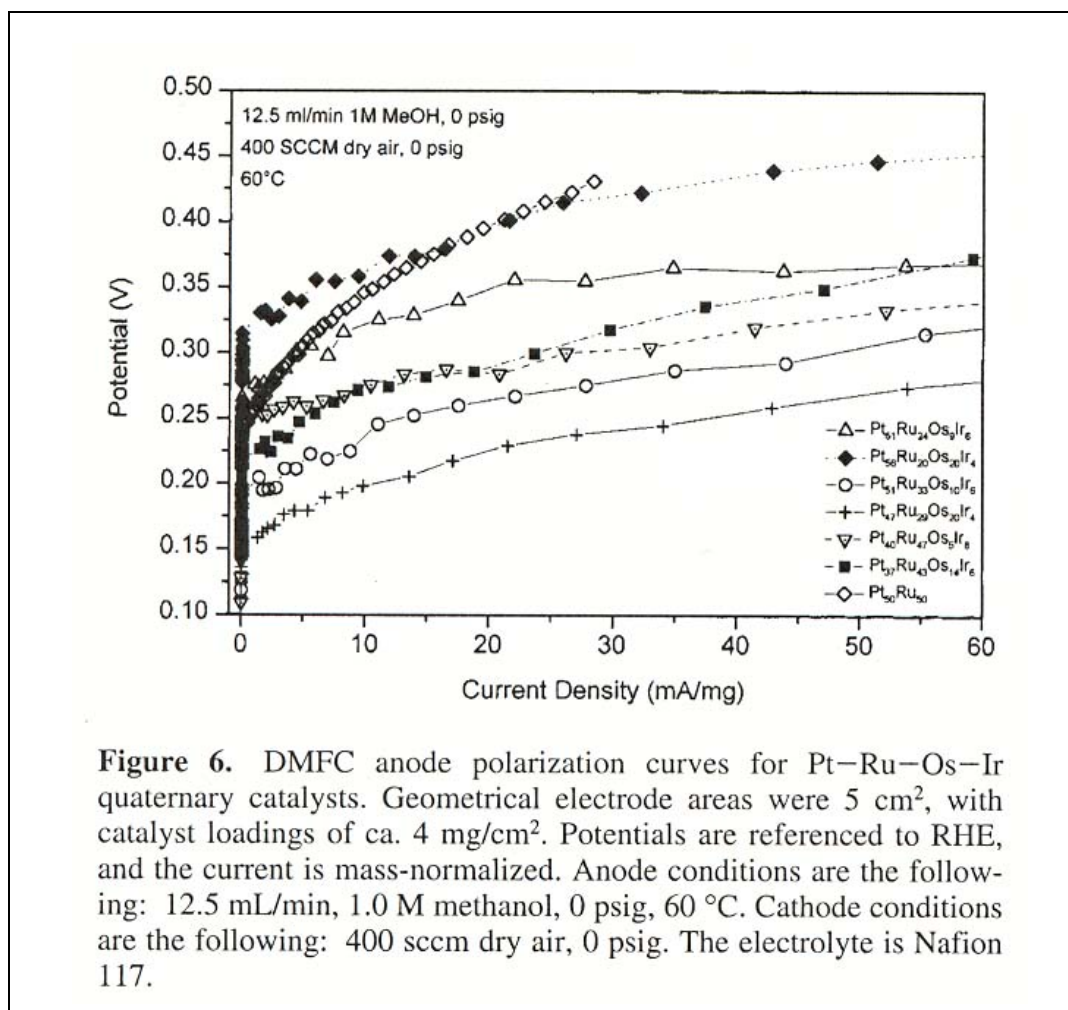


Figure 2.4b Quantitative comparison of electrocatalysts without verifying the potential of the pseudo reference electrode or the cathode for figures in [18] despite evidence in [10] and recent re-verification [67].

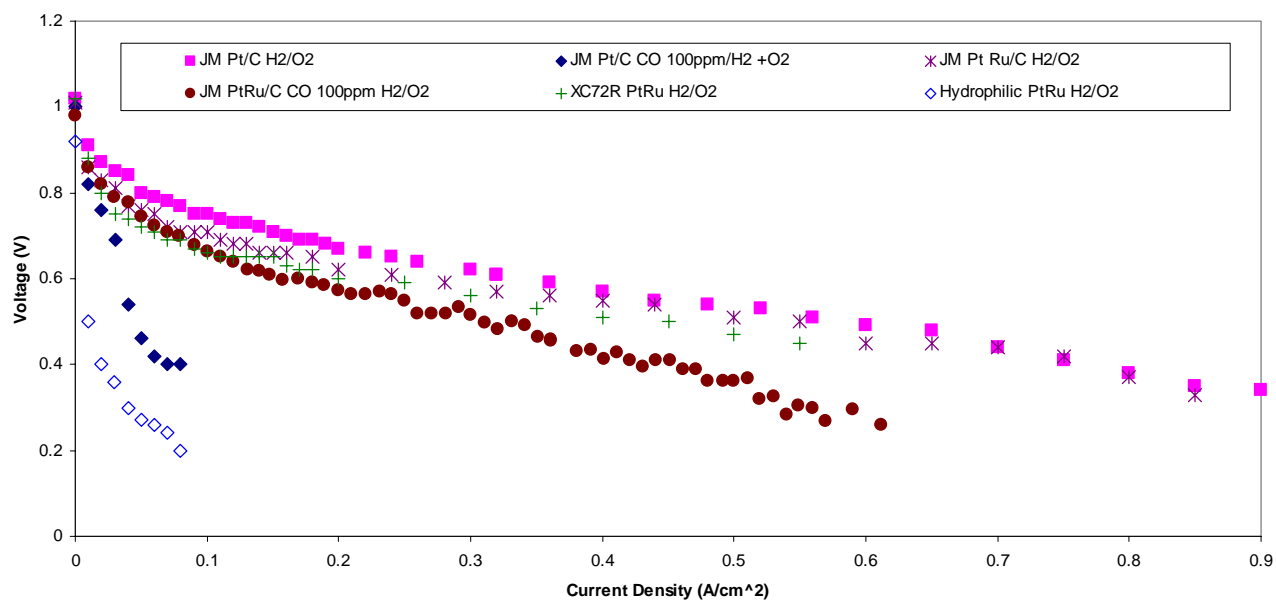


Figure 2.5 Polymer Electrolyte Membrane (PEM) fuel cell results for commercial catalysts from Johnson Matthey (JM Pt and JM PtRu) and two homemade catalysts in a membrane electrode assembly (MEA) as a function of current density at 0.07 and 0.14 slpm flow rates of fuel and oxidizer respectively (slpm refers to standard cubic liters per minute). The voltage values are accurate to +/- 5 mV (deviation from average).

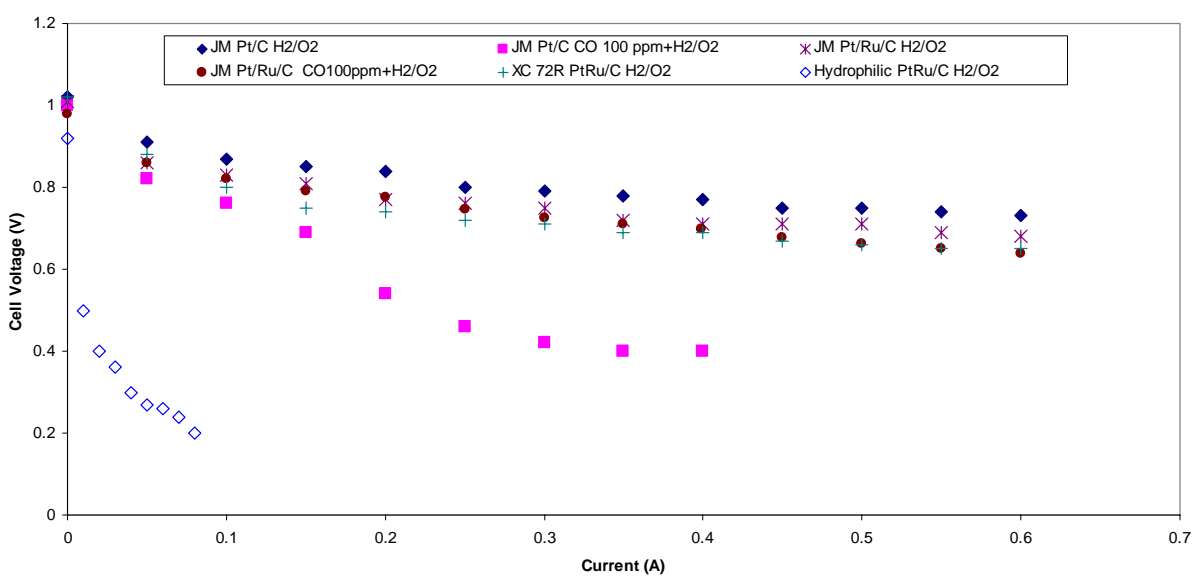


Figure 2.6 Polymer Electrolyte Membrane (PEM) fuel cell results for commercial catalysts from Johnson Matthey (JM Pt and PtRu) and two homemade catalysts in a membrane electrode assembly (MEA) as a function of current under the same conditions as figure 5. The voltage values are accurate to +/- 5mV (deviation from average).

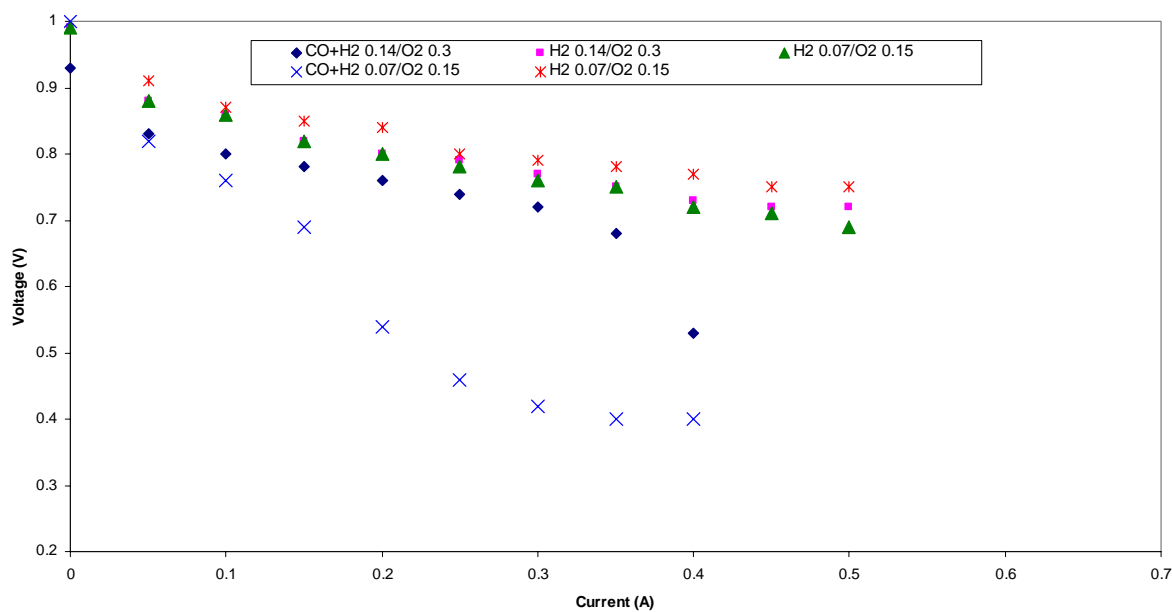


Figure 2.7 Flow rate effects and reproducibility in fuel cell tests for Johnson Matthey Pt on carbon. Numbers following gases refer to flow rates in standard cubic liters per minute. The voltage values are accurate to +/- 5mV (deviation from average).

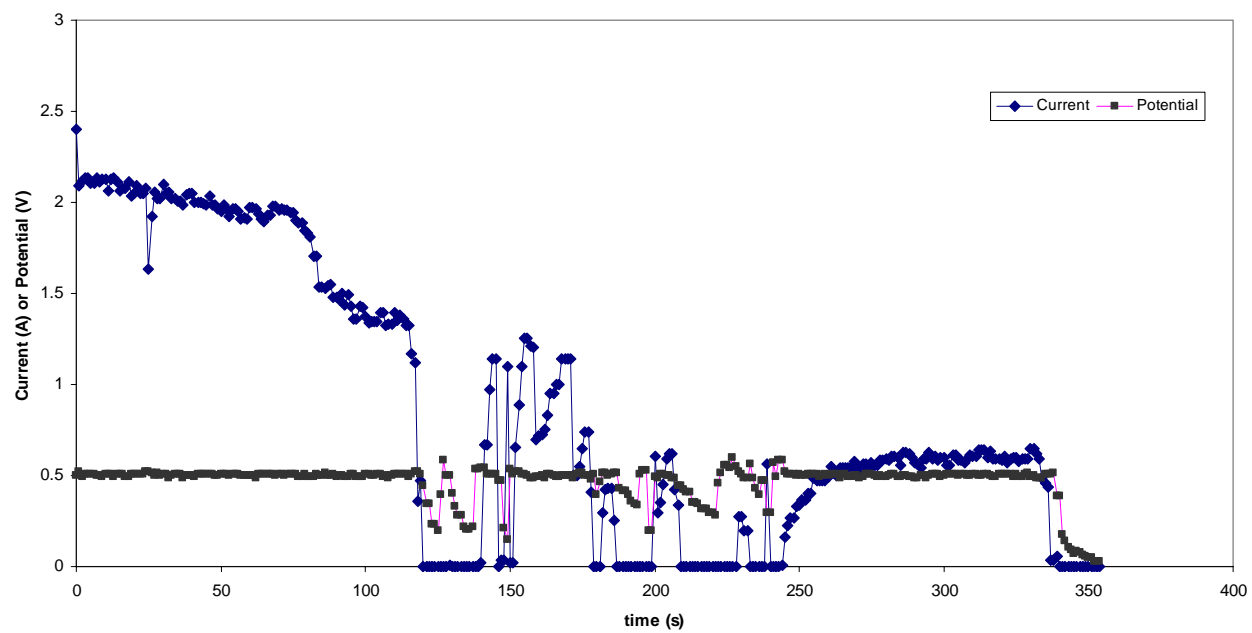


Figure 2.8 Current vs time of PSU catalysts at 0.5 V on the introduction of 100 ppmCO/H₂

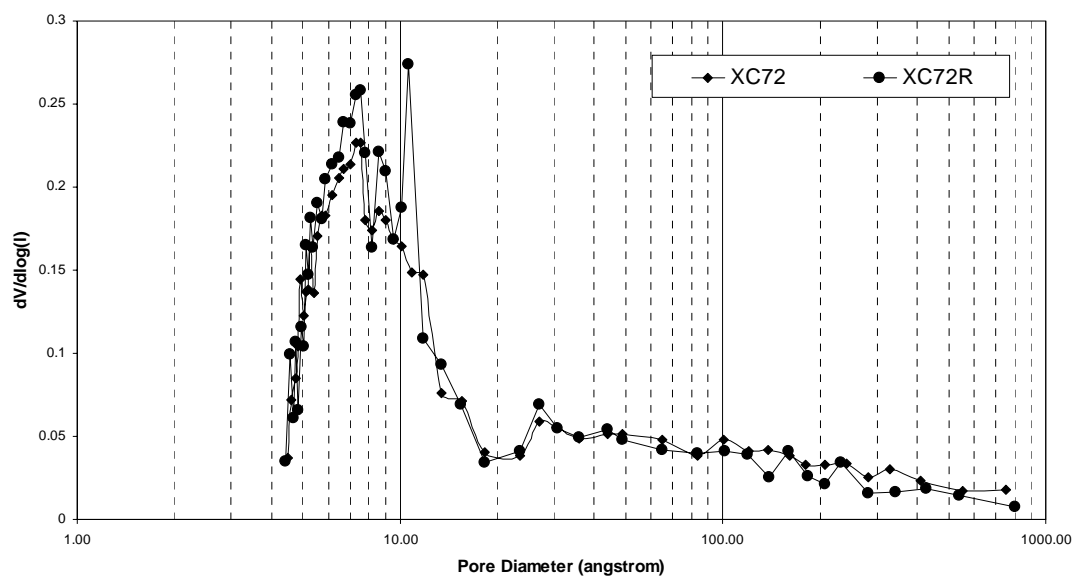


Figure 2.9 Pore diameter Distribution of XC72 and XC72R carbon using chloromethane as probe molecule (lines are guide to the eye)

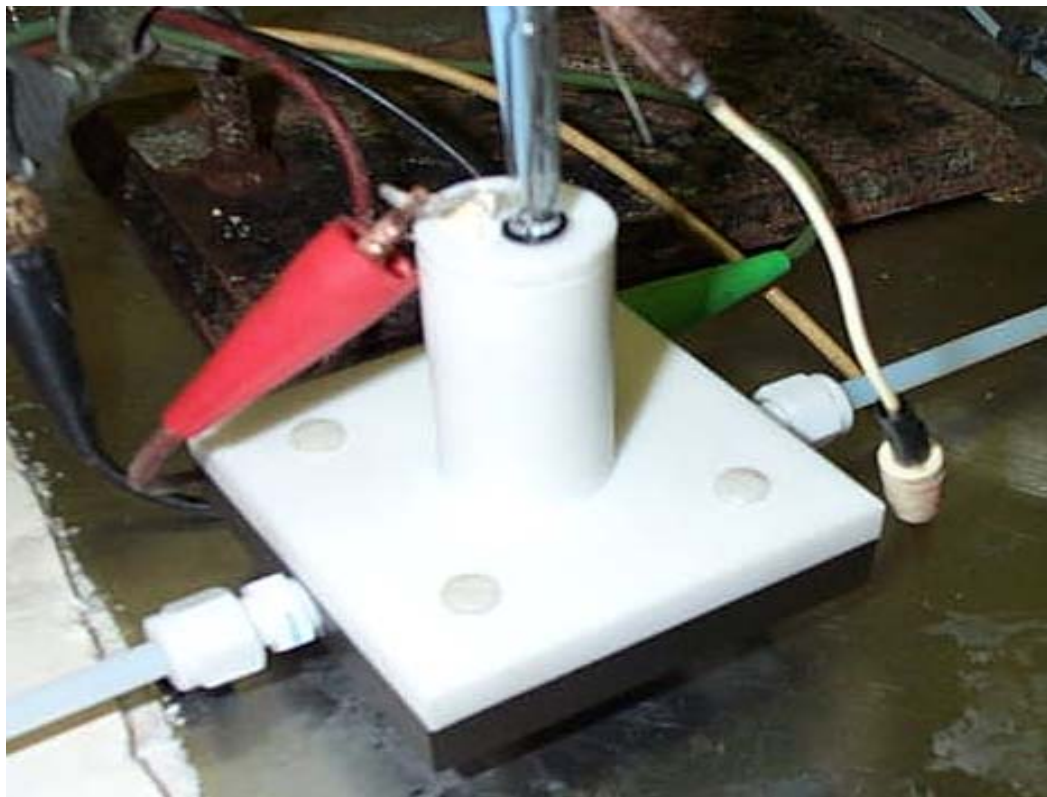


Figure 2.10 Gas diffusion half cell used in evaluating electrocatalysts for oxygen reduction. Oxygen enters through the Swagelok fitting on the left diffuses through the carbon cloth held in the middle by four nuts and exits to the right through the Swagelok fitting. The bottom plate serves as the working electrode, the clip to the left is a counter electrode and the glass pipet holds a dynamic hydrogen electrode.

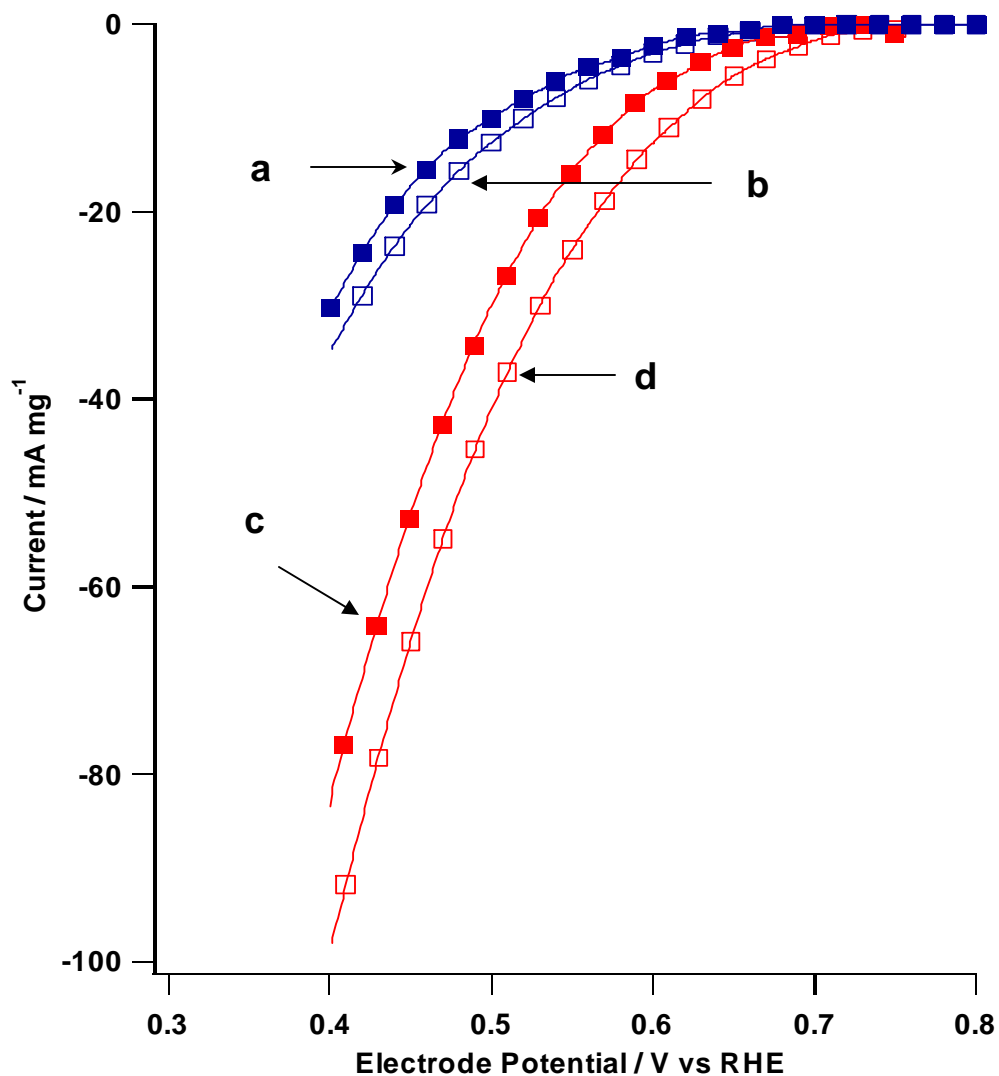


Figure 2.11 Current-Voltage characteristics of Ru based electrocatalysts for the reduction of oxygen at 60°C in the presence and absence of methanol in the electrolyte. Similar trends were observed at room temperature. Voltage values are +/- 5mV (deviation from average). Currents are negative due to a cathodic oxygen reduction with an oxygen flow rate of 70 mlpm (mlpm refers to standard milli liters per minute).

a) RuSnSe with methanol; b) RuSn Se without methanol; c) RuMoSe with methanol; d) RuMoSe without methanol. RuSnSe a) and b) refers to $\text{Ru}_7\text{Sn}_1\text{Se}_1$ and RuMoSe c) and d) refers to $\text{Ru}_3\text{Mo}_{0.08}\text{Se}_2$.

Chapter 3 Coupling Reaction and separation using microporous carbon as gas diffusers

This work was done in collaboration with Ramakrishnan Rajagopalan and Prof. Henry Foley of the Chemical Engineering Department at Penn State and published in Materials Research Society Symposium Proceedings, Volume 801 (Materials and Technology for Hydrogen Economy), 2004. Ramakrishnan Rajagopalan fabricated the membranes used in this work and characterized them using permeance tests. I tested the membranes in a fuel cell in our lab and analyzed and calculated results from experiments.

Introduction

The combinatorial approach described in the previous chapter did not help solve the CO poisoning problem through a catalytic route. We sought for other ways of minimizing the poisoning effect of CO on anode kinetics. We could envision raising the temperature to about 150 °C in order to desorb CO preferentially [6, 7]. Other options include looking at electrocatalyst clusters such as Pt-Ru and Pt-Mo that improve anode kinetics [5], or, selectively oxidize CO to CO₂ in the presence of water using catalysts based on Cu-ZnO-Al₂O₃ and Pt-CeO₂ [9], or use catalytic filters [6,7] that may also function as adsorbents for CO. Other options may include designing cells having compartments for regenerating electrolytes [8]. The routes described above were based on thermal and or catalytic solutions to the poisoning problem. A different strategy is to couple reaction and separation in chemical and electrochemical systems. We sought to increase the selectivity to H₂ over CO non-catalytically by incorporating membranes on the anode side of the fuel cell that would selectively transport H₂ and not CO to the electrocatalyst.

Pioneering work by Philip Walker in the Fuel Science Department at Penn State in the early 1960s [38, 39] helped establish carbon as a catalytic support and a separator, following the demonstrated application of zeolites to catalysis by Paul Weisz and co-workers at Mobil [37]. Carbon has the added advantage of being electrically conductive for electrochemical purposes. Walker and his group found that carbon with pore diameter

in the range of 4-5 Å (called microporous carbon henceforth) possess excellent size and shape selective properties, helping them preferentially separate gases based on their size and molecular weight. These forms of carbon are typically derived from polymers like polyfurfuryl alcohol (PFA), polyvinylidene chloride (PVDC) and polyvinylchloride (PVC). The ease of synthesis of these materials in powder form and thin membranes on supports provides the flexibility to process these materials for different applications including catalysis and gas separation [1-4]. We investigated the potential of microporous carbon as a selective separator for fuel cell poisons.

Experimental Section

Synthesis of Carbon Membranes A known concentration of polyfurfuryl alcohol (Polymer & Dajac Laboratories Inc., Feasterville, PA) was dissolved in acetone to form the polymer solution. This polymer solution was coated onto a 0.2-micron porous stainless steel disc (1.8" diameter, Chand Metallurgical, Worcester, Massachusetts) using a home-built spin coater. The porous stainless steel support was mounted on the shaft of a hand-drilling machine. 2 ml of polymer solution was applied on the rotating stainless steel discs very slowly until a uniform film of the polymer was formed on the support. This process was repeated after every pyrolysis. The coated stainless steel support was then pyrolyzed under argon in a tube furnace at 600 °C for 4 hours. The sample was weighed before and after each pyrolysis and the amount of carbon deposited on the substrate was calculated. This process was repeated until a supported carbon membrane was obtained. The same procedure was followed to coat carbon from PFA on a carbon web (B-1 carbon cloth from E-Tek®).

Synthesis of Membrane Electrode Assemblies (MEA) Membrane electrode assemblies were synthesized using the procedure described on page 86 (Chapter 2) with the microporous carbon membranes coated stainless steel plates or PFA coated carbon web replacing the carbon cloth. The pore diameter distribution of the carbon is shown in Figure 3.1 indicating a narrow pore diameter of 5 Å as described in the work of Foley *et*

al. [1-4] and Walker *et al.* [12,13]. Figure 3.2 shows an optical micrograph of PFA coated carbon web and a schematic of transport through the web.

Permeance Experiments The permeance of various gases through the microporous carbon membranes was measured using a testing unit. The membranes used in this study were sealed using Viton gaskets into a stainless steel module shown in Figure 3.3, set up to measure the transport of a single gas through the membrane. The module was evacuated and the gas introduced at the top face (core side) at pressure, P_{cs} . The bottom of the module (shell side) was sealed from vacuum and subsequent rise in pressure was used to evaluate the instantaneous derivative of time dependent flux. The pressure was measure using an MKS Barton pressure transducer (0-1000 torr) and the setup interfaced to a PC that controlled the start and duration of the experiments using electronically actuated solenoid valves. The pressure rise was not permitted to exceed a minimum value (10 torr), enabling the measurement of steady state flux as a function of driving force (pressure P_{cs}).

Fuel cell testing Testing was carried out by placing the fuel cell assembly in a modified Lynntech test stand (Lynntech Industries, College Station, TX) described on page 86 of Chapter 2.

Results and Discussion

We measured the flux of pure gases through the membranes using a permeation unit in Figure 3.3. Following Shiflett and Strano *et al.* [1-4], we can write a mass balance for the permeating species as a function of a membrane area averaged flux as:

$$(1/A) * \frac{(dm)}{(dt)} = J * M \quad (1)$$

where,

(dm/dt) is the time derivative of increase in mass of the gas of molecular weight M

A , the membrane area in m^2 and

J is the flux across the membrane in $molm^{-2}s^{-1}$

Equation (1) can be re-written as $(1/A) \cdot (dn/dt) = J$, where n represents the total number of moles of a gas of molecular weight n diffusing across an interface. Equation (1) does not distinguish between molecules free to move through the membrane and those adsorbed onto the pore walls of the membrane and assumes a linear relation between the two based on Weisz's suggestion [11b].

The flux J across the membrane can be written as a function of the driving force (pressure) following [15,16] as:

$$J = \frac{(\pi)}{(\delta)} * (P_{cs} - P_{ss}) \quad (2)$$

Using the ideal gas law for total moles, equation (1) can be re-written as

$$J = d(P * V / ART) / dt = (V / ART) * (dP / dt) \quad (3)$$

Equating (2) and (3) we can write

$$d(P * V / ART) / dt = \frac{(\pi)}{(\delta)} * (P_{cs} - P_{ss}) \quad (4)$$

$$[V / ART] * [dP / (P_{cs} - P_{ss})] = [(\pi / \delta) * t] \quad (5)$$

Replacing pressure (P) and volume (V) by shell side pressure and volume; holding initial shell side pressure zero at zero time (due to experimental conditions) and integrating (5) with respect to time, we can obtain a time dependent pressure rise following Strano and Shiflett et al [1-4], as

$$\{(V_{ss}) / (ART) * \ln [(P_{cs} - P_{sso}) / (P_{cs} - P_{ss})]\} = [(\pi / \delta) * t] \quad (6)$$

$$\{(V_{ss}) / (ART) * \ln [(P_{cs}) / (P_{cs} - P_{ss})]\} = [(\pi / \delta) * t] \quad (7)$$

where,

V_{ss} , shell side volume in m^3 ,

A , membrane area in m^2 ,

R , gas constant in $J \text{ gmol}^{-1} \text{ K}^{-1}$ or $m^3 \text{ Pa gmol}^{-1} \text{ K}^{-1}$,

T , temperature in K ,

P_{cs} and P_{ss} , pressures on the core side and shell side of the tubular membrane, respectively in Pa

P_{sso} , pressure at $t=0$ on the shell side of the tubular membrane in Pa (zero in these experiments)

π , gas permeability in $\text{mol m}^{-1} \text{s}^{-1} \text{Pa}^{-1}$,

δ , membrane thickness in m,

Flux of each gas through the membrane was measured by a plot of pressure rise versus time and multiplying the linear part of the plot with the ratio of shell side volume over product of membrane area, gas constant and temperature, following equation 3. The slope of the plot of the left hand side of equation 7 versus time gave permeance of the gas in $\text{molm}^{-2}\text{Pa}^{-1}\text{s}^{-1}$. The slope of the same plot provided flux divided by pressure. Figure 3.4 shows the results of flux of various gases examined in this study. Tables 3.1 and 3.2 show permeance ratios of different gases, derived from the slope of Figure 3.4. The linear dependence of steady state flux on driving force from Figure 3.4 also suggested that adsorption on these membranes are in the regime of Henry's law [1-4]. From table 3.1, we see that the kinetic diameter for O_2 (3.46Å) is very close to that of N_2 (3.64Å). The experimental separation factor of 0.96 for O_2/N_2 was characteristic of a Knudsen type diffusion behavior [16] for the separation of these gases. Under these conditions, the movement of molecules inside the narrow pore channels is mainly hindered by collisions with the pore walls rather than with each other and the diffusivity scales as the $m^{-1/2}$ where m is the molecular weight [16]. An alternative explanation was that the presence of cracks in the membrane resulted in no net separation of O_2/N_2 [1-4] as the experimental separation factor of 0.96 is close to the theoretical separation factor of 0.93 by the Knudsen model.

We experimented with two ways of testing the separation and reaction hypothesis. The first involved sandwiching a stainless steel supported carbon membrane between the two flanges used in the permeation experiment and placing it close to the gas cylinders. This led to very low flux of gases through the carbon coated stainless steel membrane. Figure 3.5 a) and 3.5 b) shows the results from a typical experiment. The results indicated that

these membranes are insufficient in providing constant flux of gases in fuel cells, unless the separator system was redesigned. The time lag in steady flow during these experiments suggested that the membrane provides restriction to flow of gas, characteristic of ink-bottle pores [17] i.e., the gas flow is at a continuum only when sufficient pressure built up in the pores of the membrane, resulting in adsorption-desorption hysteresis. This effect therefore has applications in delayed release of chemicals, modulated by pressure changes [20].

We then sought to use the carbon coated membranes as the gas diffuser and separator, by reducing the diffusion distance between the source of the fuel and the fuel cell. We were interested in *optimizing three parameters* (i) operating in a regime relevant to fuel cells (ii) operating in a regime free of external transport effects (iii) operating at a large H₂/CO separation factor.

We cut the carbon coated stainless steel disks used in permeation experiments to 5 cm² strips, and used the same as the anode gas distributor. This led to poor electrical contact with the graphite plates and no current. We then tested PFA coated carbon web as the anode carbon cloth. As a comparison, Pt/C MEAs were also tested in the fuel cell assembly. Current voltage curves were collected at a backpressure of 33 psig (206 kPa) across the cell for the PFA carbon MEA and at 15psig (101 kPa) across the standard Pt/C. This was essential to increase the flux through the PFA carbon MEA. From Figure 3.4, the limiting current density at 206 kPa (based on external flux from permeation experiments), for the PFA carbon MEA is 2.4 A cm⁻² (product of steady state flux and Faraday's constant). This suggested that we were not limited by external flux of fuel to the electrocatalyst surface, under the present experimental conditions.

Figures 3.6 and 3.7 show the current-voltage data obtained as a function of fuel and oxidizer flow rates for the different MEAs. We observe from these figures, a lack of the separation effect based on current-voltage on Pt-based MEAs, to microporous carbon (having Knudsen selectivity for O₂/N₂, H₂/CO and H₂/CO₂) as the backing layer. These results were very surprising as pure component permeation results indicated a large

separation factor. The confusion was partly resolved by comparing the feed in fuel cell tests (100 ppm CO in H₂) against pure component permeation experiments and pointed out the importance of using the same feed in both tests. We currently postulate that strong adsorption of CO and CO₂ onto the carbon membranes and perhaps concentration of CO in the micropores is responsible for the lack of separation using the PFA derived carbon as shown in Table 3.2 and Figure 3.7.

The adsorption phenomena can also be partially explained by the accumulation effect postulated by Wei and Weisz [11]. According to Wei and Weisz [11], the Knudsen model, which applies to dilute gas phase diffusivities in narrow pores, assumes that interactions between molecules and the pore walls are inelastic and that molecules have no memory of the angle of incidence. The assumption of Knudsen diffusion may break down for linear molecules within the confines of the molecular sieve pores where the tendency of the membrane to concentrate molecules increases the probability of collisions with other molecules versus collisions with the pore walls. Quantifying this effect in zeolites continues to be a challenge [18]. The closest study that attempted this difficult task experimentally is the work of Haag and Weisz [19]. Attempts to adapt the same to study of zeolitic carbon to try and draw structure property relations have been hampered by difficulty in assigning a structure to microporous carbon and growing crystals of the proposed structure [21].

To check to see if Weisz's [11] hypothesis was validated in our experiments, we measured the permeance of CO and CO₂ (Table 3.2 and Figure 3.4). We find that the experimental ratios of H₂/CO and H₂/CO₂ (Table 3.2) are lower than the values predicted by theory, even though the kinetic diameters (from table 3.1) of CO (3.69Å) and CO₂ (3.94Å) are comparable to O₂ (3.46Å) and N₂ (3.64Å). The small changes in kinetic diameter resulting in large changes in experimental ratios of H₂/CO and H₂/CO₂ (Table 3.2) lead us to speculate that accumulation or more likely strong adsorption of CO and CO₂ in the pores of the polyfurfuryl alcohol derived carbon. The permeation experiments involved increase in pressure as a signal and could not distinguish pressure rise due to individual components of a mixture. Lack of analytical data for composition of the shell

side gas during the earlier experiments prevented identity of gas mixture and quantification.

Membranes containing Pd or Pd-Ag alloys are attractive candidates to solve the problem of selectively transporting H₂ and not CO to the electrocatalyst, but suffer from CO poisoning problems with time [22]. The technological solution to the problem could be two membranes, one cleaning up CO and the other being simultaneously regenerated after CO poisoning. An interesting idea would be to try membranes containing Pd or Pd-Ag alloys dispersed in PFA derived carbon with the technological solution to the problem being the same; i.e., two membranes, one cleaning up CO and the other being simultaneously regenerated after CO poisoning.

Conclusions

Carbon membranes with pore diameter of 4-5 Å were tested in working fuel cells for separation of small amounts of CO (100ppm) in H₂. These were compared to traditional Pt/C membrane-electrode assemblies. Current-voltage results indicate a lack of any advantage for using carbon membranes having Knudsen selectivity (based on O₂/N₂ tests) in Pt based MEAs. Future exploratory ideas could include synthesizing membranes with higher selectivity to check for tolerance of these assemblies to low amounts of CO and check the anode and cathode exhausts for CO/H₂ ratio at the exit. Using gas mixtures coupled with analytical methods in future experiments to check for selectivity of these membranes to mixtures rather than pure gases should help match realistic conditions of fuel cell and permeation tests. An interesting approach would be to use these membranes as a catalytic filter to concentrate CO and CO₂, prior to its introduction into the fuel cell assembly or use these materials in applications requiring delayed release of chemicals.

References

1. a) Strano, M. S. and Foley, H. C., *AIChE Journal*, **2001**, *47*, 66.; b) Mariwala R. K. and Foley H. S., *IECR*, **1994**, *33*, 2314.

2. Shiflett, M. B. and Foley, H. C., *J. Membr. Sci.*, **2000**, 179, 275.
3. Shiflett, M. B. and Foley, H. C., *Carbon*, **2001**, 39, 1421.
4. Rajagopalan, R. and Foley H. C., *Mat. Res. Soc. Symp. Proc.*, **2003**, 752, 225.
5. Lee, S. J., Mukherjee, S., Ticanelli, E. A. and McBreen, J., *Electrochimica Acta*, **1999**, 44, 3283 and references therein.
6. Balasubramanian, L., Huang, W. and Weidner, J. W., *Electrochemical and Solid-State Letters*, **2002**, 5(12), A267 and references therein.
7. Adcock, P. A., Brosha, E. L., Garzon, F. H., Uribe, F. A., *Mat. Res. Soc. Symp. Proc.*, **2003**, 756, 365.
8. Simons, E. L., Cairns, E. J., *Materials Protection*, **1967**, 6(9), 51.
9. Handbook of heterogeneous catalysis, Vol. 4, p1801-1900, ed. by G Ertl, H Knözinger, and J Weitkamp, VCH, Weinheim, **1997**.
10. (a) Wilson, M. S., Gottesfeld, S., *J. E. Soc.*, **1992**, 139(2), L28; (b) Wilson, M. S.; Valerio, J. A. and Gottesfeld, S., *Electrochimica Acta*, **1995**, 40(3), 355.
11. a) Weisz, P. B.; Frillette, V. J., *J. Phys. Chem.*, **1960**, 64, 382; b) Weisz, P. B., *IECR*, **1995**, 34(8), 2692; c) Haag, W. O., Lago, R. M. and Weisz, P. B., *Faraday Discussions of the Chemical Society*, **1981**, 72, 317; d) Wei, J., *J. Catal.*, **1982**, 75, 433.
12. Metcalfe, J. E. III; Kawahata, M.; Walker, P. L., Jr., *Fuel*, **1963**, 42, 233.
13. Kotlensky, W. V.; Walker, P. L., Jr., *Proc. Conf. Carbon, Buffalo*, **1959**, 423.
14. (a) Weisz, P. B., "Polyfunctional Heterogeneous Catalysis", *Advances in Catalysis*, Academic Press Inc., New York, NY, **1962**, 13, 137; (b) Weisz, P. B., *Science*, **1973**, 4072(179), 433.
15. Cussler, E. L., "Diffusion: mass transfer in fluid systems", Cambridge University Press, New York, **1997**.
16. Bird, R. B., Stewart, R. E., Lightfoot, E. N., "Transport phenomena", John Wiley and Sons, NY, **2002**.
17. a) McBain, J. W., *JACS*, **1935**, 57, 699; b) Vishnyakov, A. and Neimark, A V., *Langmuir*, **2003**, 19(8), 3240 and references therein.
18. Degnan, T. F. Jr., *J. Catal.*, **2003**, 216 (1-2), 32.
19. a) Arsenova-Hartel, N.; Bludau, H.; Haag, W. O.; Karge, H. G., *Microporous and Mesoporous Materials*, **2000**, 35-36, 113. ; (b) Frillette, V. J.; Haag, W. O.; Lago, R. M.,

J. Catal., **1981**, *67(1)*, 218; (c) Haag, W.O.; Lago, R.M.; Weisz, P. B., *Faraday Discussions of the Chemical Society*, **1982**, *72*, 317.

20. a) LaVan, D. A.; Padera, R. F.; Friedmann, T. A.; Sullivan, J. P.; Langer, R.; Kohane, D. S., *Biomaterials*, **2005**, *26(5)*, 465; b) Hsieh, D. S. T.; Rhine, W. D.; Langer, R., *Journal of Pharmaceutical Sciences*, **1983**, *72(1)*, 17.; c) Rhine, W. D.; Hsieh, D. S. T.; Langer, R., *Journal of Pharmaceutical Sciences*, **1980**, *69(3)*, 265.

21. Smith, M. A.; Foley, H. C.; Lobo, R. F., *Carbon*, **2004**, *42(10)*, 2041.

22. Wilhite, B. A.; Schmidt, M. A.; Jensen, K. F., *IECR*, **2004**, *43(22)*, 7083 and references therein.

Gases	Permeance (* 10⁻⁷ mol/(m²*s*Pa))	Kinetic Diameter (Å)
O ₂	3.35	3.46
N ₂	3.49	3.64
CO ₂	4.14	3.94
CO	4.22	3.69
H ₂	12.9	2.9

Table 3.1 Permeance of pure component gases from the slope of Figure 3.4

Gases	H ₂ /CO	H ₂ /CO ₂	O ₂ /N ₂
Theoretical permeation ratios (Knudsen model)	3.74	4.69	0.93
Experimental Permeation ratios	3.06	3.12	0.96

Table 3.2 Permeance ratios of pure component gases from Figure 3.4

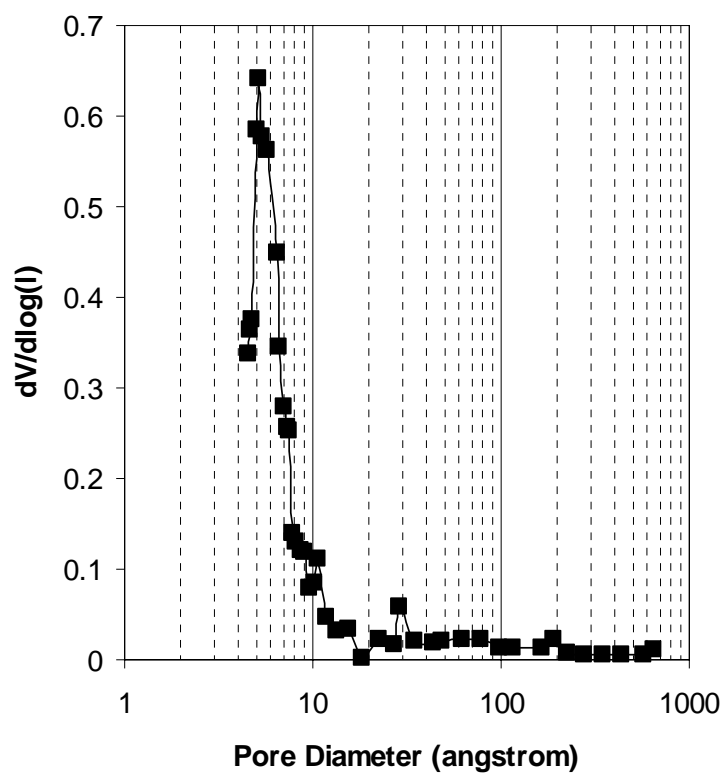


Figure 3.1 Pore Diameter Distribution of polyfurfuryl alcohol (PFA) derived carbon using chloromethane as probe molecule with pores size maximum at 5 Å. (line drawn as a guide to the eye)

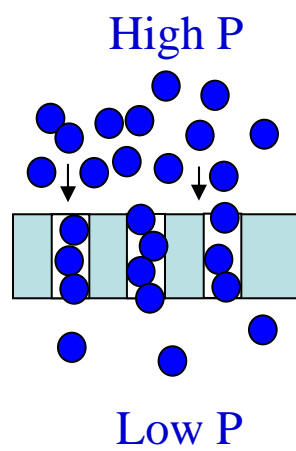


Figure 3.2 Photograph of polyfurfuryl alcohol (PFA) derived carbon web (2.5x 2.5 cm) and a schematic of transport through the web.

Gas in



Vaccum

Pressure Transducer

Figure 3.3 Membrane Module for Permeation Experiments. The carbon web shown in Figure 3.2 was held between the stainless steel flanges using Viton® gaskets.

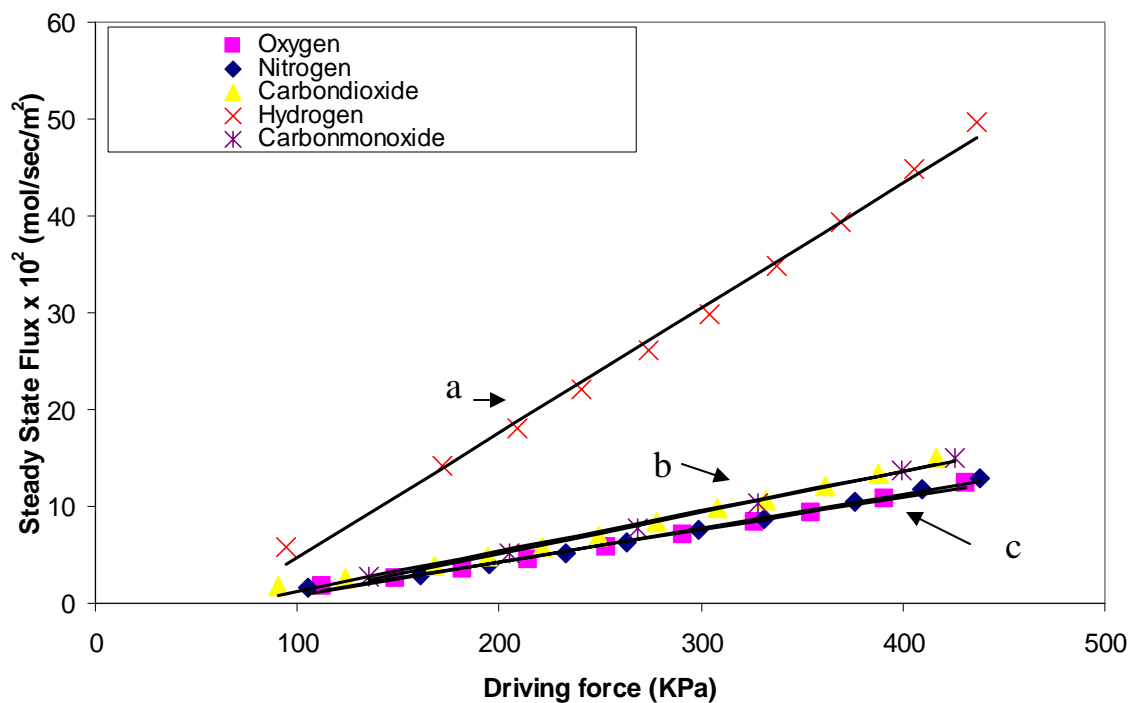


Figure 3.4 Steady state flux of different gases through carbon membrane a) H₂ b) CO and CO₂ c) O₂ and N₂. Linear behavior suggests adsorption is in the regime of Henry's Law.

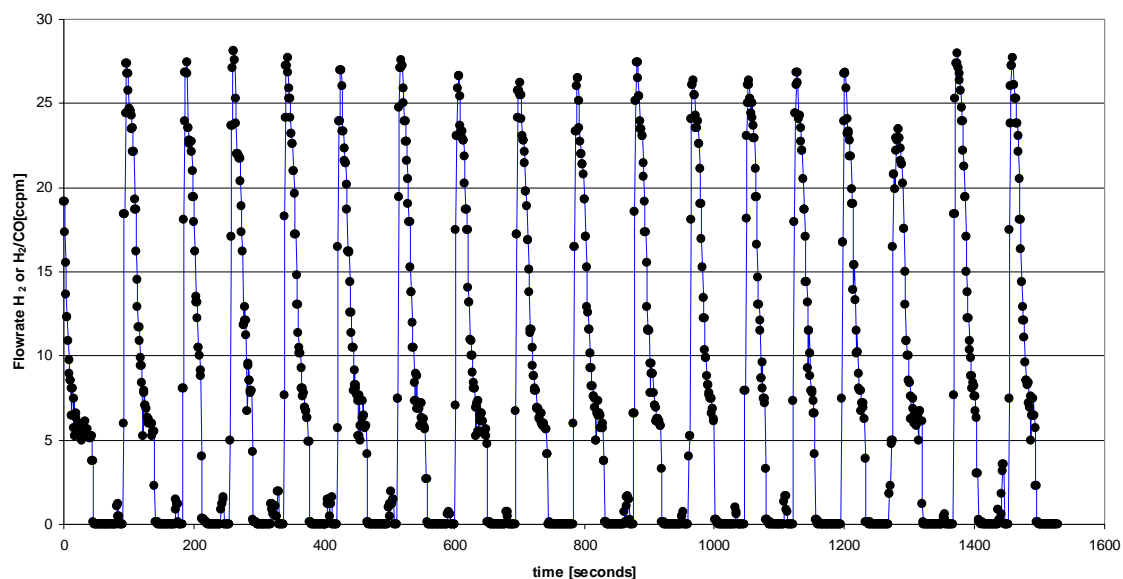


Figure 3.5a Flow rate of fuel (H_2 or H_2/CO) as a function of time with the membrane held between the gas cylinder and inlet to the flow meter.

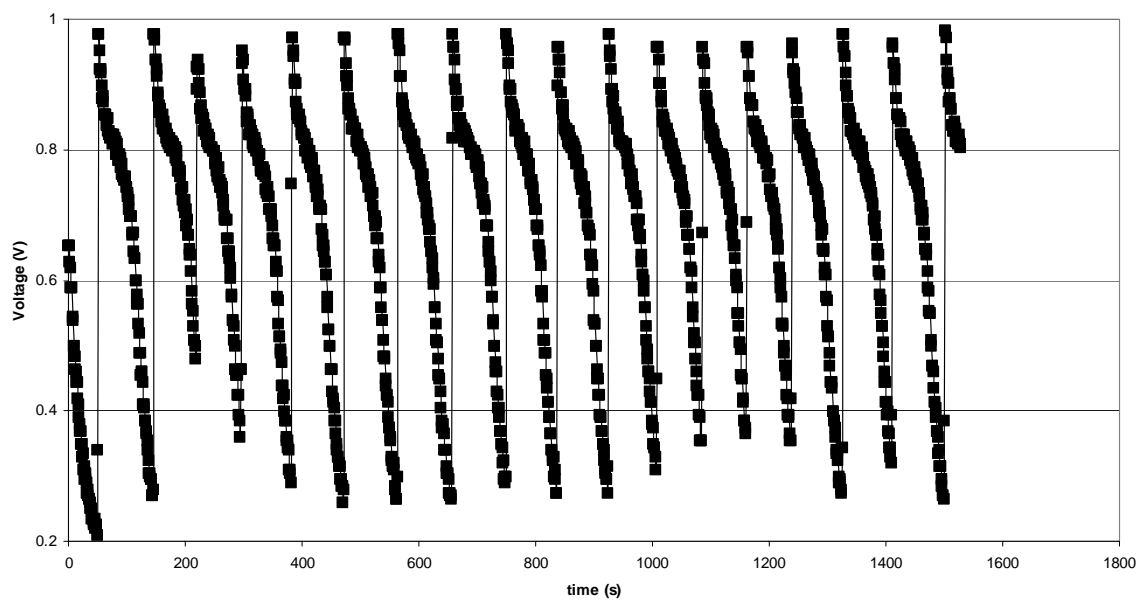


Figure 3.5b Voltage of fuel cell (H_2 or H_2/CO) as a function of time with the membrane held between the gas cylinder and inlet to the flow meter.

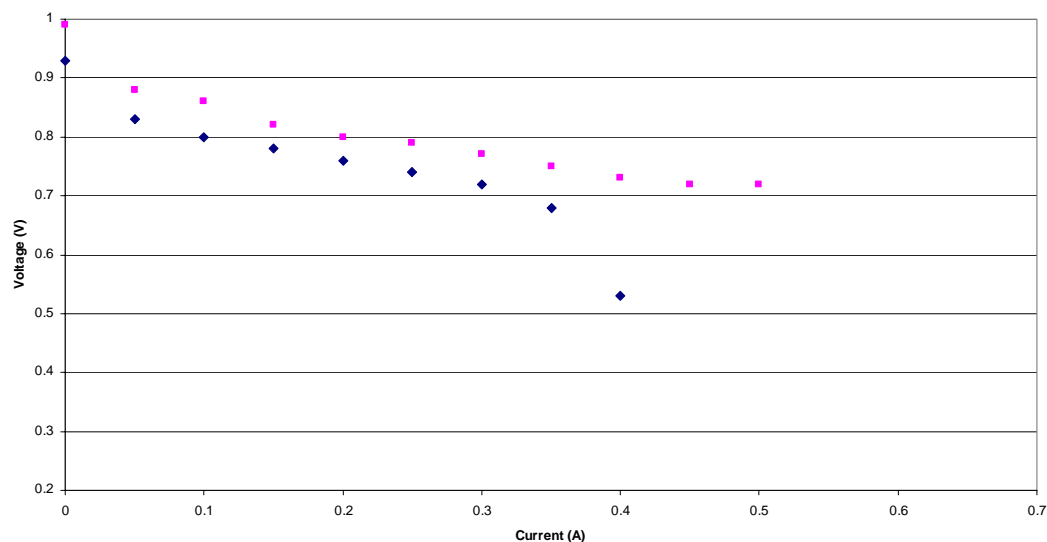


Figure 3.6 Current- Voltage curves for Johnson Matthey Pt on carbon membrane electrode assembly (MEA) tested in fuel cells as a function of different flow rates of H₂ (square) and H₂/CO (diamond) as the fuel and O₂ as the oxidizer (in 0.14 and 0.3 standard liters per minute respectively)

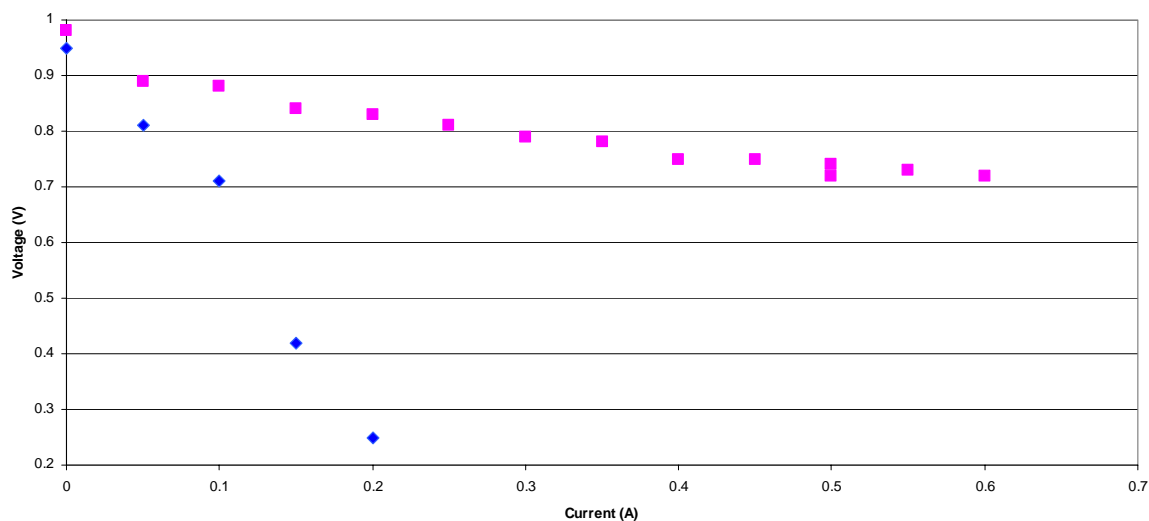


Figure 3.7 Current- Voltage curves for Johnson Matthey Pt on polyfurfuryl alcohol (PFA) derived carbon membrane electrode assembly (MEA) tested in fuel cells for H₂ (square) and H₂/CO (diamond) as the fuel and O₂ as the oxidizer (in 0.14 and 0.3 standard liters per minute respectively)

Appendix A Direct Sort Algorithm

```
C      FORTRAN PROGRAM DIRECTSORT

C      PERFORMS SPLIT-POOL OPERATIONS USING BEADS
C      IN RECTANGULAR 96 (12 X 8), 384 (24 X 16),
C      OR 1536 (48 X 32) WELL PLATES

C      DEFINE ARRAY VARIABLES

CHARACTER*12 SEQOLD(16,48,32)
CHARACTER*12 SEQNEW(16,48,32)
CHARACTER*10 AT(16)
CHARACTER*40 HEADER1
CHARACTER*40 HEADER2
CHARACTER*40 HEADER3
CHARACTER*40 HEADER4
CHARACTER*40 HEADER5
INTEGER COMPOLD(16,48,32)
INTEGER COMPNEW(16,48,32)

INTEGER NROW
INTEGER NCOL
INTEGER NCOMP
INTEGER NIND
INTEGER NINF
INTEGER NSTEP
INTEGER FACT1
INTEGER FACT2
INTEGER NPOSS

INTEGER NCOMB
INTEGER NSEQ
INTEGER IPLUS
INTEGER JPLUS
INTEGER NT(16)
INTEGER JT

CHARACTER*1 INCR(16)
INCR(1) = "1"
INCR(2) = "2"
INCR(3) = "3"
INCR(4) = "4"
INCR(5) = "5"
INCR(6) = "6"
INCR(7) = "7"
```

```

INCR(8) = "8"
INCR(9) = "9"
INCR(10) = "T"
INCR(11) = "E"
INCR(12) = "W"
INCR(13) = "H"
INCR(14) = "O"
INCR(15) = "I"
INCR(16) = "X"

```

```

HEADER1="STEPS  NCOMP  ROWS  COLS  PLATE"
HEADER2="NUMBER OF UNIQUE COMPOSITIONS"
HEADER3="NUMBER OF POSSIBLE COMPOSITIONS"
HEADER4="NUMBER OF UNIQUE SEQUENCES"
HEADER5="TOTAL NUMBER OF WELLS"

```

```

C      DEFINE WELL PLATE SIZE AND NUMBER OF S-P STEPS

```

```

C      NCOMP = NUMBER OF COMPONENTS (= NUMBER OF PLATES)
C      NCOL = NUMBER OF COLUMNS, NROW = NUMBER OF ROWS
C      NSTEP = NUMBER OF SPLIT POOL STEPS

```

```

NCOMP = 4
NCOL = 16
NROW = 24
NSTEP = 4

```

```

OPEN(UNIT=5, FILE='OUTPUT2', STATUS='NEW')

```

```

C      INITIALIZE WELL PLATES

```

```

DO 30 J=1, NCOMP
  DO 20 K=1, NROW
    DO 10 L=1, NCOL
      COMPOLD(J, K, L)=10**(J-1)
      COMPNEW(J, K, L)=10**(J-1)
      SEQNEW(J, K, L)=INCR(J)
      SEQOLD(J, K, L)=INCR(J)

```

```

10      CONTINUE
20      CONTINUE
30      CONTINUE

```

```

C      MAIN DIRECTED SORTING LOOP

```

```

DO 180 I=1, NSTEP/2

```

```

C      SHUFFLE ROWS

```

```

  DO 80 J=1, NCOMP
    DO 70 K=1, NROW
      JT=IFIX(((K+I-2)*NCOMP/NROW)*1.)

```

```

        JNEW=JT+J
        IF (JNEW.GT.NCOMP) JNEW=JNEW-NCOMP
        IF (JNEW.GT.NCOMP) JNEW=JNEW-NCOMP
C      WRITE(5,500) I, J, K, JT, JNEW
        DO 60 L=1,NCOL
            SEQNEW(JNEW,K,L)=SEQOLD(J,K,L)
            COMPNEW(JNEW,K,L)=COMPOLD(J,K,L)
60     CONTINUE
70     CONTINUE
80     CONTINUE
C      UPDATE ARRAY VALUES
        DO 110 J=1,NCOMP
            DO 100 K=1,NROW
                DO 90 L=1,NCOL
                    SEQNEW(J,K,L)=TRIM(SEQNEW(J,K,L))/INCR(J)
C      WRITE (5,510) SEQNEW(J,K,L)
                    SEQOLD(J,K,L)=SEQNEW(J,K,L)
                    COMPNEW(J,K,L)=COMPNEW(J,K,L)+10**(J-1)
                    COMPOLD(J,K,L)=COMPNEW(J,K,L)
90     CONTINUE
100    CONTINUE
110    CONTINUE
C      SHUFFLE COLUMNS
        DO 140, J=1,NCOMP
            DO 130, L=1,NCOL
                JT=IFIX((L+I-2)*NCOMP/NCOL)*1.)
                JNEW=JT+J
                IF (JNEW.GT.NCOMP) JNEW=JNEW-NCOMP
                IF (JNEW.GT.NCOMP) JNEW=JNEW-NCOMP
                DO 120, K=1,NROW
                    SEQNEW(JNEW,K,L)=SEQOLD(J,K,L)
                    COMPNEW(JNEW,K,L)=COMPOLD(J,K,L)
120    CONTINUE
130    CONTINUE
140    CONTINUE
C      UPDATE ARRAY VALUES
        DO 170 J=1,NCOMP
            DO 160 K=1,NROW
                DO 150 L=1,NCOL
                    SEQNEW(J,K,L)=TRIM(SEQNEW(J,K,L))/INCR(J)
C      WRITE (5,510) SEQNEW(J,K,L)
                    SEQOLD(J,K,L)=SEQNEW(J,K,L)
                    COMPNEW(J,K,L)=COMPNEW(J,K,L)+10**(J-1)
                    COMPOLD(J,K,L)=COMPNEW(J,K,L)
150    CONTINUE
160    CONTINUE
170    CONTINUE

```

```

180 CONTINUE

C COMPUTE NUMBER OF UNIQUE COMBINATIONS AND SEQUENCES
NCOMB=0
NSEQ=0
NIND=0
  DO 300 I=1, NCOMP
    DO 290 J=1, NROW
      DO 280 K=1, NCOL
        NIND=NIND+1
        NINF=0
        IPLUS=1
        JPLUS=1
        DO 270 L=1, I
          DO 260 M=1, NROW
            DO 250 N=1, NCOL
              NINF=NINF+1
              IF (NINF.GE.NIND) GOTO 250
              IF ((I).NE.(L)) GOTO 240
              IF ((J).NE.(M)) GOTO 240
              IF ((K).NE.(N)) GOTO 240
              GOTO 250
240 IF (COMPNEW(I,J,K).EQ.COMPNEW(L,M,N)) THEN
          IPLUS=0
          ENDIF
          IF (SEQNEW(I,J,K).EQ.SEQNEW(L,M,N)) THEN
            JPLUS=0
            ENDIF
250 CONTINUE
260 CONTINUE
270 CONTINUE
C IF (IPLUS.EQ.1) WRITE(5,500) COMPNEW(I,J,K)
      NCOMB=NCOMB+IPLUS
      NSEQ=NSEQ+JPLUS
280 CONTINUE
290 CONTINUE
300 CONTINUE
C COMPUTE NUMBER OF POSSIBLE COMBINATIONS
FACT1=1
FACT2=1
FACT3=1
DO 320 J=1, NCOMP-1
  FACT1=FACT1*J
320 CONTINUE
DO 330 J=NSTEP+2, NSTEP+NCOMP
  FACT2=FACT2*J
330 CONTINUE

```

```

NPOSS = FACT2/FACT1
C   OUTPUT DATA
WRITE(5,420) HEADER1
WRITE(5,400) NSTEP, NCOMP, NROW, NCOL, NROW*NCOL
WRITE(5,400)
WRITE(5,420) HEADER5
WRITE(5,400) NCOMP*NROW*NCOL
WRITE(5,400)
WRITE(5,420) HEADER2
WRITE(5,410) NCOMB
WRITE(5,410)
WRITE(5,420) HEADER3
WRITE(5,410) NPOSS
WRITE(5,410)
WRITE(5,420) HEADER4
WRITE(5,410) NSEQ
WRITE(5,410)

400  FORMAT(I8, I8, I8, I8, I8)
410  FORMAT(I8)
420  FORMAT(A45)

C   OUTPUT ARRAYS
DO 450 J=1,NCOMP
    DO 440 K=1,NROW
        DO 430 L=1,NCOL
            NT(L) = COMPNEW(J,K,L)
            AT(L) = SEQNEW(J,K,L)
430  CONTINUE
        WRITE(5,510)
AT(1),AT(2),AT(3),AT(4),AT(5),AT(6),AT(7),AT(8)
C   WRITE(5,510)
AT(9),AT(10),AT(11),AT(12),AT(13),AT(14),AT(15)
C   WRITE(5,510) AT(16)
        WRITE(5,500)
NT(1),NT(2),NT(3),NT(4),NT(5),NT(6),NT(7),NT(8)
C   WRITE(5,500)
NT(9),NT(10),NT(11),NT(12),NT(13),NT(14),NT(15)
C   WRITE(5,500) NT(16)
440  CONTINUE
        WRITE(5,500)
450  CONTINUE

500  FORMAT(I9,I9,I9,I9,I9,I9,I9,I9)
510  FORMAT(A9,A9,A9,A9,A9,A9,A9,A9,A9)
END

```

Appendix B Total number of physical manipulations for a n component, m step library in a 96 well plate format

$$\text{Bead Transfer} = n + m[n(n-1)]+n$$

$$\text{Solution Transfer} = n(m+1)$$

$$\text{Total number of physical manipulations} = \text{Bead Transfer} + \text{Solution Transfer}$$

$$= n + m[n(n-1)]+ n + n(m+1)$$

$$= m(n^2+1) + 3n$$

$$= \text{Order } (n^3) \text{ for every } m \text{ that can be expressed as function of } n$$

Total number of steps for a four component, four step, 96 well plate library = 66

Total number of theoretical compositions for a four component, four step, 96 well plate library = 52

Total number of theoretical sequences for a four component, four step, 96 well plate library = 256

Total number of steps for a eight component, four step, 96 well plate library = 276

Total number of theoretical compositions for a eight component, four step, 96 well plate library = 52

Total number of theoretical sequences for a eight component, four step, 96 well plate library = 256

We see that the algorithm pays for effort (fewer physical manipulations) resulting in more compositions and sequences only for large libraries.

VITA
RAMNARAYANAN RAMANATHAN (Ramna)

EDUCATION

The Pennsylvania State University, University Park, PA

- Ph. D., Intercollege Graduate Program in Materials, Engineering Option
Thesis: Synthesis and Characterization of catalysts and electrocatalysts using combinatorial methods

Clarkson University, Potsdam, NY

- M.S. Chemical Engineering
Thesis: Directional Solidification of Al-Si eutectic December 1999

Central Electrochemical Research Institute, Karaikudi, India

- B.Tech. Chemical and Electrochemical Engineering May 1997

PUBLICATIONS

1. R. Ramnarayanan, T. E. Mallouk et al., and R.R. Willis et al., "Directed Sorting method for Synthesis of Bead-based Combinatorial Libraries of Heterogeneous Catalysts," in preparation.
2. Ramnarayanan Ramanathan, B.C.Chan, M.A.Salvitti, T. E. Mallouk, F. M. Falih, D. B. Galloway, S. R. Bare, and R. R. Willis, "Directed sorting method for synthesis of supported metal catalysts for methylcyclohexane dehydrogenation", accepted in *Preprints of Symposia - American Chemical Society, Division of Petroleum Chemistry*, **2005**.
3. R.Ramnarayanan, R. Rajagopalan, H. Foley, and T. E. Mallouk, "Using nanoporous carbon membranes in fuel cells," *Materials Research Society Symposium Proceedings*, **2004**, 801 (*Materials and Technology for Hydrogen Economy*), 185.
4. H. Liu, R. Ramnarayanan and B. E. Logan, "Production of electricity during waste water treatment using a single chamber microbial fuel cell," *Environmental Science and Technology*, **2004**, 38, 2281.
5. Min, Booki; Ramanathan, Ramnarayanan; Cheng, Shaoan; Logan, Bruce E. , "Electricity Production in salt bridge and membrane microbial fuel cells," *Preprints of Extended Abstracts, Division of Environmental Chemistry*, **2004**, 44(2), 1498.
6. Guoying Chen, Chad C. Waraksa, R. Ramnarayanan, Hungoo Cho, Digby D. Macdonald, and Thomas E. Mallouk, " EIS Studies of Porous Oxygen Electrodes with Discrete Particles 1. Impedance of Oxide Catalyst Supports," *J. E. Soc.*, **2003**, 150, E423 and *J. E. Soc.*, **2004**, 151 (5), L1.
7. U. Turaga and R. Ramnarayanan, "Catalytic Naphtha Reforming: Revisiting its importance in the modern refinery," *Journal of Scientific & Industrial Research*, **2003**, 62 (10), 963.
8. Y. Sun, B. C. Chan, R. Ramnarayanan, W. M. Leventry, T. E. Mallouk, S. R. Bare, and R. R. Willis, "The Split-Pool Method for Synthesis of Solid-State Materials Combinatorial Libraries," *J. Combi. Chem.*, **2002**, 4, 569.

PATENTS

1. Mallouk, Thomas E.; Ramanathan, Ramnarayanan R.; Willis, Richard R.; Gillespie, Ralph D., "Method of assembling particle libraries", *PCT Int. Appl.* **2004**, WO 2004102197.

AWARDS and PRESENTATIONS

1. Richard Kokes Travel Award, 19th North American Catalysis Society Meeting, 2005
2. Braddock Graduate Fellowship, The Pennsylvania State University, 1999
3. Three technical presentations in international meetings (MRS and ACS)